HYDRAULIC ANALYSIS OF FREE-SURFACE FLOWS INTO HIGHLY PERMEABLE POROUS MEDIA AND ITS APPLICATIONS

BIDUR GHIMIRE

June, 2009

HYDRAULIC ANALYSIS OF FREE-SURFACE FLOWS INTO HIGHLY PERMEABLE POROUS MEDIA AND ITS APPLICATIONS

BIDUR GHIMIRE

June, 2009

HYDRAULIC ANALYSIS OF FREE-SURFACE FLOWS INTO

HIGHLY PERMEABLE POROUS MEDIA AND ITS

APPLICATIONS

A thesis submitted

by

Bidur Ghimire

to

The Department of Urban Management

in partial fulfillment of the requirements

for the degree of

Doctor of Philosophy

Kyoto University

June, 2009

Abstract

In this study, a comprehensive approach including mathematical, numerical and experimental study has been taken in order to develop new models for describing free surface flow behavior in porous media. The study suggested that modeling free-surface flow in porous media is possible using a single equation capable of showing proper transition between inertial and classical Darcian flow, based on the similarity distribution functions of depth and velocity. The developed integral model inherits both the flow regimes as depicted in the analysis. For both laminar and turbulent flows through porous media, the integral models give satisfactory results. Also the proposed algorithm for numerical simulation is capable of solving various problems of free-surface flow through porous media.

This study adds a new dimension to fluid flow in porous media by replacing Darcy's equation with new models that are capable of representing both Darcy and non-Darcy flow behaviors. These are new nonlinear ordinary differential equations inherited both the flow regimes investigated. Integral formulations for unsteady depth distribution, velocity and front speed under constant water level and constant flux discharge inlet conditions have been developed based on similarity law. The formulations presented provide additional analytical insight about the intrusion dynamics. It is pointed out that, based on the self-similarity analysis, the temporal intrusion processes can be categorized into the inertia-pressure (IP) and the pressure-drag (PD) regimes. The early inertia-pressure regime is followed by the pressure-drag regime. In addition, the integral models proposed can be successfully used for the solution of a host of other nonlinear problems that admit self-similarity. The analytical and numerical solutions for constant inlet water level condition are verified with experimental observations. The unsteady distributions of flow depth, inflow velocity and front speeds are compared for various porous

media characterized by its corresponding porosity and permeability. Analyses indicate that the integral models clearly represent the nonlinear flow behavior in porous media both in laminar and turbulent flow conditions. The integral model results are in agreement with those obtained by similarity solution for the temporal change of velocity, depth at inlet and front positions.

The thesis also presents a computational fluid dynamics (CFD) model developed for the analysis of unsteady free-surface flows through porous media. Vertical two-dimensional numerical simulations are carried out for the free-surface flow inside the porous media governed by a set of Navier-Stokes equations extended for porous media flow. This model includes the convective and local inertia terms along with viscous diffusion term and resistance term comprising Darcy's linear resistance and Forchheimer's inertial resistance terms. The Finite volume method is applied using constrained interpolated propagation (CIP) method and highly simplified marker and cell (HSMAC) type pressure solver for the numerical solution. The evolution of moving free surface is governed by volume of fluid (VOF) method, adapted for the flow through porous media. To prevent the spurious oscillation and generate diffusion-free sharp interface, a third order monotone upstream-centered schemes for conservation laws (MUSCL) type total variation diminishing (TVD) schemes is used to solve the VOF convection equation.

The power law derivation and validation for the general flux inflow condition are made for a channel having a backward facing step. The result of theoretical analysis is compared with that of the numerical simulation and it shows a good agreement. The model can be a tool for the proposition of some empirical flow relationships using multivariate correlation.

In the case of rapid vertical infiltration of water through a vertical column filled with porous media, a number of experiments and analytical investigations are carried out to see the effect of acceleration in the intrusion process. It is concluded that the conventional infiltration models

like Green-Ampts infiltration model cannot account for the acceleration effect in the case of high velocity flow. It is revealed that it takes certain time for intruding water to be accelerated to its peak velocity before decreasing to almost constant velocity. The investigations are made for two different cases: constant water level and variable water level above the porous media. For porous media having low permeability, the effect of acceleration was not so significant.

In the case of dam break flow over horizontal porous strata, the model is applied to a complicated domain regarding both geometry and flow boundary conditions. Single set of governing equation is implemented to simulate the complex phenomenon. The model shows its capability in simulating the flow where interface between pressurized and open channel flow moves forward. The vertical acceleration has a significant effect on the rapid vertical infiltration which the shallow water equations cannot account for. In particular, it is shown that vertical two dimensional numerical solution that couples the fluid and solid systems simultaneously at macroscopic scale are feasible and extremely beneficial, shedding a new light into the phenomena unavailable otherwise.

It is also found that the proposed numerical model can be used for the determination of storm water storage in porous sub-base in a typical road section. The capability of the model is assessed by using the unsteady inflow condition so as to simulate the condition during high precipitation. The model could be a promising tool for planners and decision makers for effective drainage calculations to mitigate urban flood. The model successfully simulates the free surface flow in the bulk fluid as well as in the porous region. The velocities and stresses are assumed to be continuous at the interface of free and porous media so that a single set of governing equations could be solved. The robustness of the model is demonstrated by the capability of the numerical approach proposed in this thesis.

Acknowledgement

The research work presented in this thesis was conducted in River System Engineering and Management Laboratory, Department of Urban Management. Many people have contributed towards the completion of this study. Most of them I am mentioning herein, however, I am taking this opportunity to apologize to those I have inadvertently omitted from the list.

First of all, I would like to express my deep appreciation and sincere gratitude to my supervisor, Professor **Dr. Takashi Hosoda**, for all his inspiring guidance, encouragement and valuable suggestions throughout the completion of this work. I thank him for his time spent during our many discussions and for his invaluable advices. His deep knowledge and scientific integrity had been of great help whenever I encountered problems. I believe this will accompany me for the rest of my life. From him I have learned not only physics and numerical techniques, but also the attitude and the philosophy for conducting the research as a scientist.

I am highly indebted to Professor **Dr. Keiichi Toda** and Associate Professor **Dr. Kiyoshi Kishida** for their thorough review of first draft of this thesis which helped immensely to improve in this form by their invaluable suggestions and comments.

My special thanks are due to Research Assistant **Dr. Shinichiro Onda** for his kind help in many issues right from my first day in Japan. I also appreciate Pioneer Researcher **Dr. Shinichiro Nakashima** for providing valuable suggestions and his useful comments in many issues. Many results of this work are the outcome of the discussion with him.

I am thankful to my senior research colleagues **Nenad Jacimovic** and **Md. Shahjahan Ali**, who are already graduated. They were very kind, friendly, and supportive in all aspect. I would also like to thank my colleague **Mr. How Tion Puay** for his assistance and fruitful discussions over many issues.

I wish to extend my thanks to all the staff in the Graduate School of Engineering Division at the Kyoto University for the help from them.

I would like to take this opportunity to acknowledge my previous supervisors Prof. **Dr. Narendraman Shakya** and Prof. **Dr. Raghu Nath Jha** for their ample guidance which gave me the insights into the transport phenomena. I also thank **Dr. Padma Bahadur Shahi** for his suggestion and help to pursue research work in Kyoto University.

I am much indebted to my lovely wife **Bhagabati** and my little daughter **Bristi** for all their love, support and patience.

Finally but not the least, I wish to acknowledge gratefully the financial support from the Japanese Government Scholarship *Monbukagakusho*, which enabled me this great opportunity to live and study in Japan.

Dedication

*Dedicated to my mother **GAURI DEVI GHIMIRE***
...whose unconditional love has made me whatever I am today.

Preface

This manuscript of *Ph.D. Thesis* includes the contents of the following published and/or submitted journal and conference papers:

1. Ghimire, B., Hosoda, T. and Nakashima, S., An investigation on lateral intrusion process of water into porous media under different upstream boundary conditions, *Journal of Applied Mechanics*, *JSCE*, Vol. 10, pp.839-846, September, 2007.

2. Ghimire, B., Nakashima, S. and Hosoda, T., Lateral inflow characteristics of rain water from permeable road ditch into granular sub-base, *Proceedings of Annual Conference*, *The Japan Society of Fluid Mechanics*, *JSFM*, Kobe, pp.259, September 4-7, 2008.

3. Ghimire, B., Nakashima, S. and Hosoda, T., Study of various flow regimes in the water intrusion process into porous media under different upstream boundary conditions, *Eighth International Conference on Hydro-Science and Engineering*, *ICHE*, Nagoya, Vol. VIII, pp.81, September 8-12, 2008.

4. Ghimire, B., Nakashima, S. and Hosoda, T., Numerical solution of the Navier-Stokes equations for incompressible free surface flow in porous media under forced drainage condition, *Proceedings of Second Workshop on Present and Future Technology*, *NEA-JC*, Tokyo, October 12, 2008.

5. Ghimire, B., Nakashima, S. and Hosoda, T., Formulation of integral model and numerical simulation for the unsteady free-surface flows inside porous media under various inlet conditions, *Advances in Water Resources*, *Elsevier*, February, 2009. (under review)

6. Ghimire, B., Nakashima, S. and Hosoda, T., Application of spatial integral models to water intrusion process into porous media and its verification, *Journal of Applied Mechanics*, *JSCE*, Vol. 12, September, 2009. (accepted)

Table of Contents

List of Figures

List of Tables

Chapter 1
INTRODUCTION

1.1 General background

Due to its ever-broader range of applications in engineering, science and industry, the study of flow through porous media has recently gained extensive attention. This interdisciplinary field is of interest to civil engineers, fluid dynamicists, mathematicians, geologists and ecologists etc. In a broader sense, the study of porous media embraces fluid and thermal sciences, and materials, chemical, geothermal, petroleum and combustion engineering.

The equation most widely used for describing the flow of a fluid through a saturated porous medium is the well-known Darcy's law. This is a reduced form of the equation of fluid motion which predicts a linear relationship between the fluid velocity relative to the solid and the pressure head gradient. Over the years, Darcy's law has been extended to more generalized forms in order to describe more complex flow situations. In addition, it has been observed that the proportionality between head gradient and fluid velocity does not hold for high rates of fluid flow [Raptis and Perdikis, 1983]. This phenomenon has been the subject of many experimental and theoretical investigations. These studies have centered upon two important issues: (i) establishing an upper bound for the range of validity of Darcy's equation and providing generalized relationships which predict the nonlinear flow behavior properly, (ii) providing a physical basis for the generalized equation of motion and identifying mechanisms which are responsible for the nonlinear flow behavior. The latter issue is tried to address in this thesis.

Models are usually, but not always, formulated in terms of classical continuum mechanics, with equations of motion often being highly non-linear. Related problems are further complicated by the presence of a free boundary, and most modern computer methodology has been applicable only under highly restrictive assumptions. In this work we develop a method for general, continuum formulated, free surface with moving boundary, unsteady porous flow problems. Accordingly, applications that are more complex usually require appropriate and, in most cases, more sophisticated mathematical and numerical modeling. Obtaining the final numerical results, however, may require the solution of a set of coupled partial differential equations involving many coupled variables in a complex geometry. This research work shall review important aspects of resistance laws in porous media depending upon the porous material and flow characteristics and develop analytical as well as numerical methods, including treatment of multidimensional flow equations, discretization schemes for accurate solution.

A macroscopic balance of forces containing all mechanisms relevant to the fluid flow is presented as the starting point. Then a similarity theory considering one dimensional depth averaged flow equation is employed to study the nonlinear flow behavior. The study shows the solid-fluid drag force is much larger than inertial forces. Based on the spatial distribution functions for flow variables, a class of nonlinear integral models is also derived. Finally, based on principles of continuum mechanics and the general equation of the balance of forces, a physical basis for the high-velocity flow equations found in the literature is provided for multidimensional numerical solution. The generality of the approach allows one to avoid making restrictive assumptions about the pore geometry, fluid compressibility, microscopic velocity distribution, rigidity of the medium, and so forth.

1.2 Statement of problem

Flow in porous media is difficult to be accurately modeled quantitatively. Richards equation can give good results, but needs constitutive relations. These are usually empirically based and require extensive calibration [Van Genuchten, 1980; Pullan, 1990]. The parameters needed in the calibration are amongst others: capillary pressure and pressure gradient, volumetric flow, liquid content, irreducible liquid content, and temperature. In practice it is usually too demanding to measure all these parameters. Moreover, Richard's equation is applicable for the soils having very low value of permeability. In the high velocity flow through the porous media where a distinct free surface is observed, one can expect the inertial flow. In the model

introduced in this dissertation no such constitutive relations are used, but a description of flow in terms of physical parameters of the porous medium and the fluids. These parameters are amongst others: viscosity, porosity and permeability. The concept of a Representative Elementary Volume (REV) implicitly replaces part of the constitutive relations. The newly derived mathematical model can be used in drainage modeling and in the following applications where the Buckingham-Darcy or Richards equation are not directly applicable, e.g. gravity current flow of fluids in porous media with free surface.

A granular porous material is composed of distinct particles that interact with their neighbors through complex contact mechanisms. A system of several particles under the action of surface tension and capillary forces is complicated to model. Our assumption is that their effect is not so significant because one can expect the highly porous media would have less effect on the gross flow characteristics. There is perhaps no perfect scheme to simulate all these details of granular materials, but an attempt has been made by the author to select a simple system capable of capturing the fundamental features of free surface flow inside the porous formation in the unsteady intrusion. The processes include the evolution of the orientation of moving free surface. A study of this nature in the laboratory is complicated if not impossible to conduct, yet an adequate analysis requires the quantification of this information. Therefore, alternative procedures, such as computer simulations, have to be employed.

In the present form the newly derived equations are not suitable for infiltration models, for the description of fingering flow, for flow of non-Newtonian fluids, and for flow with drag along the fluid-fluid interfaces. The model can be extended to include additional processes like surface-tension, capillary forces, heat transport, and electrical conductivity, by directly averaging these processes with the aid of the REV approach.

1.3 Objectives and scope of the Study

The objective of this dissertation is to analyze and develop a macroscopic model for the movement of a wetting liquid in a rigid porous medium in the presence of a gas phase having negligible viscosity. Firstly, various flow regimes in the unsteady intrusion is investigated using similarity principle and then integral models are derived which inherit those characteristics obtained in the similarity solution. Also this dissertation uses the method of spatial averaging to change the scales in the description of flow in porous media. The results of the integral models are compared with the results of numerical simulation in vertical 2D.

The main objective of this study is to develop a CFD approach using finite volume method (FVM) for incompressible free-surface flow algorithm that incorporates fundamental physical processes involved in the unsteady intrusion of water into the porous media. The scope of the study is to introduce this novel approach as a research tool to study the composite flow phenomena in which a part of the domain is bulk fluid region and part is porous media or vice versa.

In this work, the starting point of the research will be the recent scientific developments in the flow inside the porous media and its implementation to predict the various hydrologic parameters. Thus it necessitates a physically based mathematical model which can predict the unsteady storage rate inside granular sub-base. The main objective of the study is to develop a predictive model based on the physics of multi phase flow and investigate the temporal and spatial distribution of water so that the model can be used to quantify the flow with free surface through porous media. Such model has its various uses in calculating various flow parameters. In point wise they can be enlisted as:

(i) To analyze various flow regimes in the transient free-surface flow inside porous media considering both laminar and turbulent flow

(ii) To derive the integral model from the result of analysis that can represent all the flow regimes

(iii) To develop a multidimensional mathematical model based on multiphase flow physics to predict unsteady movement of water into a granular media

(iv) To develop a numerical algorithm that will be applicable in the composite flow domain consisting of both free and porous region

(v) To refine the model to a robust one to ensemble various flow regimes inside and outside of the porous media

1.4 Organization of the thesis

This thesis contains a detailed description of analytical approaches to investigate the flow regimes and development and applications of the numerical algorithm for multidimensional unsteady free-surface flow through porous media.

The remainder of this thesis is organized as follows. Chapter 2 presents an account of literature

survey with particular emphasis on the single phase unsteady flow through the porous media. It gives a theoretical background for the governing equations for inertial unsteady flows with free surface inside porous media which are numerically solved in this study. This section also discusses about the spatial averaging the governing equation to treat the free surface flow in porous media as a continuum. A brief introduction to fractional volume of fluid (VOF) concept is provided which is used in the chapters that follow.

Chapter 3 introduces the equations of motion used in the unsteady free-surface flows through highly porous media where one can expect nonlinear inertial flows inside the porous media. A description of the basic concepts needed to develop the finite volume code is illustrated in this chapter. The Navier-Stokes equations extended for porous media with the inclusion of drag resistance term is presented. A detail of the solution technique is also provided in this chapter for later use in the application of the numerical model. Recently emerged CIP method for solving hyperbolic system of equation along with HSMAC type pressure solver is described in detail. The coupled free surface tracking VOF method and its modification for use in the porous media is also dealt with. The model validation will be accomplished through the comparison of the numerical solution to the analytical solution and experiments. Further verification is also provided in the following chapters by comparisons with analytical solutions and laboratory experiments, where different types of flows are treated.

The theoretical insight into various flow regimes in the lateral intrusion of fluid into porous media is described in Chapter 4. The similarity solution for self-similar propagation of fluid into porous media is described. Temporal powers in the unsteady moving boundary propagation are derived by similarity transformation technique. Finally the integral model formulations are done for the problems with moving free surface boundaries and representing the entire flow regime. A rigorous theoretical analysis is made in this chapter and its validation is done independently by the results from the developed algorithm for multidimensional unsteady free surface flow through porous media.

Chapter 5 reports a theoretical approach to treat domain with complex geometry in which the flow geometry consists of a back-step channel filled with porous media. Results of theoretical derivations carried out for general flux inflow condition is compared with the numerical results. The effect of permeability on the intrusion rate under upstream pressure boundary is also examined. The method employed to describe the free surface evolution are explained to gain

insight into the moving boundary definition. The effects of the size of the porous material used are also examined. The comparison of the results showed that the implemented algorithms are capable of reproducing the experimental tests.

Chapter 6 is devoted to explain the effects of acceleration on the rapid vertical infiltration. The vertical distribution of the pressure profile is also explained in the case of abrupt release of water from the top of a vertical column filled with porous media. The effect of the value of permeability on the infiltration rate is also described by comparing the results from various analytical models.

In Chapter 7, we further refine the model for its robustness to apply it in the case of complex domain. The single domain approach to deal with the dam break flow over a porous stratum is adopted for the application of model. The calculation domain consists of both free and porous media having moving free-surface in the flow which is the usual case in many groundwater flow systems. The interface treatment for conservation of volume and comparisons with the experiment is presented. The complicated phenomenon in which the interface between pressurized and open channel flow moves has been simulated by the model.

In Chapter, 8 we present an application of the model for the unsteady lateral intrusion of water into granular porous sub-base stratum. The phenomenon is likely to be useful in urban flood mitigation by allowing some water to be stored during high storm.

Chapter 9 summarizes the overall results and the major conclusions drawn from the present research, presents some recommendations for future research and discusses the limitations of the model.

The thesis can be grouped into five broad groups. The first two chapters deal with the introduction part and a short history. Third chapter deals with the model formulations. The integral model formulation based on the similarity distribution is explained in fourth chapter. Then fifth, sixth, seven and eighth chapters deal with application and modification side of the model to suit various boundary and domain conditions. At the end, the overall conclusion and recommendations for future research are given. A flow chart [see Fig. 1.1] is provided on the following page shows the flow of the chapters of this thesis for more clarity.

Introduction & History

CH: 1, 2

Numerical Model Development

CH: 3

Similarity Solution &
Integral Model Formulations

CH: 4

Applications:

•Flow in Backstep Channel

•Study of Rapid Vertical Infiltration

•Dambreak Flow Over Porous Bed

•Unsteady Storm-Water Storage

CH: 5,6,7,8

Conclusion and Recommendations
for future research

CH: 9
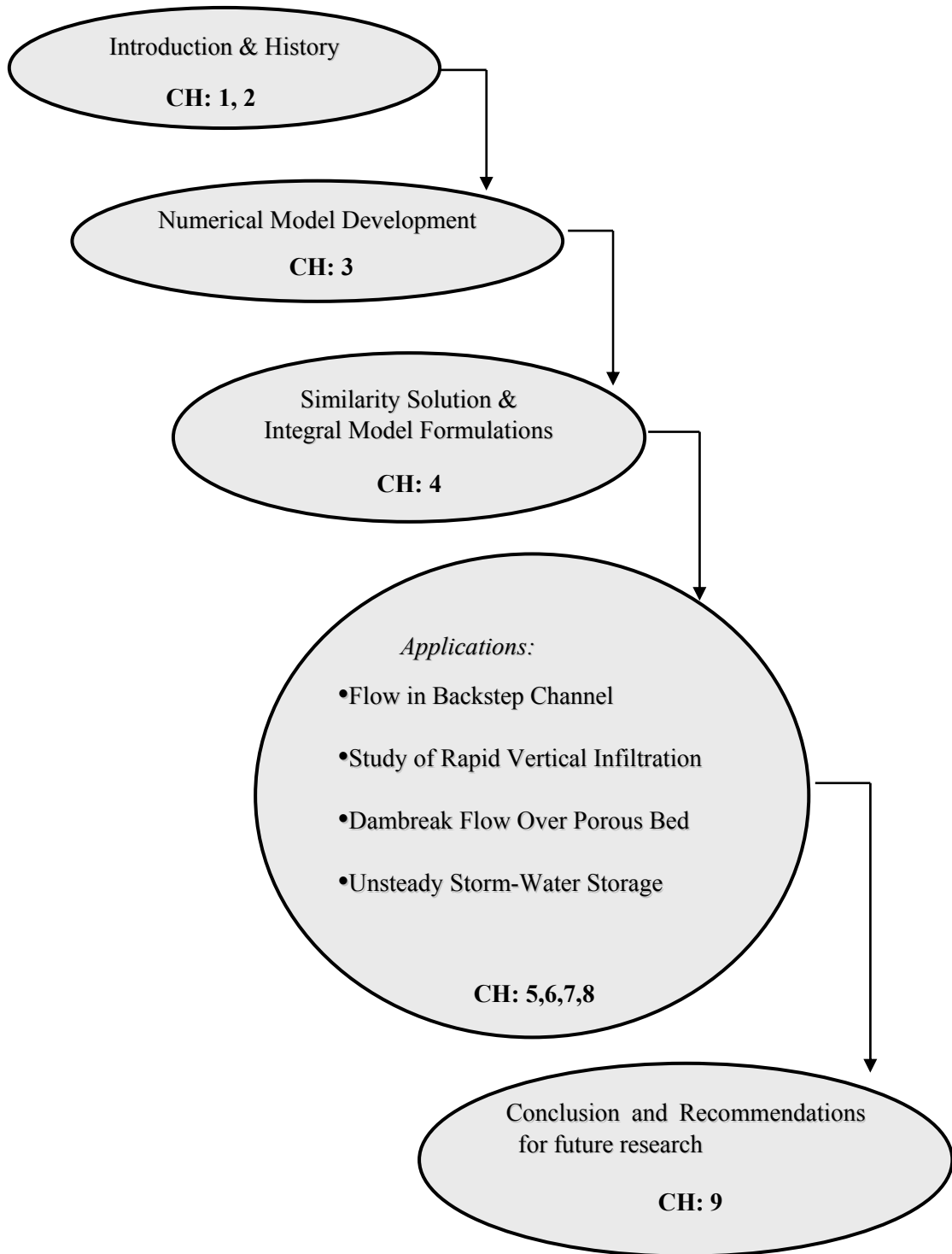
Figure 1.1 Thesis organization flow chart

Chapter 2
LITERATURE REVIEW

This chapter provides an overview and gives a historical perspective of the study of flow in porous media. Steady and unsteady flows at the pore scale are described, basic equations are introduced, and concepts of the different flow mechanisms are explained. Thereafter different methods for upscaling to a continuum description of flow in porous media are introduced and the basics of volume averaging are explained.

2.1 Preliminaries

Current equations describing fluid transport in porous media are based on empirical equations derived in the 19th century [Darcy, 1856] for single-phase flow and in the 20th century for multi-phase flow [Buckingham, 1907; Washburn, 1921; Richards, 1931; Buckley and Leverett, 1942]. The current standard equations used in soil physics are called the Buckingham-Darcy equation and Richards equation. These equations try to describe the "average" behavior of a mixture of a porous medium and one or more fluids. They have since then been put on a firm basis by theoretical investigations of Hubbert [1956], Anderson and Jackson [1967], Whitaker [1966, 1969], Slattery [1967, 1969], and Gray and Hassanizadeh [1991]. In order to find a solution, constitutive relations are needed between water content and pressure head, and relative hydraulic conductivity and water content. At very low water contents, often unrealistic solutions

are obtained due to the form of the constitutive relations used [Fuentes et al., 1992]. Due to the nonlinear character of Richard's equation only a limited number of analytical solutions are known. Usually one resorts to numerical solution techniques, which normally involve discretisation and integration.

At the end of the last millennium Gray and Hassanizadeh [1991], and Hassanizadeh and Gray [1997, 1993] proposed more general, theoretically obtained equations to describe multi-phase flow in porous media. These equations were derived by volume averaging and thermodynamics. Volume averaging has been used in the last decennia, mostly for single-phase flow in porous media, although examples of multi-phase flow are described in Bear and Bensabat [1989] and Hassanizadeh and Gray [1997].

The description of the behavior of fluids in porous media having high permeability is based on knowledge gained in studying these fluids in pure form. Flow and transport phenomena are described analogous to the movement of pure fluids without the presence of a porous medium. The presence of a permeable solid influences these phenomena significantly. The individual description of the movement of the fluid phases and their interaction with the solid phase is modeled by an upscaled porous media flow equation. The concept of upscaling from small to large scale is widely used in physics. Statistical physics translates the description of individual molecules into a continuum description of different phases, which in turn is translated by volume averaging into a continuum porous medium description. The common procedure is to obtain the governing equations at the macroscopic scale. This change, from the microscopic to macroscopic scale is accomplished through the application of appropriate averaging procedure for various types of flows. If we consider only Eulerian averaging techniques, several averaging procedures can be found in the literature: volume averaging, time averaging, both time and volume averaging and statistical averaging [e.g. Ishii, 1975; Drew and Prassman, 1999]. In the theoretical analysis of flows in porous media, the volume averaging over some representative elementary volume (REV) [Bear, 1972], is the most common way to obtain macroscopic governing equations. This volume represents mathematical point at the macroscopic scale, at which the quantities of all available phases in the system are defined. Through this change of the scale, hydraulic variables and parameters become continuous variables of time and space. In fact, obtained fictive, continuum represents the overlapping continuum for every available phase. Fortunately, the engineering practice is most often concerned with gross (macroscopic) properties, without the need to know the exact locations of the particular phase in the system. In

addition, the measurement of specific properties is only possible as some kind of average (e.g. time, mass or volume average) of microscopic quantities. Volume averaging procedure is well established in the literature. Since understanding of origins of several terms in macroscopic balance equations is of great importance in terms of their numerical modeling, a brief explanation of averaging procedure is given in this chapter. These terms are a consequence of scale change from microscopic to macroscopic, as it will be shown in the following sections.

2.2 Flow Regions and governing equations

A porous medium is defined as a volume, consisting of a solid permeated by pores filled with a fluid, being liquid or gas. The solid is referred to as "the solid matrix", whereas the space filled with fluid is "the void space". The picture in Fig. 2.1 shows the solid matrices of glass beads (diameters: 12mm, 5mm and 1mm) taken separately in the experiments for this research. The complexity of the matrix makes it an almost impossible task to describe the geometry in an exact manner. However, it does, combined with the fact that the pores are in the micrometer scale, make it possible and advantageous to describe the porous medium as a continuum, where the hydraulic resistance in each pore is averaged to a hydraulic resistance of the medium. This resistance is dependent on both fluid properties and on the properties of the solid matrix of the medium.

Figure 2.1: Solid matrix of spherical glass beads

The hydraulic conductivity of a porous medium is denoted by the intrinsic permeability k [m^2], and it is typically used to provide an indication of the capacity of a porous medium for allowing fluid to penetrate; a high permeability means a high through put. One of the macroscopic properties which rely to the permeability in a porous medium is the porosity ϕ. It is defined as the ratio of the volume of the void space in the medium,

$$\phi = \frac{V_{void}}{V_{total}} \qquad\qquad (2.1)$$

Since the nineteenth century, Darcy's law has traditionally been used to obtain quantitative information on flow in porous medium. This law is reliable when the representative Reynolds number is low whereas the viscous and pressure forces are dominant. As the Reynolds number increases, deviation from Darcy's law grows due to the contribution of inertial terms to the momentum balance [Bear, 1972; Kaviany, 1991]. It has been shown that for all investigated media, the axial pressure drop is represented by the sum of two terms, one being linear in the velocity (viscous contribution) and the other being quadratic in velocity (inertial contributions). The inertial contribution is known as Forchheimer's modification of the Darcy's law [Reynolds, 1900]. Basically, the pressure drop occurring in a porous medium is composed of two terms. Later Beavers and Sparrow [1969] proposed a similar model for fibrous porous media.
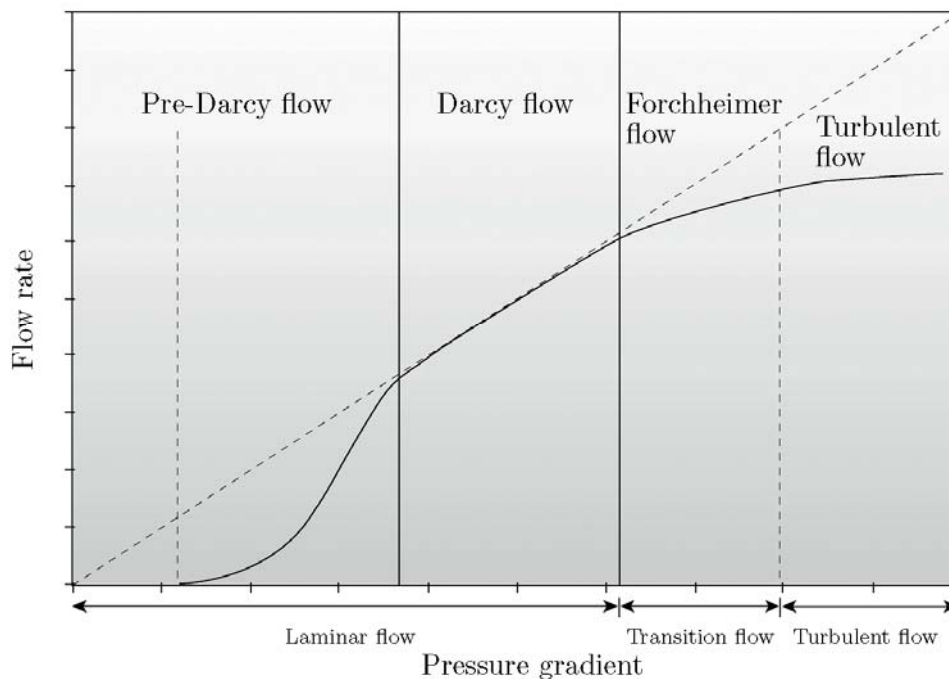
Figure 2.2 Graph of relationship between the regions of the flow. Pre-Darcy flow and regular Darcy flow occurs in the laminar region, the transition between laminar and turbulent flow is called the Forchheimer flow, and finally the fully turbulent region, where viscous forces are neglected.

While applying the continuum approach to the porous matrix, the flow in porous media can be divided into four regions on phenomenological ground: pre-Darcy flow, Darcy flow, Forchheimer flow and turbulent flow. Darcy flow means that it is governed by the linear Darcy's law. The transitions between these regions are smooth, which means that it is difficult

to determine the flow in the transition zones. Fig. 2.2 shows the general relationship between each region. Usually, Reynolds number is taken as a criterion for the demarcation of the flow regimes between laminar and turbulent. There is a smooth transition of flow from laminar to fully developed turbulent flow. In this study we have considered the pore Reynolds number Re_p, as the demarcation parameter, based on the mean diameter D of porous media and volume averaged interstitial velocity u_i i.e. $Re_p = u_i D / \nu$; where ν is the kinematic viscosity of the fluid. The demarcation is considered [Hlushkou and Tallarek, 2006] as below,

        (i) $Re_p \leq 1$:   creeping or Darcian laminar regime

        (ii) $1\sim10 < Re_p < 500$:   nonlinear laminar regime

        (iii) $Re_p \geq 500$:   turbulent regime

According to the second criteria above, the Darcy law can still be applicable upto $Re_p = 10$ without introducing significant error. These values represent a range of pore Reynolds number because a sharp demarcation of the different flow regimes in the porous media is impossible due to the gradual transition between them. As there is a general agreement on the existence of the four flow regions, the values are subject to disagreement in the porous media flow community [Fand et al., 1987].

Pre-Darcy flow is governed by molecular effects, and is thus dependent on the individual flow parameters. There does not exist a generally accepted theory for describing this flow region. Darcy flow, on the other hand, can be described by Eq. (2.2), which is an expression of conservation of momentum. It describes a linearity between flow rate and applied pressure and is similar to Ohm's law in electricity, and Fourier's law in heat conduction. Darcy's law is developed experimentally by Darcy in 1856, by using a sand filter; however, Darcy's law can also be derived from a spatial average of Stoke's equation [Whitakar, 1986] to

$$-\nabla p = \frac{\mu}{k} V_D \qquad (2.2)$$

where V_D is the macroscopic velocity defined as $V_D = Q/A$, and k the permeability (m^2). When inertial effect starts to influence the flow, Darcy's law is no longer applicable. This is due to the initiation of turbulence in the flow, as described in section 2.1. When turbulence occur, eddies will be generated, which gets energy from the main flow. Eq. (2.3) is Forchheimer's equation, and is an extension of Darcy's law, to describe the flow in this region. The energy extracted by the turbulence is converted to kinetic energy of the eddies, therefore an extra term is added to Darcy's law in the flow as given by:

$$-\nabla p = \frac{\mu}{k} V_D + \beta \rho V_D^2 \qquad (2.3)$$

where β is known as inertial coefficient.

A further extension was the addition of a second viscous term $\mu_e \nabla^2 V_D$ credited to Brinkman μ_e is called the effective viscosity; though it is usually different from μ ,both quantities are assumed to be equal following the common practice in absence of reliable experimental data. The Brinkman equation is:

$$-\nabla p = \frac{\mu}{k} V_{\mathrm{D}} + \beta \rho V_{\mathrm{D}}^2 + \mu_e \nabla^2 V_{\mathrm{D}} \tag{2.4}$$

2.3 Flow at the pore Scale

Recent applications of Lattice-Boltzmann methods provide pore-scale information and give promising results [Martys & Hagedorn, 2002; Manz & Gladden, 1999]. The major difficulties in those approaches are how to model flows in heterogeneous materials and how to properly handle the interfacial boundary conditions between fluid and solid matrix at the pore scale [Bauer, 1993; Thompson & Fogler, 1997; Thompson, 2002].

Flow at the pore scale is governed by the specific geometry of the solid phase, which determines the boundary with the fluid phases. This boundary exerts a resistance due to viscous drag on a moving fluid. If multiple fluid phases are present, their interaction gives rise to a phenomenon called capillarity. Capillarity is a manifestation of the interaction between the fluids and the solid, and the cohesion in the fluids, called surface tension. This overview mainly deals with unsteady flow at the pore scale, which can be neglected at the continuum scale.

2.3.1 Steady pore flow

For the steady and laminar flow of fluid in the porous media Darcy law has been extensibly used since 1856. It is valid for low fluid velocity only. Based on the experiments Forchheimer [1901] indicated that Darcy law breaks down when flow velocity becomes sufficiently large and proposed a relation expressed by Eq. (2.3). For the flow in porous media with high permeability, Brinkman [1947] suggested that the viscous shear stresses acting on the pore flow should be added into the momentum equation given by Eq. (2.4).

2.3.2 Unsteady pore flow

In single-phase flow, one fluid phase is present in the voids of the porous medium. When the fluid starts moving, friction develops at the fluid solid interface and inside the fluid. For an incompressible Newtonian fluid with no other body forces than gravity, motion is described by the momentum balance equations (Navier-Stokes equations):

$$\rho\left[\frac{\partial \mathbf{v}}{dt} + \nabla\bullet(\mathbf{vv})\right] = -\nabla p + \mu\nabla^2\mathbf{v} + \rho\mathbf{g} \tag{2.5}$$

with ρ the density, $\mathbf{v}$ the velocity vector, t time, p the pressure, μ the dynamic viscosity, and $\mathbf{g}$ the gravitational acceleration. Together with the mass balance equation:

$$\nabla\bullet(\rho\mathbf{v}) = 0 \tag{2.6}$$

which for incompressible flow becomes:

$$\nabla\bullet\mathbf{v} = 0 \tag{2.7}$$

a consistent set of equations with variables p and $\mathbf{v}$ is obtained. This system of equations describes the temporal and spatial evolution of the fluid movement. It is still under-determined without initial and boundary conditions. Initial conditions are the starting configuration of the fluid at $t = t_0$, and the boundary conditions describe the space-time boundaries of the flow domain. The interaction between the different fluids and the solid surface at the pore scale determines the fluid distribution and behavior [Buckingham, 1907]. If the cohesive forces in the fluids are larger than the adhesive forces between the fluids, they form a sharp interface and are immiscible [Dracos, 1991]. An example are water and air (possibly including water vapor), or oil and water. Miscible fluids, for example, are alcohol and water. The concept of miscibility depends on the thermodynamic state of the fluids. At the pore, scale surface forces usually play a much more important role than gravity. If the porous media is of high permeability such effects, e.g. of surface tension, can be neglected.

2.4 Continuum approach and space averaging

Fluid transport is usually modeled using the continuum approach in terms of appropriate averaged parameters in which the real pore structure and the associated length scales are neglected. In order to formulate mathematical model of free surface flow in porous media, it is necessary to address several concepts, which will enable us to apply differential apparatus in describing the flow of fluid-porous system. One of the most important concepts is Continuum approach in dealing with such multiphase (solid, air, water, etc.) system. According to this concept, the system with several phases is replaced by fictive continuum, in which for every point it is possible to assign any property, of any phase in the system. A multiphase system is composed of inter-penetrating phases, with each phase occupying only part of the whole system. Phases are divided by the highly irregular interface surface boundaries, which may have some

thermo-mechanical properties, such as surface tension. Through the interface, there is exchange of extensive quantities (e.g. mass, momentum, energy). Each phase is characterized by its thermodynamic quantities, which are continuous for that phase, but discontinuous over the whole system. Locally, the standard balance laws can be applied for each of the phases. Those equations, supported by the appropriate boundary conditions and with conditions at the interface surfaces may provide, in principle, the state of the system. Since the solution of those equations at this, microscopic scale is a formidable task.

Volume averaging procedure is presented by several researchers [Slattery, 1969; Whitaker, 1969; Neuman, 1977; etc.]. However, probably the most general approach is reported by Hassanizadeh and Gray [1979a; 1979b; 1980]. The derivation presented here, mainly follows the study reported by Hassanizadeh and Gray [1979a], which is here slightly adapted for the types of flows which will be numerically treated in this thesis. For now, the main concern is mechanical phenomena and therefore, only derivations of the macroscopic mass and momentum balance equations will be presented, under isothermal conditions
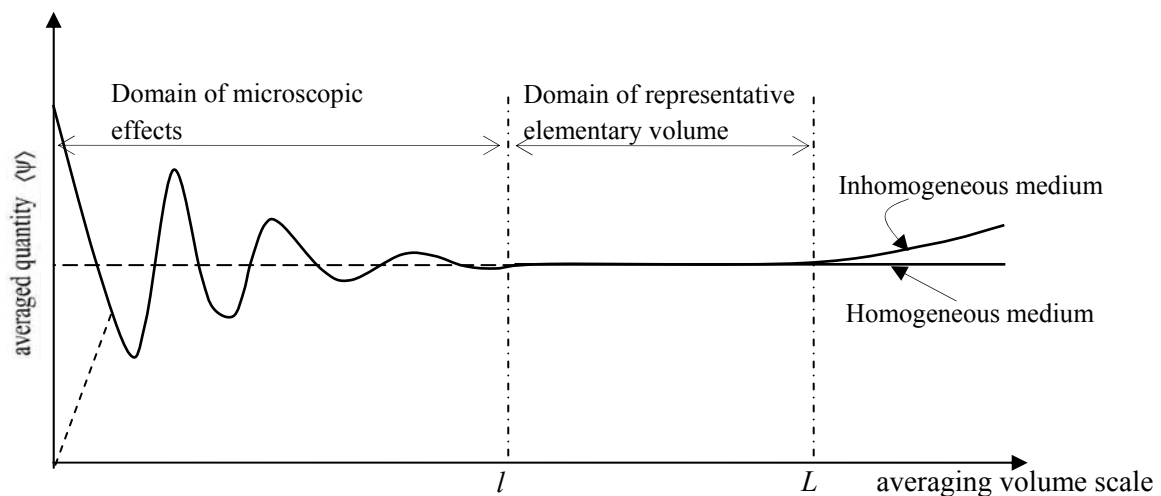
Figure 2.3 Dependence of averaged quantity on the averaging scale after Bear[1972]

In order to obtain the macroscopic equations, Eqs. (2.5) and (2.6) are averaged over the small volume dV which is bounded by the surface dA. This volume, contains all fluids of interest and in order that obtained averaged quantities do not depend on the size of this volume, it is necessary that the scale of volume dV satisfies certain conditions. If we denote this scale by D, condition can be expressed as [Whitaker, 1969]

$$l \ll D \ll L \tag{2.8}$$

where l is the characteristic microscale length and L is the scale of the gross inhomogeneities

which may cause the change of the averaging quantities. This can be seen in Fig. 2.3; if the averaging volume is too small, of the scale *l*, the local condition affects the averaging quantity (for example, if the averaging volume contains only one fluid, the averaged quantities of the other fluids are all zero). If the condition (2.8) can not be fulfilled from some reason, the averaging procedure can not obtain valid macroscopic equations.

Fig. 2.4 shows the volume dV which is characterized by its center vector **x** in some reference coordinate system. Any point in the averaging volume can be referenced with a position vector **r** in the same reference, or by the vector ξ in the local coordinates parallel to reference coordinates. The center represents the macroscopic point for which the averaged quantities are defined. The local volume-averaging method is a more practical approach than the analytical counterpart. The local averaging performs the averaging of the microscopic equations over a representative elementary volume
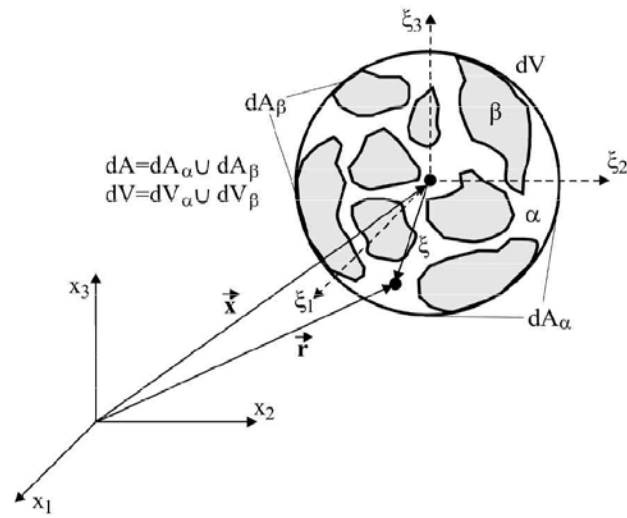
Figure 2.4 REV containing two phases α and β.

(REV) as shown in the figure. Note here, the REV is the smallest volume possessing local averaged quantities that are statically meaningful. Its definition and the relevant mathematical operations for partial differential equation (e.g. N-S equations) may be found in Slattery [1967] and Kaviany [1991].

The macroscopic conservations for convective flow in a porous medium can be obtained by a volume averaging of the microscopic conservation equations over a representative volume. In this section, a brief discussion of the volume averaging process will be presented.

Consider a representative volume *dV* in a porous medium consisting of an α-phase and a β-phase. If W_α is a quantity associated with the α-phase, an intrinsic phase average of W_α is defined as

$$\overline{W_\alpha} = \frac{1}{dV_\alpha} \int\limits_{dV_\alpha} W_\alpha dv \qquad (2.9)$$

where the volumetric integration is to be carried out over $dv = dx'\, dy'\, dz'$ with (x', y', z') denoting the microscopic coordinates. In Eq. (2.9) dV_α is the volume occupied by the α-phase in dV, and $dV_\alpha + dV_\beta = dV$, with dV_β being the volume occupied by the β-phase in dV.

To derive the macroscopic equations from the microscopic equations, the following averaging theorems similar to those obtained by Whitaker [1967] and Slattery [1967] relating the volume average of a spatial derivative to the spatial derivative of the volume average are needed :

$$\frac{1}{dV}\int_{dV_\alpha} \nabla W_\alpha dv = \overline{\nabla}\left[\frac{1}{dV}\int_{dV_\alpha} W_\alpha dv\right] + \frac{1}{dV}\int_{dA_{\alpha\beta}} W_\alpha da \tag{2.10a}$$

$$\frac{1}{dV}\int_{dV_\alpha} \nabla\bullet\mathbf{W}_\alpha dv = \overline{\nabla}\bullet\left[\frac{1}{dV}\int_{dV_\alpha} \mathbf{W}_\alpha dv\right] + \frac{1}{dV}\int_{A_{\alpha\beta}} \mathbf{W}_\alpha\bullet da \tag{2.10b}$$

where $A_{\alpha\beta}$ is the interface between the α- and β-phase in dV, $d\mathbf{a}$ is a surface vector, and W_α and $\mathbf{W}_\alpha$, are a scalar and a vector, respectively. In Eq. (2.10), we define the gradient operators in the microscopic (x', y', z') and macroscopic coordinates (x, y, z) by ∇ and $\overline{\nabla}$ as

$$\nabla = \mathbf{i}\frac{\partial}{\partial x'} + \mathbf{j}\frac{\partial}{\partial y'}\mathbf{k}\frac{\partial}{\partial z'} \tag{2.11}$$

$$\overline{\nabla} = \mathbf{i}\frac{\partial}{\partial x} + \mathbf{j}\frac{\partial}{\partial y}\mathbf{k}\frac{\partial}{\partial z} \tag{2.12}$$

Eq. (2.10) can easily be obtained by applying the gradient and divergence theorems to a representative elementary control volume dV.

2.4.1   Averaging of the mass balance equation

The microscopic continuity equation for an incompressible flow is given by

$$\nabla\bullet\mathbf{v}_f = 0 \tag{2.13}$$

where $\mathbf{v}_f$ is the microscopic velocity vector. Integrating Eq. (2.13) with respect to a representative volume in a porous medium, dividing the resulting expression by dV and with the aid of Eq. (2.10b) yields

$$\overline{\nabla}\bullet\{(1-C)\overline{\mathbf{v}}_f\} = 0 \tag{2.14}$$

where C is the volumetric concentration of the solids and $(1-C)$ represents the porosity while $\overline{\mathbf{v}}_f$ is the volumetric average (macroscopic) velocity vector. Eq. (2.14) can be rewritten as

$$\overline{\nabla}\cdot\mathbf{V}_D = 0 \tag{2.15}$$

where $\mathbf{V}_D = (1-C)\overline{\mathbf{v}}_f$ is the Darcy velocity vector.

2.4.2   Averaging of the momentum balance equation

The microscopic momentum equation for an incompressible flow in a porous medium is given by the Navier-Stokes equation

$$\rho_f\left[\frac{\partial \mathbf{v}_f}{\partial t} + \nabla\cdot(\mathbf{v}_f\mathbf{v}_f)\right] = -\nabla p_f + \mu_f\nabla^2\mathbf{v}_f + \rho_f\mathbf{g} \tag{2.16}$$

where ρ_f and μ_f are the density and viscosity of the fluid while p_f is the pressure of the fluid. Integrating the above equation with respect to a representative elementary volume and with the aid of Eq. (2.10) gives

$$\rho_f\left[\frac{\partial(1-C)\overline{\mathbf{v}}_f}{dt} + \overline{\nabla}\cdot\left((1-C)\overline{\mathbf{v}_f\mathbf{v}_f}\right)\right] = -(1-C)\overline{\nabla p_f} + \mu_f\overline{\nabla}^2(1-C)\overline{\mathbf{v}}_f + \rho_f\mathbf{g}(1-C) + \mathbf{R} \tag{2.17}$$

where $\mathbf{R}$ is the total drag force per unit volume due to the presence of solid particle and in terms of macroscopic velocity vector its value is given by

$$\mathbf{R} = -\left[\frac{\mu_f(1-C)^2\overline{\mathbf{v}}_f}{k} + \rho_f\frac{F_{ch}(1-C)^3\overline{\mathbf{v}}_f\left|\overline{\mathbf{v}}_f\right|}{\sqrt{k}}\right] \tag{2.18}$$

where F_{ch} is the Forchheimer's inertia coefficient. The detail of the derivation can be found from [Ingham, 2002]

2.5 Single phase saturated flow in porous media

Concerning analytical studies, Darcy's law ignores the effects of solid boundary or the inertial forces on fluid flow. While these effects become significant near the boundary and in highly porous materials, relatively little attention had been directed to study these effects. Notably, Brinkman [1947] proposed a model to account for the presence of solid boundary by adding a

viscous term to the Darcy's law. Muskat [1946] took inertial effect into account by adding a velocity squared term to the Darcy's law. However, both works do not consider boundary and inertia effects simultaneously. Vafai and Tien [1981] used a volume-averaged momentum and energy equations to numerically study both effects simultaneously.

Saturated flow in porous media can be considered as a special case of multiphase flow with solid and fluid phase present. Since the establishment of the Darcy's law in 1856, as a generally accepted empirical macroscopic equation of motion in porous media for small Reynolds numbers [e.g. Bear, 1972], many authors have reported theoretical studies of flow in porous media. Some of them tried to derive the Darcy's law theoretically [Hubbert, 1956; Hall, 1956; Whitaker, 1966; Neuman, 1977] by averaging Navier- Stokes equations over a representative volume of porous media. Ahmed and Sunada [1969] used the same approach to derive macroscopic equation of motion for flows with greater Reynolds numbers, where linear dependency of hydraulic gradient and flux is not valid any more. Probably the most significant step toward theoretical analysis of flow in porous media was derivation of the theorem which relates volume averages of space derivatives and space derivatives of volume averages [Slattery, 1967; Whitaker, 1969]. Some other authors presented an alternative approach by treating the flow in porous media as a stochastic process [Scheidegger, 1954; Bachmat, 1965], or by simplifying the structure of the pores to give a conceptual model [Bear, 1972]. In this case. the porous media is represented as a system of capillary tubes in some arrangement, with Hagen-Poisseuille's law as a starting governing equation. Originally, the Darcy's law was established as an empirical correlation between the hydraulic gradient and volumetric flux for one-dimensional flow of a single fluid through the porous column.

As velocity increases, the inertial effects increase, and in turn, deviations from Darcy law become more significant. In the early investigations, this deviation was prescribed to the turbulence by analogy with flow in pipes, where after reaching specific Reynolds numbers; the hydraulic gradient has quadratic dependency in terms of velocity. However, experimental investigations revealed that deviation from Darcy law occurs significantly earlier in comparison with onset of turbulence [e.g. Bear 1972]. Therefore, this deviation is prescribed to the inertial effects, as a consequence of curvature of fluid velocity streamlines on the microscopic level. It can be shown that obtained volume-averaged equation for momentum balance Eq. (2.17) can be reduced to Darcy's law.

2.6 Free surface flow through porous media.

In many flow problems, at least one of the domain boundaries represents a free fluid surface. After obtaining a velocity and pressure field by using an appropriate solver (such as HSMAC method), the position of free surface has to be updated. In the original marker and cell (MAC) method massless markers are used, for which the velocity vectors are interpolated from the cell boundaries, and used for calculation of their new position [Harlow and Welch, 1965]. A mesh cell containing markers, but having a neighboring cell with no markers, is defined as containing a free surface. It is obvious that this approach suffers from large amount of additional memory required to keep a track of each marker and additional computational time required to calculate a new position for the each marker. Hirt and Nichols [1981] proposed a volume of fluid (VOF) method for free surface tracking. This was not the first proposed method for volume tracking [Kothe et al., 1996], however, it is probably the most often used. In the method, a volume fraction occupied by the fluid is introduced as a new property and this volume fraction function is advected at each time step. Exact geometry of the free surface inside the cell is not known; it is reconstructed under conservation condition that free surface truncates the cell by the volume equal to the volume of fluid property. The method has been later significantly improved [e.g. Youngs, 1982; Kothe et al., 1996; Rider and Kothe, 1998].

The free surface evolution inside the porous media is an important feature of this study. The method introduces a volume of fluid function to define the water region and its saturation within the cell. The evolution of the free surface is traced using VOF method (Hirt and Nichols, 1981) which is discussed in the subsequent section.

Evolution of Free Surface

Consider a function f which represents the fractional cell saturation defined in a continuous domain as

$$f = \begin{cases} 1 & \text{for full cell} \\ 0 & \text{for empty cell} \\ 0{\sim}1 & \text{for surface cell} \end{cases} \tag{2.19}$$

For a cell (i, j) of volume $V_{i,j}$, a volume function $f_{i,j}$, is defined as

$$f_{i,j} = \frac{1}{(1-C)V_{i,j}} \int_{v_{i,j}} f dV \tag{2.20}$$

where $d\mathcal{V} = (1-C)dxdy$. The time evolution of the free surface flow inside the porous domain is governed by the following equation.

$$\frac{\partial f}{\partial t} + \nabla \bullet (\mathbf{v}f) = 0 \tag{2.21}$$

where f represents the fractional saturation of fluid in a cell. Eq. (2.21) is the material derivative of the saturation volume of fluid within a cell [Jacimovic et al., 2005]. This equation is solved after the velocity field is calculated because the position of fluid surface cannot be known a priori. Given the volumetric nature of function f and in order to maintain a sharp interface, the discretization of Eq. (2.21) requires special treatment. In this study, the donor-acceptor concept [Hirt and Nichols, 1981] along with MUSCL type TVD [Van Leer, 1979] scheme is used for the non-oscillatory convection of the VOF function.

2.7 Summary

The free surface flow of viscous and incompressible fluid in porous media thus can be described by a set of continuity and momentum equation given by Navier-Stokes type equations extended with the resistance terms to account the resistance due to porous matrix as below,

$$\frac{\partial(1-C)}{\partial t} + \frac{\partial(1-C)u_i}{\partial x_i} = 0 \tag{2.22}$$

$$\frac{\partial(1-C)u_i}{\partial t} + \frac{\partial(1-C)u_iu_j}{\partial x_j} = (1-C)g_i - \frac{(1-C)}{\rho}\frac{\partial p}{\partial x_i} + v\frac{\partial^2(1-C)u_i}{\partial x_j\partial x_j} + \frac{R_i}{\rho} \tag{2.23}$$

where u_i is the velocity vector, also called the pore water velocity in the porous medium, C is the volumetric concentration of the solids in the porous medium, R_i the flow resistance term due to porous matrix, p the pressure and v the kinematic viscosity of the fluid. As we are dealing with highly permeable porous media, the term volumetric solid concentration C is preferred to the term porosity. The model can account the spatial variability of permeability and porosity. The above equations for the conservation of mass and momentum can be used for anisotropic porous media. According to the volume averaging procedure [Hsu and Cheng, 1990], the Darcy's flux is equal to the product of spatially averaged pore fluid velocity as used in above expressions and the porosity of the medium given by

$$V_{Di} = (1-C)u_i \tag{2.24}$$

where V_{Di} denotes the Darcy's flux vector, also called superficial velocity sometimes. The total drag resistance due to the presence of the solid particles per unit volume R_i in the momentum balance equation represents the sum of the viscous drag and form drag. The total drag resistance force per unit volume of the fluid for a wide range of flow as expressed by Ergun [1952] correlation can be written as

$$\frac{R_i}{\rho} = -\left[\frac{v(1-C)^2 u_i}{k} + \frac{F_{ch}(1-C)^3 u_i |u_i|}{\sqrt{k}} \right] \tag{2.25}$$

where k is the permeability (m^2) and F_{ch} the Forchheimer's inertia factor. For a randomly packed bed of spheres such coefficients can be expressed in terms of the solid concentration C and the mean diameter of the particles d_p in the porous medium as

$$k = \frac{(1-C)^2 d_p{}^2}{150C^2} \quad \text{and} \quad F_{ch} = \frac{1.75}{\sqrt{150}\sqrt{(1-C)^3}} \tag{2.26}$$

It should be noted that the Eqs. (2.22) and (2.23) governing the flow in porous media is very much similar to the classical continuity and Navier-Stokes equations for the open channel flow. The equations can also be used in free domain by switching suitably the values of C and k. In doing so, the terms used for the drag resistance of the solid matrix will be vanished outside the porous media which eventually results the equation for the flow in free domain.

Chapter 3

MODEL DEVELOPMENT FOR FREE-SURFACE FLOW THROUGH POROUS MEDIA

3.1 Preliminaries

In this chapter, numerical model developed for simulation of free-surface flow of water through porous media is presented and in the following chapters, the model results are compared with the results of integral models and experiments to test its validity for different type of flows. Since the flow in porous media is also considered under assumption that solid phase is stagnant and rigid, in that case the model could also be considered as two or three phase models, respectively.

The models developed in this study basically rely on the MAC (Marker and Cell) method, the first method proposed for numerical integration of Navier-Stokes equations for two-dimensional flows with free-surface boundary [Welch et al., 1965; Harlow and Welch, 1965], and later applied for simulation of three-dimensional flow domains [Hirt and Cook, 1972]. In the original MAC method, pressure field is obtained from the Poisson equation, in which the source term is function of velocity field; formulated in order to satisfy the incompressibility condition. From obtained pressure field, the velocity field at the new time step is explicitly calculated from Navier-Stokes equations. At the end of the time step, the massless particles are advected in order to trace the movement of the free surface. The Poisson equation for pressure field requires

a special care of boundary conditions in the original MAC method. This inconvenience was significantly improved in the later versions of the MAC method. For example, in SMAC (Simplified MAC) method by Amsden and Harlow [1970], or HSMAC (Highly Simplified MAC) method [Hirt and Cook, 1972], which was inspired by the work of Chorin [1968] and Viecelli [1971]. In the latter method, the solution of Poisson equation is completely avoided by introduction of an iterative procedure in which both the pressure and velocity fields are iteratively updated until the incompressibility condition is achieved. This numerical scheme is used in the thesis, and will be described in more detail in this chapter.

A porous medium is a two-phase material in which the solid matrix usually assumed to be rigid, constitutes one phase, and the interconnected voids or pores constitutes the other. One of the main characteristics of porous media is the irregular shape and size of its pores which are randomly distributed; considering the flow through this heterogeneous formation is very complex. Our interest will be to determine the flow through the porous formation, with typical length scales much larger than the characteristic pore size. The complex internal geometry of a porous medium, artificial or natural, is difficult if not impossible to determine. Furthermore, in general, in the groundwater engineering field there is a lack of interest in knowing the internal details of the structure or the microscopic flow. In fact, in most circumstances our interest will be in determining the characteristics of the flow in large portions of the porous structure under consideration, introducing an averaging process in the analysis of the flow. The averaging process has a smoothing effect, filtering out small-scale variations associated with the media heterogeneity and porous irregularities.

The numerical modeling of the free-surface flow through porous media is done in this study using continuity and momentum equations extended for use in porous media with the inclusion of distributed resistance terms.

3.2 Discretization of governing equations

The governing equations for the free-surface flow through porous media are discretized by the finite volumes, with staggered arrangement in which velocity components are defined at the cell boundaries and scalar quantities (pressure, volume fractions, permeability etc.) are defined at the cell centers (Fig. 3.1). The flow domain is divided into the grid cells by planes parallel to the coordinate axes. It is generally accepted that staggered arrangement is more accurate in

comparison with ordinary grid arrangements, and that conservation of extensive quantities (mass, momentum. etc.) is more easily accomplished. The staggered arrangement is also convenient in terms of imposing different types of boundary conditions [Ferziger, 1987]. It should be noted that control volumes, over which the specific terms in governing equations are integrated, do not necessarily need to coincide with the grid volumes, (see Fig. 3.1). For the
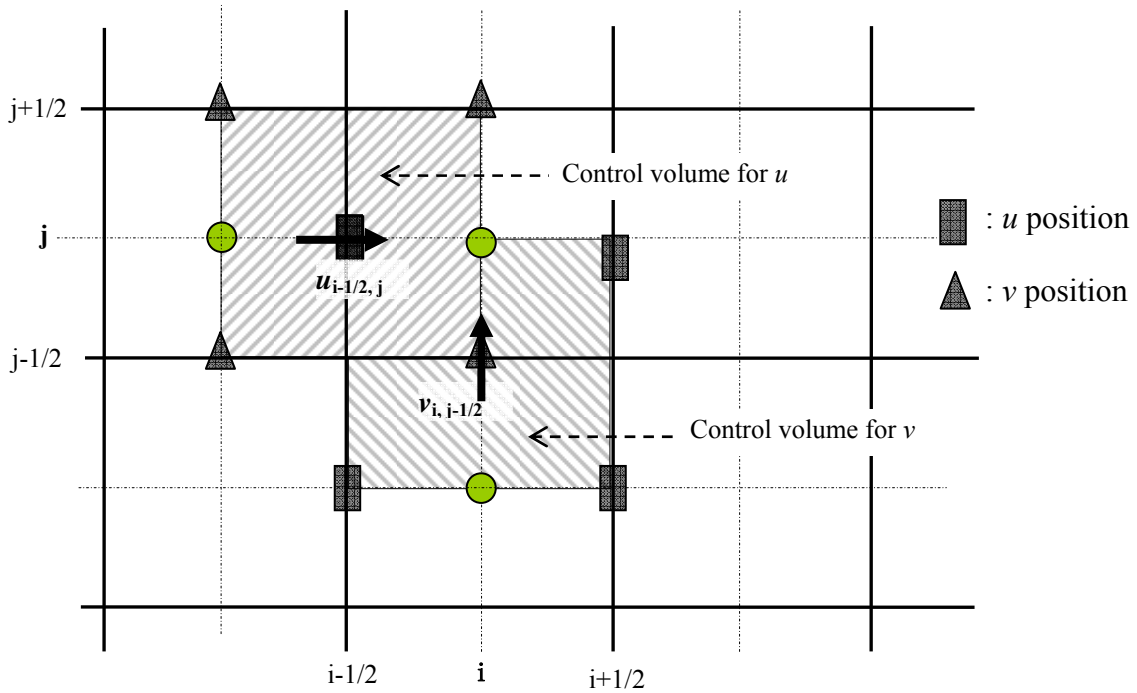
3.1(a)
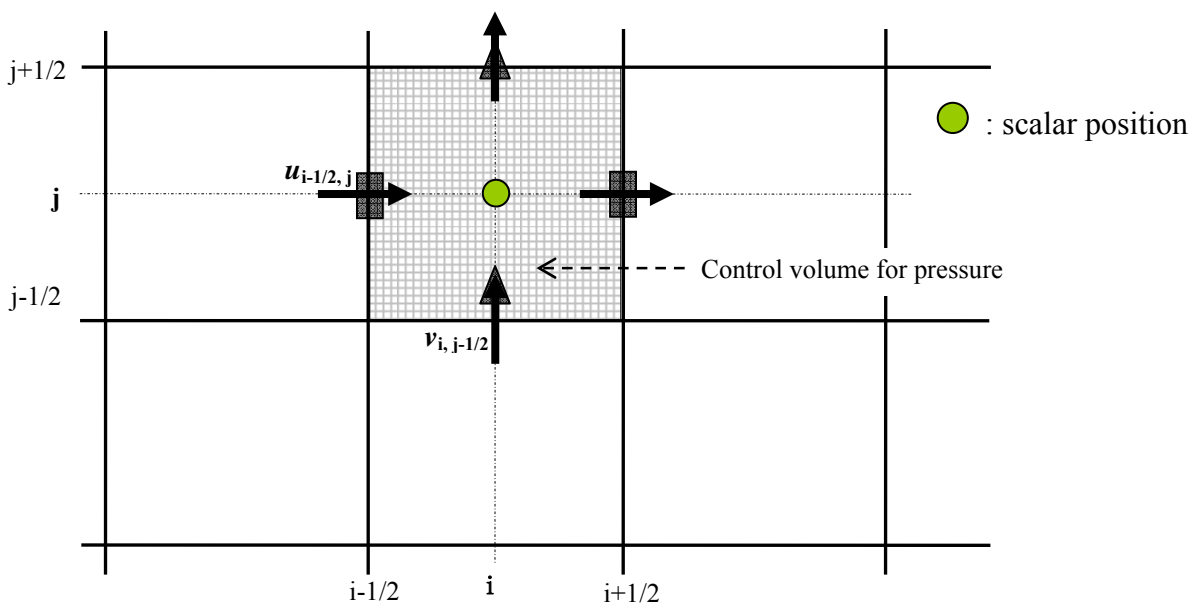
3.1(b)

Figure 3.1 Control volumes in staggered grid arrangement for (a) vectors: u, v (b) scalars: p, f, k etc.

momentum equations, control volumes are shifted for half of the cell size, so that corresponding velocity comes into the center of the control volume. The governing equations for free-surface flow of viscous and incompressible fluid in porous media given by a set of continuity and momentum equation are rewritten as:

Continuity:
$$\frac{\partial(1-C)u_i}{\partial x_i} = 0 \tag{3.1}$$

Momentum:
$$\frac{\partial(1-C)u_i}{\partial t} + \frac{\partial(1-C)u_iu_j}{\partial x_j} = (1-C)g_i - \frac{(1-C)}{\rho}\frac{\partial p}{\partial x_i} + \nu\frac{\partial^2(1-C)u_i}{\partial x_j\partial x_j} + \frac{R_i}{\rho} \tag{3.2}$$

where all the terms have their usual notations.

3.2.1 Discretization of continuity equation

The continuity equation can be discretized as follows

$$(1-C)\frac{\partial u_i}{\partial x_i} = D_{i,j} = \frac{(1-C)u_{i+1/2,j}^{n+1} - (1-C)u_{i-1/2,j}^{n+1}}{\Delta x} + \frac{(1-C)v_{i,j+1/2}^{n+1} - (1-C)v_{i,j-1/2}^{n+1}}{\Delta y} = 0 \tag{3.3}$$

where superscripts n and n+1 denote current and next time step, respectively, and halfway subscripts represent the corresponding cell face position.

3.2.2 Discretization of momentum equations

For a given time step *n*, a predicted velocity field for the next time step is found from the momentum equation with the explicit values:

$$(1-C)u_i^{n+1} = (1-C)u_i^n + \Delta t(CONV^n + DIFF^n) + \Delta t(1-C)g_i - \Delta t(1-C)\frac{\partial p^{n+1}}{\partial x_i} + \Delta t\frac{R_i^n}{\rho} \tag{3.4}$$

where *CONV* and *DIFF* are respectively the convective and diffusive terms in the momentum equation; and Δt is the time interval. The predicted velocity field does not fully satisfy the continuity equation, and the deviation *D* is found as the divergence of the predicted velocity field using Eq. (3.1)

The difference between the correct velocity field and the predicted velocity field is due to the effect of the change of the pressure Δp at the new time step, the corrected velocities are then found iteratively using HSMAC method which is described in the next section. It is known that most of errors are due to inaccurate approximations of convective terms in the momentum equation. To get an approximation with high accuracy for the predicted velocity, the step for the predicted velocity using Eq. (3.4), it is split into two phases, namely advection and

non-advection. The convective terms in the momentum equations are included in the advection phase, in which the CIP (Constrained Interpolation Profile) method proposed by Yabe and Aoki [1991a, 1991b] is used as a solver which will be explained in section 3.4.

3.3 HSMAC method

The original HSMAC method for numerical solution of Navier-Stokes equations is slightly adapted to suit the CIP method and an additional resistance term due to the porous media, in momentum Eq. (3.4). Here, the method will be presented for the flow through porous media having free surface. Extension to the multi-phase flow in porous media and to three dimensional domain is straightforward. The method includes an iterative procedure which consists of two steps. In the first step predicted values of fluid fluxes are calculated from the discretized form of momentum Eq. (3.4). After obtaining predicted fluxes, the divergence for each discretization cell is computed by Eq. (3.3). In the second step, the pressure is corrected iteratively using

$$\delta p_{i,j} = -\frac{\omega D_{i,j}}{2\Delta t\left[\dfrac{1}{\Delta x^2} + \dfrac{1}{\Delta y^2}\right]} \qquad (3.5)$$

where ω is relaxation coefficient, Δx and Δy are the uniform size of the cell in x and y direction respectively. In this study the value of ω is taken as 1.0. The iteration for pressure correction and subsequent velocity prediction is repeated until the continuity is satisfied, i.e. some prescribed criteria for the divergence-free field. A flow chart of the iterative procedure is shown in Fig. 3.2. While choosing the value of Δt, the CFL criteria has to be satisfied i.e. the fluid is not allowed to move through more than one cell length because the differential equations assume fluxes only between adjacent cells. Therefore the time increment must satisfy the inequality

$$\Delta t < \min\left\{\frac{\partial x_i}{u_{i,j}}, \frac{\partial y_j}{u_{i,j}}\right\} \qquad (3.6)$$

Also from the diffusion criteria the time step should satisfy

$$\Delta t < \frac{1}{2\mu}\left\{\frac{\Delta x_i^2 \partial y_j^2}{\Delta x_i^2 + \Delta y_j^2}\right\} \qquad (3.7)$$

to ensure that momentum does not diffuse more than approximately one cell in one time step. For the slow flows like we are dealing with, this viscous criterion for the stability is very important and an adaptive time step is implemented for stability in some cases.
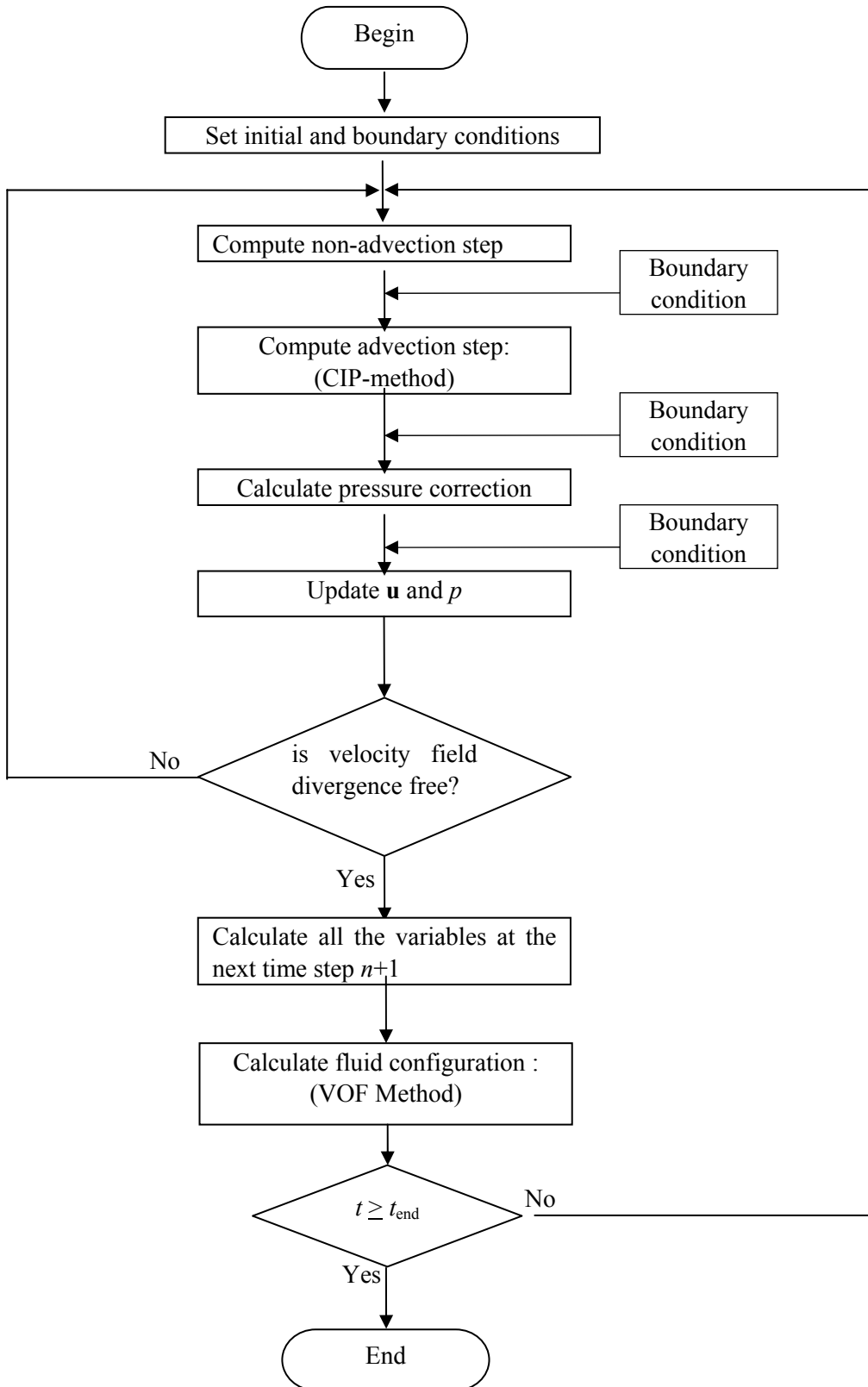
Figure 3.2 Flow chart of numerical solution by CIP-HSMAC method

3.4 CIP method

In this section we present the detail of the solution algorithm in vertical 2D simulation for the flow in channel filled with porous media. The governing Eqs. (3.1) and (3.2) are solved numerically on a uniform staggered Cartesian grid by finite volume method. The constrained interpolated propagation (CIP) method [Yabe and Aoki, 1991a, 1991b] is adopted as the base scheme for the numerical solution. The basic idea of the CIP method is that for advection computation of any flow variable, not only the transportation equation but also the transportation equation of its spatial gradients are solved. For the ease in compactness, the equations are written here in vector notation. Referring to the momentum equation (3.2), its spatial derivatives can be written as

$$(1-C)\frac{\partial \mathbf{u}_x}{\partial t} + \left((1-C)\mathbf{u}\cdot\nabla\right)\mathbf{u}_x = -\left((1-C)\mathbf{u}_x\cdot\nabla\right)\mathbf{u} - (1-C)\nabla p_x + \frac{1}{\mathrm{Re}}(1-C)\nabla^2\mathbf{u}_x + \mathbf{R}_x \qquad (3.8)$$

$$(1-C)\frac{\partial \mathbf{u}_y}{\partial t} + \left((1-C)\mathbf{u}\cdot\nabla\right)\mathbf{u}_y = -\left((1-C)\mathbf{u}_y\cdot\nabla\right)\mathbf{u} - (1-C)\nabla p_y + \frac{1}{\mathrm{Re}}(1-C)\nabla^2\mathbf{u}_y + \mathbf{R}_y \qquad (3.9)$$

where density of the fluid is absorbed in the pressure term itself and Re is the reciprocal of the kinematic viscosity of fluid. The subscripts *x* and *y* denote the spatial derivatives with respect to x and y directions respectively. The governing equations are split into two steps: non-advection and advection phase. The non-advection phase is solved by usual finite difference scheme whereas the advection phase is solved by the CIP method.

To use CIP method, we consider transient conditions in Eqs. (3.1) and (3.2). Then to reach a steady state, we need to continue the calculation until the solution is at steady state, that is, the velocities, pressure and the spatial derivatives of the velocities no longer change with time. Thus applying the fractional time step approach, the numerical solution of the governing equations can be divided into the following two steps

3.4.1 Non advection step

The governing equations for the non-advection phase are

$$(1-C)\frac{\hat{\mathbf{u}}-\mathbf{u}^n}{\Delta t} = -(1-C)\nabla p + \frac{1}{\mathrm{Re}}(1-C)\nabla^2\mathbf{u}^n + \mathbf{g}(1-C) + \mathbf{R}^n \,,$$

$$(1-C)\frac{\hat{\mathbf{u}}_x - \mathbf{u}_x^n}{\Delta t} = -((1-C)\mathbf{u}_x^n \cdot \nabla)\mathbf{u}^n - (1-C)\nabla p_x + \frac{1}{\text{Re}}(1-C)\nabla^2 \mathbf{u}_x^n + \mathbf{R}_x$$

and $$(1-C)\frac{\hat{\mathbf{u}}_y - \mathbf{u}_y^n}{\Delta t} = -((1-C)\mathbf{u}_y^n \cdot \nabla)\mathbf{u}^n - (1-C)\nabla p_y + \frac{1}{\text{Re}}(1-C)\nabla^2 \mathbf{u}_y^n + \mathbf{R}_y \qquad (3.10)$$

In order to avoid considering the pressure derivatives p_x and p_y as nodal variables and updating them for each time step in the second and third equations in Eq. (3.10), the right hand side terms are replaced by the velocity terms from the first equation. Then, the second and third equations can be written as

$$(1-C)\frac{\hat{\mathbf{u}}_x - \mathbf{u}_x^n}{\Delta t} = -((1-C)\mathbf{u}_x^n \cdot \nabla)\mathbf{u}^n + (1-C)\frac{\partial}{\partial x}\left(\frac{\hat{\mathbf{u}}_x - \mathbf{u}_x^n}{\Delta t}\right)$$

and $$(1-C)\frac{\hat{\mathbf{u}}_y - \mathbf{u}_y^n}{\Delta t} = -((1-C)\mathbf{u}_y^n \cdot \nabla)\mathbf{u}^n + (1-C)\frac{\partial}{\partial y}\left(\frac{\hat{\mathbf{u}}_y - \mathbf{u}_y^n}{\Delta t}\right) \qquad (3.11)$$

3.4.2 Advection step

The equations to be solved in a typical time step in this phase are written as

$$(1-C)\frac{\mathbf{u}^{n+1} - \hat{\mathbf{u}}}{\Delta t} + ((1-C)\hat{\mathbf{u}} \cdot \nabla)\hat{\mathbf{u}} = 0 ,$$

$$(1-C)\frac{\mathbf{u}_x^{n+1} - \hat{\mathbf{u}}_x}{\Delta t} + ((1-C)\hat{\mathbf{u}} \cdot \nabla)\hat{\mathbf{u}}_x = 0$$

and $$(1-C)\frac{\mathbf{u}_y^{n+1} - \hat{\mathbf{u}}_y}{\Delta t} + ((1-C)\hat{\mathbf{u}} \cdot \nabla)\hat{\mathbf{u}}_y = 0 \qquad (3.12)$$

where n denotes the beginning of the step, and $\hat{\mathbf{u}}$, $\hat{\mathbf{u}}_x$ and $\hat{\mathbf{u}}_y$ denote the velocity vector and its spatial derivatives at the end of the non-advection phase. The last two equations in Eq. (3.12) are the equations for updating the spatial derivatives of velocity.

First of all, the velocity after non-advection phase $\hat{\mathbf{u}}$ is calculated using usual finite difference technique from the first equation in Eq. (3.10) and so for the spatial derivatives using Eq. (3.11). Then new time step velocity $\mathbf{u}^{n+1}$ is obtained by applying a cubic interpolation polynomial to solve Eq. (3.12). In this phase, velocity and its spatial derivatives obtained after non-advection phase are used. Also spatial derivatives are updated for use in the next time step. Iteration is

made until the divergence of the velocity field, $\nabla \cdot (1\text{-}C)\mathbf{u}^{n+1}$, is diminished to some prescribed value so as to satisfy the continuity Eq. (3.1). Then we get the updated pressure. An iterative procedure similar to HSMAC type iteration algorithm [Jacimovic et al., 2005] is implemented to update the velocity vector and the pressure. Thus the calculations for one time step are now complete. For the next time step, we take the values $\mathbf{u}^{n+1}$, p^{n+1}, $\mathbf{u}_x^{n+1}$ and $\mathbf{u}_y^{n+1}$ to the next time step non-advection phase and repeat the calculations.

3.5 Free Surface Evolution

In the original MAC method a massless markers are used, for which the velocity vectors are interpolated from the cell boundaries, and used for calculation of their new position. A mesh cell containing markers, but having a neighboring cell with no markers, is defined as containing a free surface. It is obvious that this approach suffers from large amount of additional memory required to keep a track of each marker and additional computational time required to calculate a new position for the each marker. Hirt and Nichols [1981] proposed a Volume of Fluid (VOF) method for free surface tracking. This was not the first proposed method for volume tracking [Kothe et al., 1996], however, it is probably the most often used. In the method, a volume fraction occupied by the fluid is introduced as a new property which is advected at each time step. Exact geometry of the free surface inside the cell is not known; it is reconstructed under conservation condition that free surface truncates the cell by the volume equal to the volume of fluid property. The method has been later significantly improved [e.g. Youngs, 1982; Kothe et al., 1996; Rider and Kothe, 1998]. The main accuracy improvement comes from the linear reconstruction of the surface inside the cell, instead of the original constant approximation. Nevertheless, the original method has been widely used with satisfactorily results in many flow problems and therefore will be used in this study. An exquisite historical review of volume tracking methods is given by Rider and Kothe [1998].

In the vertical two-dimension, the free surface is approximated as shown in Fig. 3.3 The line that represents interface is either parallel to horizontal or vertical direction. In the calculation of the fluid volume function f, the flux at the cell face is calculated depending upon the direction of advection velocity and the orientation of the surface as well. The method ensures that fluid cannot exit the cell until it is full.

In order to describe the free water surface, the VOF method introduces a volume of fluid
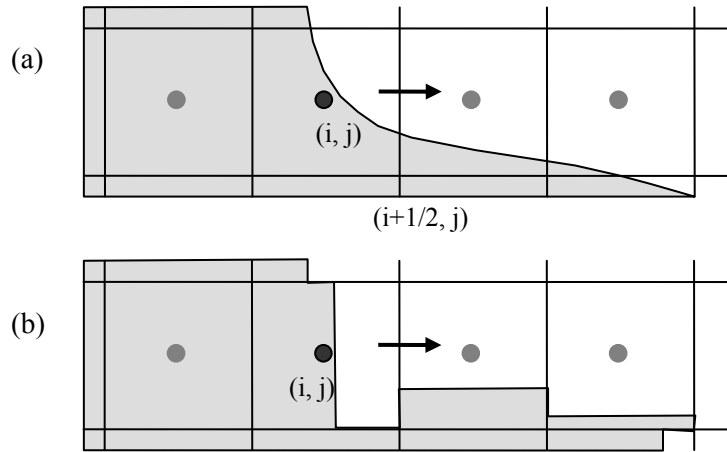
Figure 3.3 Free-surface configuration (a) actual free surface (b) VOF approximation

function $F(x, y, t)$ to define the fluid region. The physical meaning of the F function is the fractional volume of the cell occupied by the fluid. A unit value of F corresponds to a cell full of fluid, while a zero value indicates that the cell contains no fluid. Cells with F values between zero and one must then contain a free surface. The time dependence of F is governed by the equation.

$$\frac{\partial(1-C)F}{\partial t} + \frac{\partial(1-C)u_i F}{\partial x_i} = 0 \tag{3.13}$$

where $(1-C)F$ represents portion of cell occupied by the fluid (cell saturation). It should be noted that Eq. (3.13) is the material derivative of fluid function i.e. the volume of fluid function follows the fluid region. But due to the round off errors in the numerical schemes, the spurious diffusion of VOF function can be observed at the sharp interfaces. To prevent the spurious oscillation and generate diffusion-free sharp interface, a third order MUSCL-type total variation diminishing (TVD) schemes is used to discretize the convective terms in VOF convection equation

3.6 TVD Schemes

In the upwind scheme, it is implicitly assumed that value of the convected property is constant in the computational cell. Assuming its value changing linearly, we come to the second-order spatial accuracy. It is obvious that, in order to establish this linearity, we need at least two cell averaged values (Fig. 3.4). Similarly, the third-order spatial accuracy would be obtained if the change of convected quantity would be represented as a quadratic function of space. A MUSCL (after the name of code, developed by Van Leer [1979]) approach imply variable extrapolation

of averaged cell values, providing this way a higher-order accuracy. MUSCL is a second order Godunov-type method. It differs from Godunov's scheme in that it creates linear profiles of state data in each zone. It is sometimes necessary, however, to flatten the slopes of the linear profile, to ensure that the scheme provides sufficient dissipation. Unfortunately, it is shown that simple replacement of first-order upwind scheme by higher-order upwind scheme leads to similar deficiencies as encountered with central scheme. i.e. oscillations around discontinuities. In addition, it can be theoretically shown that linear, second-order upwind schemes always generate oscillations [Enquist and Osher. 1981]. Therefore, an additional treatment is required.
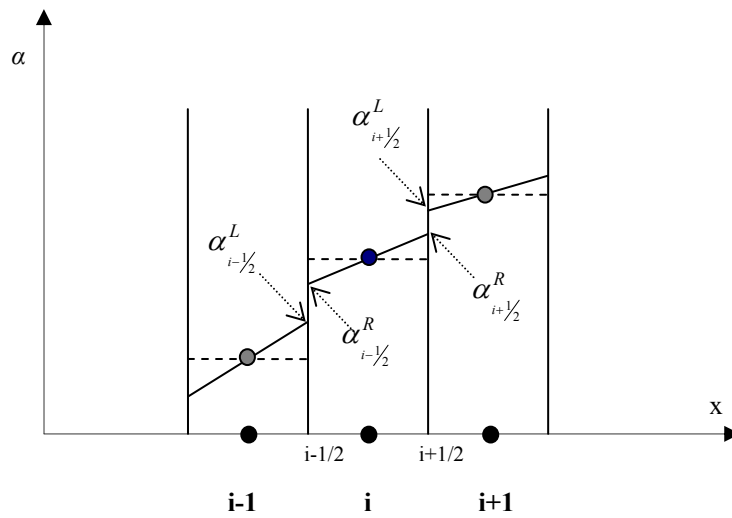
Figure 3.4 Distribution of the advected quantity in the computational cell: dashed line represents a constant approximation and the continuous line represents a linear approximation.

Harten [1983] introduced the criterion of bounded total variation in order to ensure that oscillations are not generated by the numerical scheme. Total Variation Diminishing (TVD) schemes are those in which the total variation is non-increasing with time, i.e.,

$$TV(\alpha^n) \leq TV(\alpha^{n+1}) \tag{3.14}$$

for numerical solutions α where in this case (with α piecewise constant), the total variation is

$$TV(\alpha^n) = \sum_j \left| \alpha_{j+1}^n - \alpha_j^n \right| \tag{3.15}$$

A TVD condition ensures that the scheme is a monotonicity preserving, which means that monotonicity is preserved during the solution time evolution and oscillations can not occur. It

can be easily shown that first-order upwind scheme satisfies the condition (3.14) for courant number less than unity, and therefore it is a TVD scheme.

Referring to Fig. 3.3, the value of the quantity α at the cell boundaries from the left and the right side can be approximated as [Hirsch, 1990]:

$$\alpha_{i+1/2}^{L} = \alpha_i + \frac{\varepsilon}{4}\left[(1-\kappa)\frac{\alpha_i - \alpha_{i-1}}{\Delta x_{i-1/2}} + (1+\kappa)\frac{\alpha_{i+1} - \alpha_i}{\Delta x_{i+1/2}}\right]\Delta x_i \tag{3.16}$$

$$\alpha_{i+1/2}^{R} = \alpha_{i+1} - \frac{\varepsilon}{4}\left[(1-\kappa)\frac{\alpha_{i+2} - \alpha_{i+1}}{\Delta x_{i+3/2}} + (1+\kappa)\frac{\alpha_{i+1} - \alpha_i}{\Delta x_{i+1/2}}\right]\Delta x_{i+1} \tag{3.17}$$

where parameter ε determines the spatial accuracy. For $\varepsilon = 0$, it is first order approximation, and for $\varepsilon = 1$, the scheme is of higher order. Similarly, parameter κ determines higher order accuracy. For example, in the case that $\kappa = 1/3$, Eqs. (3.16) and (3.17) represent a third order Taylor expansion, for $\kappa = 1/2$ a QUICK scheme [Leonard, 1979] can be obtained. In the case of $\kappa = -1$, we obtain a simple linear one-sided extrapolation of nodal values on the cell boundary. A third order scheme is used for the convective term in VOF evolution equation in this thesis.

In Eqs. (3.16) and (3.17) the second term on the right side brings higher order accuracy, but also produces eventual oscillations. In order to ensure the TVD condition, slope limiters can be introduced in those terms to restrict the amplitude of gradients:

$$\alpha_{i+1/2}^{L} = \alpha_i + \frac{\varepsilon}{4}\left[(1-\kappa)\psi_{i-1/2}^{+}\frac{\alpha_i - \alpha_{i-1}}{\Delta x_{i-1/2}} + (1+\kappa)\psi_{i+1/2}^{-}\frac{\alpha_{i+1} - \alpha_i}{\Delta x_{i+1/2}}\right]\Delta x_i \tag{3.18}$$

$$\alpha_{i+1/2}^{R} = \alpha_{i+1} - \frac{\varepsilon}{4}\left[(1-\kappa)\psi_{i+3/2}^{-}\frac{\alpha_{i+2} - \alpha_{i+1}}{\Delta x_{i+3/2}} + (1+\kappa)\psi_{i+1/2}^{+}\frac{\alpha_{i+1} - \alpha_i}{\Delta x_{i+1/2}}\right]\Delta x_{i+1} \tag{3.19}$$

where the limiters $\psi_{i\pm1/2}^{\pm}$ are functions of the ratio of consecutive gradients:

$$\psi_{i+1/2}^{+} = \psi(r_{i+1/2}^{+}) = \psi\left(\frac{\alpha_{i+2} - \alpha_{i+1}}{\alpha_{i+1} - \alpha_i}\frac{\Delta x_{i+1/2}}{\Delta x_{i+3/2}}\right) \tag{3.20}$$

$$\psi_{i+1/2}^{-} = \psi(r_{i+1/2}^{-}) = \psi\left(\frac{\alpha_i - \alpha_{i-1}}{\alpha_{i+1} - \alpha_i}\frac{\Delta x_{i+1/2}}{\Delta x_{i-1/2}}\right) \tag{3.21}$$

In order to simplify Eqs. (3.18) and (3.19), the limiters $\psi(r^L)$ and $\psi(r^R)$ can be defined as:

$$\psi(r^L) = \psi(r^+_{i-1/2}) \tag{3.22}$$

$$\psi(r^R) = \psi(r^-_{i+3/2}) \tag{3.23}$$

Naturally, every function of the ratio *r* can not be a gradient limiter. A detailed analysis of required limiter properties is given, for example, in the work of Sweby [1984]. In short, to satisfy the TVD condition it is necessary that limiter has the following property:

$$0 \leq \psi(r) \leq \min(2r, 2) \tag{3.24}$$

Furthermore, in order to ensure a higher order accuracy a more restrictive condition can be established [Sweby, 1984]:

$$\psi(r) = \max\{0, \min(\beta r, 1), \min(r, \beta)\} \qquad (1 \leq \beta \leq 2) \tag{3.25}$$

Several gradient limiters are reported in the literature, we use *minmod* limiter. It takes a smaller gradient for extrapolation of variables when consecutive gradients have same sign. If the consecutive gradients have different sign, an ordinary upwind scheme is utilized, to avoid the occurrence of oscillations. A *minmod* function is defined as :

$$minmod(a,b) = \begin{cases} a & \text{if } |a| < |b| & \text{and } ab>0 \\ b & \text{if } |a| > |b| & \text{and } ab>0 \\ 0 & \text{if} & ab<0 \end{cases} \tag{3.26}$$

After calculating the interpolated cell face values from both upstream and downstream side by Eqs. (3.18) and (3.19), fluxes at the left and right edge of the boundaries are given by:

$$(\alpha V)_{i+1/2} = \frac{1}{2}\left[V_{i+1/2}\left(\alpha^L_{i+1/2} + \alpha^R_{i+1/2}\right) + |V_{i+1/2}|\left(\alpha^L_{i+1/2} - \alpha^R_{i+1/2}\right)\right] \tag{3.27}$$

$$(\alpha V)_{i-1/2} = \frac{1}{2}\left[V_{i-1/2}\left(\alpha^L_{i-1/2} + \alpha^R_{i-1/2}\right) + |V_{i-1/2}|\left(\alpha^L_{i-1/2} - \alpha^R_{i-1/2}\right)\right] \tag{3.28}$$

3.7 Conclusion

The volume averaged governing equations for flow in porous medium, obtained in the previous chapter, are discretized by finite volume method with full staggered arrangement of hydraulic variables. Here, the velocity vectors are defined at cell boundaries and scalars are defined at cell centers. For the reconstruction of scalars at the cell boundaries, a higher order approach is

utilized, with a TVD slope limiter in order to avoid numerical diffusive effects, as well as occurrence of oscillations around the sharp fronts, which is characteristic for higher order schemes. In describing the free surface, the VOF method is used, which is here slightly adapted for flows in porous media. Coupled momentum and mass conservation equations are solved by extending the HSMAC method to porous media flows, where a special consideration is paid to calculate the convective terms in the momentum equations. The CIP method is employed for the convection terms. Not only the variables but also their spatial gradients are convected to preserve the inter-nodal details of the variables in this method.

Developed model will be validated by applying it to various porous media free-surface flow problems in the chapters to follow. The results of the models will be compared to both experiments and analytical results. The intention is to develop a numerical model coupling with the VOF method for free-surface flow in porous media and propose an algorithm so that it can be used as a tool for various flow types with respect to the geometry and hydraulic conditions.

Chapter 4
INTEGRAL MODEL FORMULATION

4.1 Introduction

Even though Darcy law has been used nearly exclusively in the studies of porous medium phenomena, there is considerable evidence that at high-velocity, the Darcy law does not hold in many porous and subsurface systems. Any deviations from this linear relation may be defined as non-Darcy flow. For this reason several works have been published by using the generalized Darcy law where the convective acceleration and viscous-stress are taken into account considering linear resistance law. If the flow is laminar the linear law of resistance is applicable i.e. hydraulic gradient is taken proportional to the fluid velocity and if the flow is turbulent, the hydraulic gradient is assumed proportional to the square of the velocity which is also called quadratic law of resistance for high velocity flow inside porous media. In this study, we deal with the unsteady intrusion of water into porous media consisting of large grain size, which can be applied to simulate the storm water storage into granular road sub-base from a side drain channel, under prescribed upstream boundary conditions. The typical drainage facility where one can expect the inertial effect will be described later in chapter 8 of this thesis. The unsteady transient free-surface porous media flow model could be a potential decision tool to study various temporal and spatial hydrological parameters.

The common fundamental equations for solid-liquid multiphase flows with the inertia force term, which is generally neglected in the conventional underground flows, are used as the basic model

for this study because the pervious and granular road sub-base material consists of large grain size material and one can expect inertial flows through such strata. The fundamental characteristics of intrusion process are firstly investigated with respect to various flow regimes theoretically using the depth averaged equations with the local and convective inertia term and the porous drag resistance terms in the momentum equation. Assuming the self-similarity distributions of depth and velocity, we derive the similarity solutions of intrusion process with the propagation of front, velocity and depth at entry etc. under two different boundary conditions. We also derive the spatial integral model incorporating the similarity functions of flow depth and velocity for both laminar and turbulent flows. It is pointed out that we can deal with all the possible flow regimes by using integral models.

The results derived in this study are verified by carrying out the numerical simulations and hydraulic experiments. The vertical 2D numerical simulation is carried out by applying the finite volume method coupled with CIP-VOF technique to define the moving free surface.

4.2 Problem statement

In this section, we present the theoretical background for the intrusion process of water into porous media with respect to the temporal power of depth, entry velocity and front position. The results are derived by considering the similarity distributions. These results will be verified later from the results of both numerical simulation and hydraulic experiments.

4.2.1 Theoretical considerations

The governing equations for the conservation of mass and momentum as given in the section 3.1 are taken as the basic equations for the unsteady free-surface flow through porous media. In order to investigate fundamental characteristics of intrusion process, the depth-averaged equations are used. The depth averaged continuity and momentum equations for one dimensional flow with inertia and drag resistance terms can be written as

$$\frac{\partial\{(1-C)h\}}{\partial t}+\frac{\partial\{(1-C)hU\}}{\partial x}=0 \tag{4.1}$$

$$\frac{\partial\{(1-C)hU\}}{\partial t}+\frac{\partial\{(1-C)hU^{2}\}}{\partial x}=-(1-C)gh\frac{\partial z_{s}}{\partial x}+\frac{\partial}{\partial x}\left\{(1-C)\frac{\tau_{xx}}{\rho}h\right\}-\frac{\tau_{bx}}{\rho}-\frac{R_{x}}{\rho}h \tag{4.2}$$

where t is time, x the spatial coordinate, h the flow depth, U the depth averaged velocity, z_s the free-surface elevation, τ_{xx} the viscous stress, τ_{bx} the bottom shear stress and ρ the density of water. For the analytical study, the volumetric concentration of solid particles C is taken constant for the rigid porous media. The last term of Eq. (4.2) represents the resistance offered by the porous matrix. Hence for the flow in porous media where linear and quadratic resistance laws are applied separately, the resistance term is given by

$$\frac{R_x}{\rho} = \begin{cases} C_L U & \text{for laminar flow (linear law)} \\ C_T U |U| & \text{for turbulent flow (quadratic law)} \end{cases} \tag{4.3}$$

where C_L and C_T are the constant coefficients for linear and quadratic resistance terms, respectively. The coefficients are considered to be dependent only on the characteristics of porous media in this study. The constant coefficients for linear and quadratic resistance laws can be written from the consideration of Darcy law and turbulent resistance given by

$$C_L = \frac{\nu(1-C)^2}{k} \tag{4.4}$$

$$C_T = \frac{(1-C)^3 F_{ch}}{\sqrt{k}} \tag{4.5}$$

where ν is the kinematic viscosity of the fluid, F_{ch} is the Forchheimer's inertia coefficient and k the permeability in m^2 of the porous medium. For a rigid and isotropic porous media, following set of continuity and momentum equation can be written

$$\frac{\partial h}{\partial t} + \frac{\partial hU}{\partial x} = 0 \tag{4.6}$$

$$\frac{\partial U}{\partial t} + U\frac{\partial U}{\partial x} + g\frac{\partial h}{\partial x} = -\frac{R_x}{\rho(1-C)} \tag{4.7}$$

The approximate solutions for depth and velocity distributions are derived based on the assumed similarity of depth and velocity to clarify the fundamental characteristics of intrusion of water under two boundary conditions for both laminar and turbulent resistance laws. The methods based on similarity transformation has been applied to the dam break flow of viscous fluid where temporal and spatial distribution of depth and velocity were derived analytically balancing the pressure gradient and viscous terms [Hosoda et al., 2000; Huppert, 1982]. Among others Barenblat and Vazquez [1998] used Boussinesq equation and Huppert and Woods, [1995] used

Darcy equation as the basic governing equations for similarity transformation. The inertia term in the flow equation has been neglected in most of the reported literatures though we expect its significance in the porous media having high permeability value. Nonetheless, the similarity reduction is very useful, because it allows many interesting results to be obtained, for example regarding the position of front, its speed of propagation and some other nonlinear characteristics [Chen and Bodvarsson, 1995].
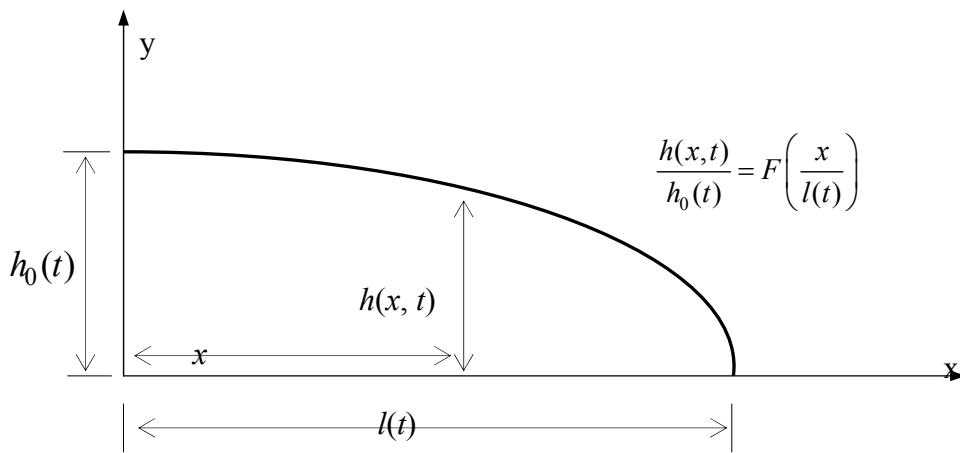
Figure 4.1 Definition sketch of similarity distribution for flow depth

Fig. 4.1 shows the similarity distribution of flow depth $h(x, t)$ in free-surface flow in terms of the depth at origin $h_0(t)$ and a non-dimensional similarity function F. In this study, we analyze first the different flow regimes by balancing the possible combinations of forces in the momentum equation under two different boundary conditions, considering similarity law and then derive the integral solutions applicable to all the flow regimes investigated. The distribution of inflow velocity U_0, depth at origin h_0, and the front position l are expressed in terms of temporal powers a, b and c as given by

$$U_0 = \alpha V_0 \left(\frac{t}{T_0}\right)^a , \quad h_0 = \beta L_0 \left(\frac{t}{T_0}\right)^b \text{ and } \quad l = \gamma L_0 \left(\frac{t}{T_0}\right)^c \tag{4.8}$$

where α, β and γ are constant coefficients; V_0, L_0 and T_0 are the characteristic velocity, length and time scales respectively. These characteristic parameters are explained for each of the cases considered in the respective section. It will be shown that the power laws with respect to time given by Eq. (4.8) are valid for the dominance of the combination of two terms of inertia-pressure (IP) and pressure-drag (PD) regimes. Also the analytical integral models based

on similarity distributions are derived. The similarity distributions of the depth $h(x, t)$ and velocity $U(x, t)$ are defined as

$$h = h_0 F(\xi) \quad \text{and} \quad U = U_0 G(\xi) \tag{4.9}$$

subject to

$$F(0) = 1, \quad F(1) = 0 \quad \text{and} \quad G(0) = U_0, G(1) = U_F \tag{4.10}$$

where ξ is the similarity variable given by $\xi = x/l(t)$, U_F is the velocity at front and the functions F and G are the non-dimensional distribution functions for depth and velocity, respectively. These similarity functions for all the time steps are expressed as:

$$G(\xi) = 1 - A\xi, \quad \text{and} \quad F(\xi) = 1 - B\xi \tag{4.11}$$

where A and B are constant coefficients to be determined using similarity law and we assume that these values do not change significantly for different flow regimes. In the subsequent sections, we derive the temporal powers a, b and c and the expressions for flow depth h, flow velocity U and front position l.

4.2.2 Flow domain and boundary conditions

Two types of flow domains are considered for the study of intrusion dynamics of fluid into the porous media. These two conditions, defined in this study as case A and case B, represent the domains subjected to constant upstream water level i.e. pressure boundary and constant upstream discharge or inflow flux boundary conditions, respectively (see Fig. 4.2).
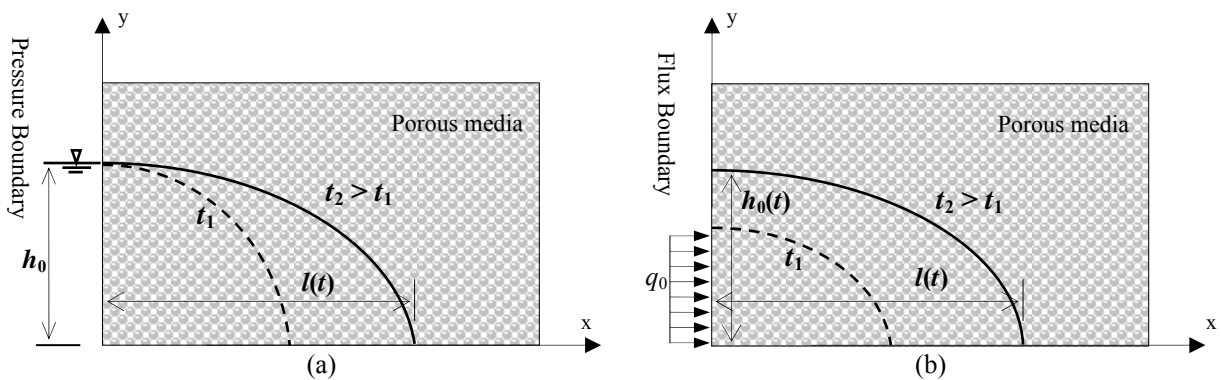

Figure 4.2 Domains subjected to constant upstream (a) water level h_0 : case A and (b)inflow discharge q_0 : case B.

For case A, a horizontal porous medium, which rests on an impermeable base, is considered and it is connected to a pool of water with a vertical boundary at the origin as shown in the Fig. 4.2(a). Initially, the water is retained at the back of this vertical boundary and to start the unsteady intrusion the gate at the origin ($x = 0$) is released instantaneously to give way to the water to intrude into the pore space being occupied by gas (air) of negligible viscosity, under the constant hydraulic head. Thus at the left boundary ($x = 0$), the hydraulic head in the pool remains constant with time i. e. the condition $h(x = 0, t > 0) = h_0$ is satisfied, where h_0 is the constant value of inlet water depth.

For case B i.e. when the upstream boundary of the domain is subjected to a constant prescribed inflow flux, the depth at the origin also varies with time as shown in Fig. 4.2(b). Thus in this case the condition $q(x = 0, t > 0) = q_0$ is satisfied, where q is the flux and q_0 is the constant value of inflow flux. In the subsequent section, we are interested in solving Eqs. (4.6) and (4.7) subject to aforementioned initial and boundary conditions.

4.3. Similarity Transformations

The power laws as expressed by Eq. (4.8) are derived for both the case of laminar and turbulent flow. The detail analysis is made for laminar flow case is shown below. The similar analysis is also made for the turbulent flow as well. The results for both the flow types are shown in Table 4.1.

4.3.1. Similarity solution for case A (Pressure inlet boundary)

This is the condition where upstream boundary is set at a constant water depth h_0. The characteristic time, length and velocity in this case are defined as

$$T_0 = \left(h_0 / g\right)^{\frac{1}{2}}, \quad L_0 = h_0 \quad \text{and} \quad V_0 = \left(gh_0\right)^{\frac{1}{2}} \tag{4.12}$$

Using Eqs. (4.8) and (4.11), the equations for continuity and momentum as expressed by Eqs. (4.6) and (4.7) are reduced to Eqs. (4.13) and (4.14) as below,

$$-\xi \frac{\gamma L_0}{T_0} c(t')^{c-1} \frac{dF}{d\xi} + \alpha V_0 (t')^a \frac{dGF}{d\xi} = 0 \tag{4.13}$$

$$\underbrace{\alpha \frac{V_0}{T_0} at'^{a-1} G - \alpha \frac{V_0}{T_0} ct'^{a-1} \xi \frac{dG}{d\xi}}_{inertia(unsteady)} + \underbrace{\frac{\alpha^2}{\gamma} \frac{V_0^2}{L_0} t'^{2a-c} G \frac{dG}{d\xi}}_{inertia(convection)} + \underbrace{\frac{\beta}{\gamma} gt'^{b-c} \frac{dF}{d\xi}}_{pressure} = \underbrace{-\frac{C_L \alpha V_0 t'^a G}{(1-C)}}_{drag} \tag{4.14}$$

where t' is the non-dimensional time defined as $t' = t/T_0$. Due to the constant water level boundary condition, h_0 is constant i.e.

$$b = 0 \tag{4.15}$$

And from Eq. (4.13), we can write

$$c - a = 1 \tag{4.16}$$

For the determination of the values of temporal power coefficients a, b and c, each combination of Eq. (4.14) such as Inertia-Pressure terms and Pressure-Drag terms are taken and solved for the coefficients. The results are as given below.

(a) Inertia-Pressure regime:

$$a = 0, \;\; b = 0 \;\; \text{and} \;\; c = 1 \tag{4.17}$$

(b) Pressure-Drag regime:

$$a = -1/2, \;\; b = 0 \;\; \text{and} \;\; c = 1/2 \tag{4.18}$$

(c) Inertia-Drag regime:

No solution is obtained for this regime.

The similarity solutions for the assumed depth and velocity distribution are found for both regimes as already depicted are presented below.

(i) Inertia-Pressure regime

The set of equation for this regime are given by

$$-\frac{\gamma L_0}{T_0} \xi \frac{dF}{d\xi} + \alpha V_0 \frac{dGF}{d\xi} = 0 \tag{4.19}$$

$$-\alpha \frac{V_0}{T_0} \xi \frac{dG}{d\xi} + \frac{\alpha^2}{\gamma} \frac{V_0^2}{L_0} G \frac{dG}{d\xi} + \frac{\beta}{\gamma} g \frac{dF}{d\xi} = 0 \tag{4.20}$$

Also the front velocity U_F can be derived by taking the time derivative of $l(t)$ as below

$$U_F = \frac{dl}{dt} = \gamma L_0 c t'^{c-1} \frac{1}{T_0} = \frac{\gamma L_0}{T_0} \tag{4.21}$$

Using the functional relationships of G and F in Eqs. (4.19) and (4.20) and after simplification we get,

$$A = -1.0, \ B = 1.0, \ \ \alpha V_0 = \sqrt{gh_0}, \ \ \beta L_0 = h_0 \ \ \text{and} \ \ \gamma L_0 = 2T_0\sqrt{gh_0} \tag{4.22}$$

The velocity and depth at origin and the front position are derived as

$$U_0 = \sqrt{gh_0} \ , \ \ h_0 = h_0 \ \ \text{and} \ \ l = 2t\sqrt{(gh_0)} \tag{4.23}$$

The flow depth and velocity are then derived as

$$h = h_0\left(1 - \frac{x}{2\sqrt{gh_0}}\frac{1}{t}\right) \ \ \text{and} \ \ U = \left(\sqrt{gh_0}\right)\left(1 + \frac{x}{l(t)}\right) \tag{4.24}$$

(ii) Pressure-Drag regime

The governing equations for this regime can be written as

$$-\frac{\gamma L_0}{2T_0}\xi\frac{dF}{d\xi} + \alpha V_0\frac{dGF}{d\xi} = 0 \tag{4.25}$$

$$\frac{\beta}{\gamma}g\frac{dF}{d\xi} = -\frac{C_L\alpha V_0 G}{(1-C)} \tag{4.26}$$

Thus using the same functional form of flow depth and velocity, Eqs. (4.25) and (4.26) yield,

$$\alpha V_0 = \frac{1}{2}\left(\frac{gh_0(1-C)}{T_0C_L}\right)^{\frac{1}{2}}, \ \beta L_0 = h_0 \ \ \text{and} \ \ \gamma L_0 = \left(\frac{4gT_0h_0(1-C)}{C_L}\right)^{\frac{1}{2}} \tag{4.27}$$

Now, using Eqs. (4.12) and (4.27), velocity and depth at origin and the front positions are derived as

$$U_0 = \frac{1}{2}\left(\frac{gh_0(1-C)}{C_L}\right)^{\frac{1}{2}} t^{-\frac{1}{2}}, \ h_0 = h_0 \ \ \text{and} \ \ l = \left(\frac{4gh_0(1-C)}{C_L}\right)^{\frac{1}{2}} t^{\frac{1}{2}} \tag{4.28}$$

Similarly the overall flow depth and velocity can be written as

$$h = h_0\left(1 - \frac{x}{l(t)}\right) \ \ \text{and} \ \ U = \frac{1}{2}\left(\frac{gh_0(1-C)}{C_L}\right)^{\frac{1}{2}}\left(1 + \frac{x}{l(t)}\right)t^{-\frac{1}{2}} \tag{4.29}$$

4.3.2. Similarity solution for case B (Flux inlet boundary)

This is the condition where upstream boundary is set at a constant flux inflow i.e. there is a constant value of inflow discharge q_0. The characteristic time, length and velocity for the case considered are defined as

$$T_0 = \left(\frac{q_0}{g^2}\right)^{\frac{1}{3}}, \quad L_0 = \left(\frac{q_0^2}{g}\right)^{\frac{1}{3}} \quad \text{and} \quad V_0 = (gq_0)^{\frac{1}{3}} \tag{4.30}$$

Using Eqs. (4.11) and (4.30), the equations for continuity and momentum as expressed by Eqs. (4.6) and (4.7) are reduced to Eqs. (4.31) and (4.32) as below

$$\beta \frac{L_0}{T_0} b(t')^{b-1} F - \beta \frac{L_0}{T_0} c(t')^{b-1} \xi \frac{dF}{d\xi} + \frac{q_0}{\gamma L_0}(t')^{-c} \frac{dGF}{d\xi} = 0 \tag{4.31}$$

$$\underbrace{\alpha \frac{V_0}{T_0} a t'^{a-1} G - \alpha \frac{V_0}{T_0} c t'^{a-1} \xi \frac{dG}{d\xi}}_{inertia(unsteady)} + \underbrace{\frac{\alpha^2}{\gamma} \frac{V_0^2}{L_0} t'^{2a-c} G \frac{dG}{d\xi}}_{inertia(convection)} + \underbrace{\frac{\beta}{\gamma} g t'^{b-c} \frac{dF}{d\xi}}_{pressure} = \underbrace{-\frac{C_L \alpha V_0 t'^a G}{(1-C)}}_{drag} \tag{4.32}$$

The upstream constant flux boundary condition gives the relationship

$$U_0 h_0 = q_0 (= \text{constant})$$

i.e. $\quad \alpha\beta V_0 L_0 (t')^{a+b} = q_0 \tag{4.33}$

With the use of Eqs. (4.30)-(4.31), the temporal powers are obtained and are shown in Table 4.1. Also the similarity solutions for various hydraulic variables are obtained and shown in Eqs. (4.34) and (4.35), in which the use of powers and the assumed distribution functions are made along with transformed governing equations for the case considered.

(i) Inertia-Pressure regime

$$h = h_0 F\left(\frac{x}{l(t)}\right) = \left(\frac{q_0^2}{g}\right)^{\frac{1}{3}}\left(1 - \frac{x}{l(t)}\right) \quad \text{and} \quad U = U_0 G\left(\frac{x}{l(t)}\right) = (gq_0)^{\frac{1}{3}}\left(1 + \frac{x}{l(t)}\right) \tag{4.34}$$

(ii) Pressure-Drag regime

$$U = \left(\frac{q_0 g(1-C)}{2C_L}\right)^{\frac{1}{3}}\left(1 + \frac{x}{3l(t)}\right) t^{-\frac{1}{3}} \text{ and } h = \left(\frac{2q_0^2 C_L}{g(1-C)}\right)^{\frac{1}{3}} t^{\frac{1}{3}}\left(1 - \frac{x}{l(t)}\right) \tag{4.35}$$

The derivations for power laws has been shown above for linear resistance law in which the resistance due to porous media is given by Eq. (4.4). Similar analysis are carried out for square resistance law [see Eq. (4.5)] as well applicable in turbulent flow. Only the results are shown here in Table 4.1.

Table 4.1 Summary of the temporal powers

Assumed resistance law	Case A (Pressure boundary)		Case B (Flux boundary)	
	IP	PD	IP	PD
laminar	$a = 0$ $b = 0$ $c = 1$	$a = -1/2$ $b = 0$ $c = 1/2$	$a = 0$ $b = 0$ $c = 1$	$a = -1/3$ $b = 1/3$ $c = 2/3$
turbulent	$a = 0$ $b = 0$ $c = 1$	$a = -1/3$ $b = 0$ $c = 2/3$	$a = 0$ $b = 0$ $c = 1$	$a = -1/4$ $b = 1/4$ $c = 3/4$

4.4 Derivation of integral model for laminar flow

In this case the hydraulic gradient is assumed to be proportional to the linear power of velocity. For the flow with small Reynolds number, the resistance coefficient in Eq. (4.3) is given by Eq. (4.4). With the help of continuity Eq. (4.6), momentum Eq. (4.7) can be converted into its conservative form and it given by:

$$\frac{\partial hU}{\partial t} + \frac{\partial hU^2}{\partial x} + g\frac{\partial}{\partial x}\left(\frac{h^2}{2}\right) = -\frac{C_L hU}{(1-C)} \tag{4.36}$$

The governing Eqs. (4) and (14) can be integrated from $x = 0$ to $x = l(t)$ at any instant as

$$\int_0^{l(t)}\left[\frac{\partial h}{\partial t} + \frac{\partial hU}{\partial x}\right]dx = 0 \tag{4.37}$$

$$\int_0^{l(t)}\left[\frac{\partial hU}{\partial t} + \frac{\partial hU^2}{\partial x} + g\frac{\partial}{\partial x}\left(\frac{h^2}{2}\right)\right]dx = -\int_0^{l(t)}\left[\frac{C_L hU}{(1-C)}\right]dx \tag{4.38}$$

Further, using similarity distribution functions as expressed by Eq. (4.9) and on simplification using Leibnitz integral rule each term in Eqs. (4.37) and (4.38) can be simplified. For the compactness, the results after simplification for each term of continuity and momentum are given in Eq. (4.39)

$$\int\limits_0^{l(t)} \frac{\partial h}{\partial t}dx = \frac{d}{dt}\int\limits_0^{l(t)} hdx - h\big|_{x=l}\frac{dl}{dt} = \frac{d(h_0 l)}{dt}\int\limits_0^1 Fd\xi \,,$$

$$\int\limits_0^{l(t)} \frac{\partial hU}{\partial x}dx = -h_0(t)U_0(t) \quad,$$

$$\int\limits_0^{l(t)} \frac{\partial hU}{\partial t}dx = \frac{d}{dt}\int\limits_0^{l(t)} hUdx - (hU)\big|_{x=l}\frac{dl}{dt} = \frac{d(h_0 U_0 l)}{dt}\int\limits_0^1 FGd\xi \,,$$

$$\int\limits_0^{l(t)} \frac{\partial hU^2}{\partial x}dx = -h_0 U_0^2 \,,$$

$$\int\limits_0^{l(t)} \frac{\partial}{\partial x}\left(\frac{h^2}{2}\right)dx = -\frac{h_0^2}{2} \quad \text{and}$$

$$\int\limits_0^{l(t)} hUdx = h_0 U_0 l\int\limits_0^1 FGd\xi \qquad\qquad (4.39)$$

Using the relations in Eq. (4.39), integral Eqs. (4.37) and (4.38) are reduced to

$$\frac{d(h_0 l)}{dt}\int\limits_0^1 Fd\xi = h_0(t)U_0(t) \qquad\qquad (4.40)$$

$$\frac{d(h_0 U_0 l)}{dt}\int\limits_0^1 FGd\xi - h_0 U_0^2 - \frac{gh_0^2}{2} = -\frac{C_L h_0 U_0 l}{(1-C)}\int\limits_0^1 FGd\xi \qquad\qquad (4.41)$$

For the integral terms comprising similarity functions in above equations, following relations can be derived

$$\int\limits_0^1 Fd\xi = \frac{(2-B)}{2} = \eta \qquad\qquad (4.42)$$

$$\int\limits_0^1 FGd\xi = 1 - \frac{(A+B)}{2} + \frac{AB}{3} = \lambda \qquad\qquad (4.43)$$

The integral models will be derived in the following section for each of the flow conditions considered that inherits both the IP and PD regime in its solution.

4.4.1 Integral model for pressure inlet condition

While making use of the special condition that the inlet water depth remains constant i. e.

$h(x= 0, t) = h_0$ (constant), Eqs (4.40) and (4.41) are changed into ordinary differential equations given by

$$\text{continuity:} \qquad \eta \frac{dl}{dt} = U_0(t) \tag{4.44}$$

$$\text{momentum:} \quad 2U_0^2 + l\frac{dU_0}{dt} = \frac{U_0^2}{\lambda} + \frac{gh_0}{2\lambda} - \frac{C_L U_0 l}{(1-C)} \tag{4.45}$$

Combining Eqs. (4.44) and (4.45), one can easily write the ODE for governing equation in terms of front position $l(t)$

$$\eta l \frac{d^2 l}{dt^2} + \left(2\eta^2 - \frac{\eta^2}{\lambda}\right)\left(\frac{dl}{dt}\right)^2 - \frac{gh_0}{2\lambda} = -\frac{C_L \eta l}{(1-C)}\frac{dl}{dt} \tag{4.46}$$

4.4.2 Integral model for flux inlet condition

Using similar approach as done for pressure inlet condition except the special constant inflow flux condition as already mentioned, we arrive to get following continuity and momentum equations by integrating Eqs. (4.6) and (4.36) for the whole domain i.e. from $x = 0$ to $l(t)$

$$\text{continuity:} \qquad \eta \frac{d(h_0 l)}{dt} = q_0 \tag{4.47}$$

$$\text{momentum:} \qquad \lambda \frac{dl}{dt} - \frac{q_0}{h_0} - \frac{gh_0^2}{2q_0} = -\frac{C_L \lambda l}{(1-C)} \tag{4.48}$$

Combining these two equations, a single ordinary differential equation is deduced as follows,

$$\frac{dl}{dt} = \frac{1}{\lambda}\left[\frac{\eta l}{t} + \frac{gq_0 t^2}{\eta^2 l^2}\right] - \frac{C_L l}{(1-C)} \tag{4.49}$$

4.5 Derivation of integral model for turbulent flow

For the case when quadratic resistance law is considered for high velocity flow through course porous media, we also have derived integral formulations. The governing equations for mass and momentum balance are given by Eqs. (4.6) and (4.7) in which the resistance coefficient in Eq. (4.3) is given by Eq. (4.5). Thus the momentum balance equation in its conservative form can be written as

$$\frac{\partial hU}{\partial t}+\frac{\partial hU^2}{\partial x}+g\frac{\partial}{\partial x}\left(\frac{h^2}{2}\right)=-\frac{C_T hU|U|}{(1-C)} \tag{4.50}$$

Integrating Eqs. (4.6) and (4.50) from $x = 0$ to $l(t)$ and making use of Leibnitz integral rule, we get following set of continuity and momentum equations

$$\frac{d(h_0 l)}{dt}\int_0^1 Fd\xi = h_0(t)U_0(t) \tag{4.51}$$

$$\frac{d\left(h_0 U_0 l\right)}{dt}\int_0^1 FGd\xi - h_0 U_0^2 - \frac{gh_0^2}{2}=-\frac{C_T h_0 U_0^2 l}{(1-C)}\int_0^1 FG^2 d\xi \tag{4.52}$$

To convert these equations into ordinary differential equations using same similarity distribution functions F and G we need one extra integral in addition to those given by Eqs. (4.42) and (4.43) i.e.

$$\int_0^1 FG^2 d\xi =1-\frac{(2A+B)}{2}+\frac{(A^2+2AB)}{3}-\frac{A^2 B}{4}=\psi \tag{4.53}$$

Hence, continuity and momentum equations are reduced to ordinary differential equations that are solved as initial value problems. The results for different boundary conditions are given in section 4.9.

4.5.1 Integral model for pressure inlet condition

For the condition considered, Eqs. (4.51) and (4.52) reduce to

$$\eta\frac{d(h_0 l)}{dt}=h_0 U_0 \tag{4.54}$$

and $\quad\lambda\frac{d\left(U_0 l\right)}{dt}-U_0^2-\frac{gh_0}{2}=-C_T\psi\left(U_0^2 l\right) \tag{4.55}$

Combining these equations we get,

$$\frac{U_0^2}{\eta}+l\frac{dU_0}{dt}=\frac{1}{\lambda}\left[U_0^2+\frac{gh_0}{2}\right]-\frac{C_T\psi U_0^2 l}{\lambda} \tag{4.56}$$

which is solved for U_0 by Runge-Kutta method in this study.

4.5.2 Integral model for flux inlet condition

The ordinary differential equation for this condition can be derived from Eqs. (4.51) and (4.52) as

$$\eta \frac{d(h_0 l)}{dt} = q_0 \tag{4.57}$$

$$\lambda \frac{dl}{dt} - \frac{q_0}{h_0} - \frac{g h_0^2}{2 q_0} = -C_T \psi l U_0 \tag{4.58}$$

Again combining these two into a single ODE we get,

$$\lambda \frac{dl}{dt} - \frac{\eta l}{t} - \frac{g q_0 t^2}{2 \eta^2 l^2} = -C_T \psi l U_0 \tag{4.59}$$

4.6 Solution of integral model formulations

The governing nonlinear partial differential equations have been changed into ordinary differential Eqs. (4.46) and (4.49) for laminar flow where the linear resistance is considered, by similarity transformation technique. Also considering quadratic resistance law Eqs. (4.56) and (4.59) are derived. The value of constant coefficients η, λ and ψ are determined for $A = -1.0$ and $B=1.0$ as already derived in the previous section for similarity law. We assume these constants do not change significantly for inertia-pressure and pressure-drag regimes. To solve these ODE's, we follow an iterative procedure using appropriate initial value. A well known fourth order Runge-Kutta method [Teukolsy et al., 1996] is implemented. All other parameters like velocity and depth at the boundaries can be found after the non-linear ODE is solved for its dependent variable. The overall process can be found from any text book dealing with nonlinear ordinary differential equation. The results are shown in section 4.9 for compactness.

4.7 Outline of laboratory tests

Laboratory experiments were carried out to evaluate both the proposed integral and numerical model. A rectangular transparent perspex flume filled with glass beads as porous media was used. In the experiment glass beads of diameter 1mm, 5mm and 12mm, taken separately, were used as porous media under constant water depth at the leftmost boundary so as to simulate case A. The summary of laboratory tests is given in the Table 4.2.

Table 4.2 Laboratory test cases

Test name	Bead size	Hydraulic conductivity	Remarks
Expt I.	1 mm	$K = 0.01$ m/s	CaseA: $h_0 = .085$m ; $C = 0.6$
Expt II.	5 mm	$K = 0.10$ m/s	
Expt III.	12 mm	$K = 0.20$ m/s	

To start with the experiment, a vertical gate at the inlet was pulled up instantaneously with the help of a nylon rope tied on the gate so as to make it as instantaneous as possible. Such an arrangement for the experiment is given in Fig. 4.3. The velocity and depth of flow with free surface were taken using a digital movie camera placed near the side of the flume. The video was converted into a series of still images at an equal time interval of 1/30 (frame rate of video camera) seconds. Then the position of front and depth distribution for different time is traced by the image interpretation manually with the help of grids drawn at 50mm interval on the perspex plate of the flume facing the camera. The time dependence and the flow profile of the intrusion behavior observed during the experiment are compared with the analytical solution and numerical simulations as well.
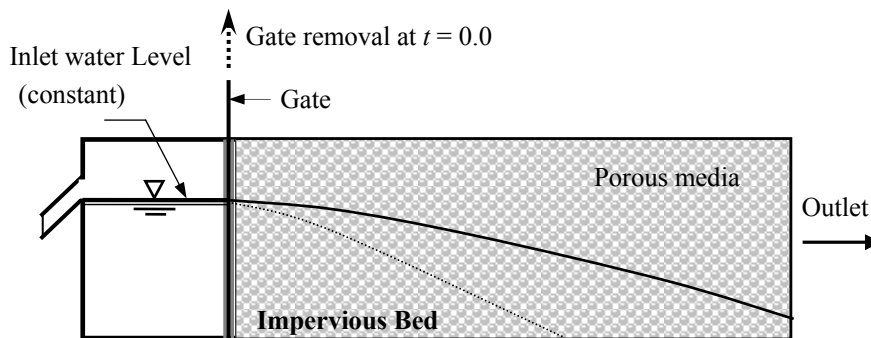
Figure 4.3 Schematic layout of the experimental set up

The experiment was carried out until a steady state condition was attained. The permeability was also calculated using the hydraulic gradient when the system attained steady state. The measured steady state discharge and the flow depths are used for the calculation of the permeability of the media for use in numerical simulation.

4.8 Numerical simulation

This section explains about the algorithm adopted for the unsteady free-surface flow through the porous media. A number of vertical two dimensional numerical simulations are carried out as

shown in Table 4.3.

Table 4.3 List of numerical runs

Numerical run	Bead size	Hydraulic conductivity	Remarks
RUN 1	1mm	$K = 0.01$ m/s	Case A :
RUN 2	5mm	$K = 0.10$ m/s	$C = 0.6$, $h_0 = 0.085$m
RUN 3	12mm	$K = 0.20$ m/s	
RUN 4	5mm	$K = 0.10$ m/s	Case B: $C = 0.6$, $q_0 = 0.005$m^3/s per m

4.8.1 Governing equations

The governing equations for free-surface flow of viscous and incompressible fluid in porous media given by a set of continuity and momentum equation are rewritten as:

$$\frac{\partial(1-C)u_i}{\partial x_i} = 0 \tag{4.60}$$

$$\frac{\partial(1-C)u_i}{\partial t} + \frac{\partial(1-C)u_iu_j}{\partial x_j} = (1-C)g_i - \frac{(1-C)}{\rho}\frac{\partial p}{\partial x_i} + \nu\frac{\partial^2(1-C)u_i}{\partial x_j\partial x_j} + \frac{R_i}{\rho} \tag{4.61}$$

where u_i is the velocity vector, also called the pore water velocity in the porous medium, C is the volumetric concentration of the solids in the porous medium, R_i is the flow resistance term due to porous matrix, p is the pressure and ν the kinematic viscosity of the fluid. The details of all the terms have been explained in chapter 3 of this thesis.

4.8.2 Boundary condition and free surface evolution

For both the cases studied here, left inlet boundary is treated as Dirichlet boundary condition where either a pressure due to water pool or a prescribed flux is supplied depending upon the case considered. At the bottom of the channel, free-slip condition is applied assuming perspex bottom friction is negligible. The downstream boundary is treated as a Neumann type where zero gradient condition for velocity and pressure is applied to ensure the continuation of the flow. At the free surface of the flow, the atmospheric pressure condition is applied. But the free surface evolution inside the porous media is not known a priori, rather is a part of the solution, an important feature of this study. The method introduces a volume of fluid (VOF) function to define the water region and its saturation within the cell. The evolution of the free surface is traced using VOF method which has been explained in the previous chapter.

4.8.3 Solution algorithm by CIP method

The governing equations [see Eqs. (4.60) and (4.61)] are solved numerically on a uniform staggered Cartesian grid by finite volume method. The CIP method is adopted as the base scheme for the numerical solution. The governing equations are split into two steps: non-advection and advection phase. The non-advection phase is solved by usual finite difference scheme whereas the advection phase is solved by the CIP method. The detail about the algorithm for numerical solution can be found in chapter 3 of this thesis.

4.9 Results and discussion

As depicted in the theoretical derivation considering the similarity distributions of variables following plots clearly show the two flow regimes in the flow through porous medium for both linear and quadratic resistance law. The results of the integral model show early inertia-pressure regime followed by pressure-drag regime.

Results of similarity solutions for linear resistance law

The theoretical results obtained from similarity analysis are verified using the results of simulations. The results correspond to the linear resistance law. Fig. 4.4 shows the position of front verses time for both the cases considered. The slopes on the plots are in agreement with the theoretical outcomes. Also the results of the numerical runs are plotted which clearly show the existence of distinct two regimes: Inertia-Pressure and Pressure-Drag for both cases. The results are in close agreement with the analytical solution derived for the assumed similarity distribution.
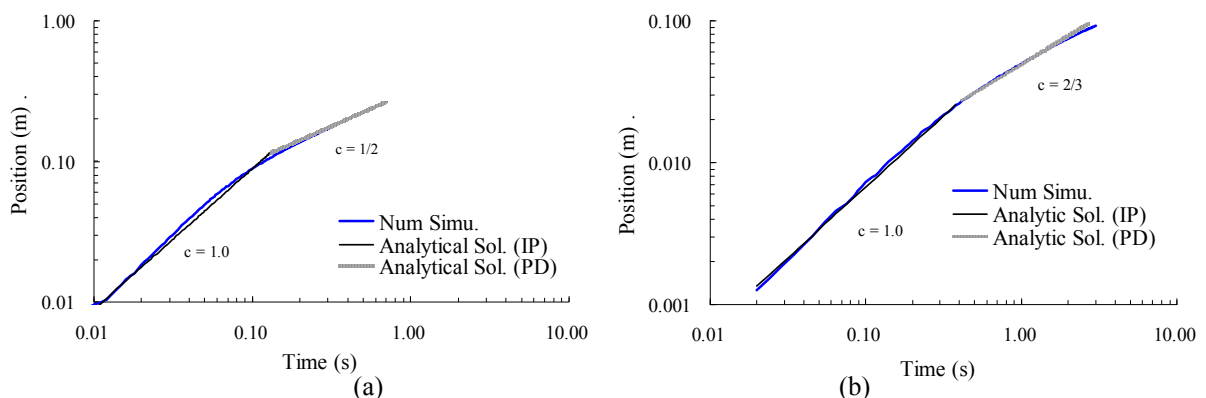

Figure 4.4 Temporal position of front (a) Case A: $K = 0.25 \text{ms}^{-1}$, $h_0 = 0.05\text{m}$ (b) Case B: $K = 0.01\text{ms}^{-1}$, $U_0 = 0.05 \text{ ms}^{-1}$, $q_0 = 0.0025\text{m}^3/\text{s}$ per m)

The flow profiles are reproduced in the numerical run which is in close agreement with that of the experiment (Fig. 4.5). The experimental depths are slightly greater than that of the simulated ones. The reason may be due to the continuous rise of capillary fringe which was observed in the experiment. The PD regime solution matches well which can be seen in the same diagram owing to the fact that inertial regime lasts for very short period of time for low permeable medium.
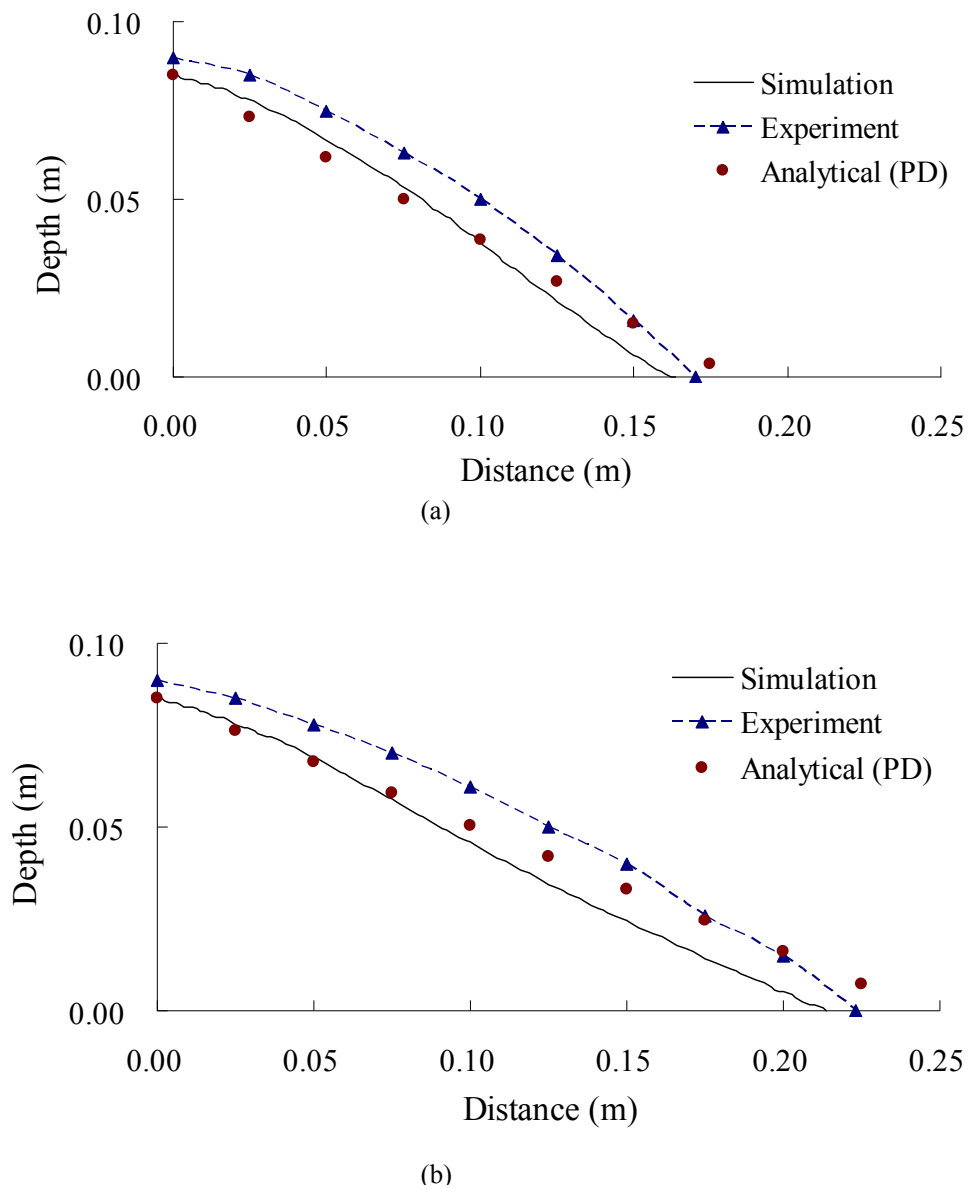

(a)

(b)

Figure 4.5 Flow Profiles for (a) 5s and (b) 10s [Case A: K=0.010m/s, C=0.6, h_0 =0.085m]

The velocity profiles obtained from the numerical experiments are shown in Fig. 4.6 for Case B. The increase in depth near the upstream boundary ($x = 0$) can be seen in Fig. 4.7. This numerical result shows two temporal powers $b =0$ and $b =1/3$ for inertia-pressure and pressure-drag regimes, respectively, agreeing the same with the theoretical results. The similarity analysis depicted the two distinct power law regimes. The solution obtained for front position, depth and velocity are valid only during the respective regime. It does not give the information about the end and start up of the new regime. Hence in the succeeding section the results of integral equation formulations are be shown. The integral formulations should inherit both the flow regimes investigated in the entire time domain.
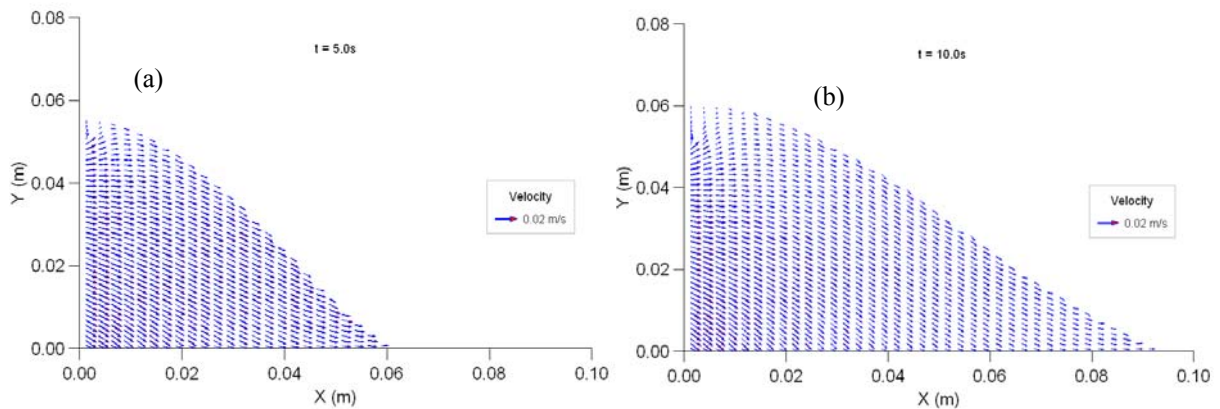

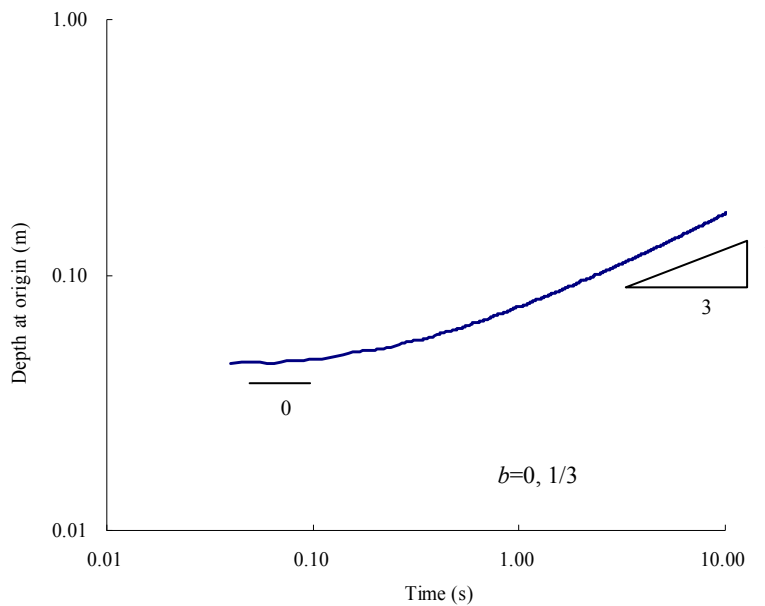**Figure 4.6** Velocity Profiles for (a) 5s and (b) 10s [Case B : K=0.005m/s, C=0.5, q_0=0.005 m^3/s per m]

**Figure 4.7** Temporal variation of depth at origin [Case B: $K = 0.01$ms^{-1}, U_0=0.05ms^{-1}, $q_0 = 0.0025$m^3/s per m]

Integral model results for linear resistance law

Figs. 4.8(a) and 4.8(b) show a log-log plot of front position and water entry velocity respectively with respect to time. The early IP regime is followed by PD regime with smooth transition. The transition time for the regime change highly depends upon the characteristics of porous media. The K values shown on the plots are the hydraulic conductivity (m/s) of porous media. The temporal powers derived theoretically are also shown on the plots to compare it with the results presented in Table 4.1 and it matches well with the results of integral formulations. It is to be noted here that there is dominance of PD regime in the flow for low permeable medium.
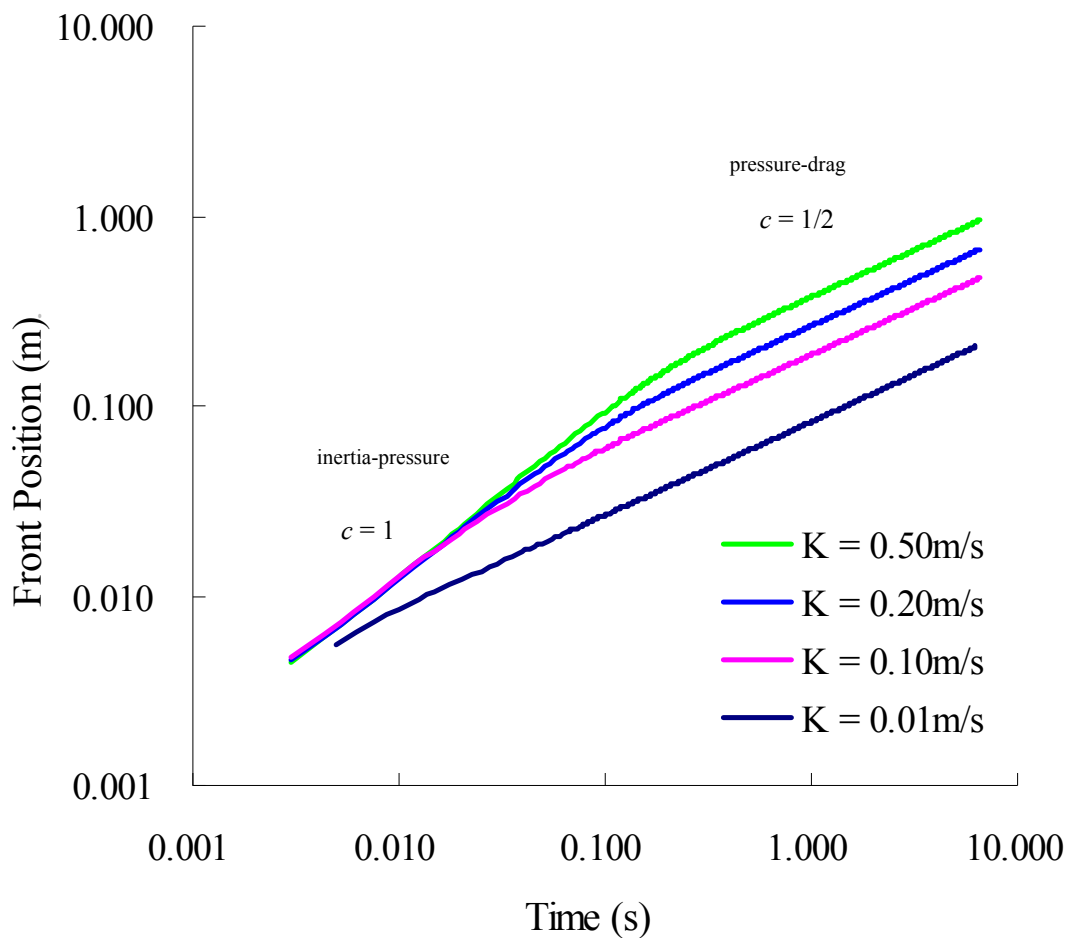

4.8(a)
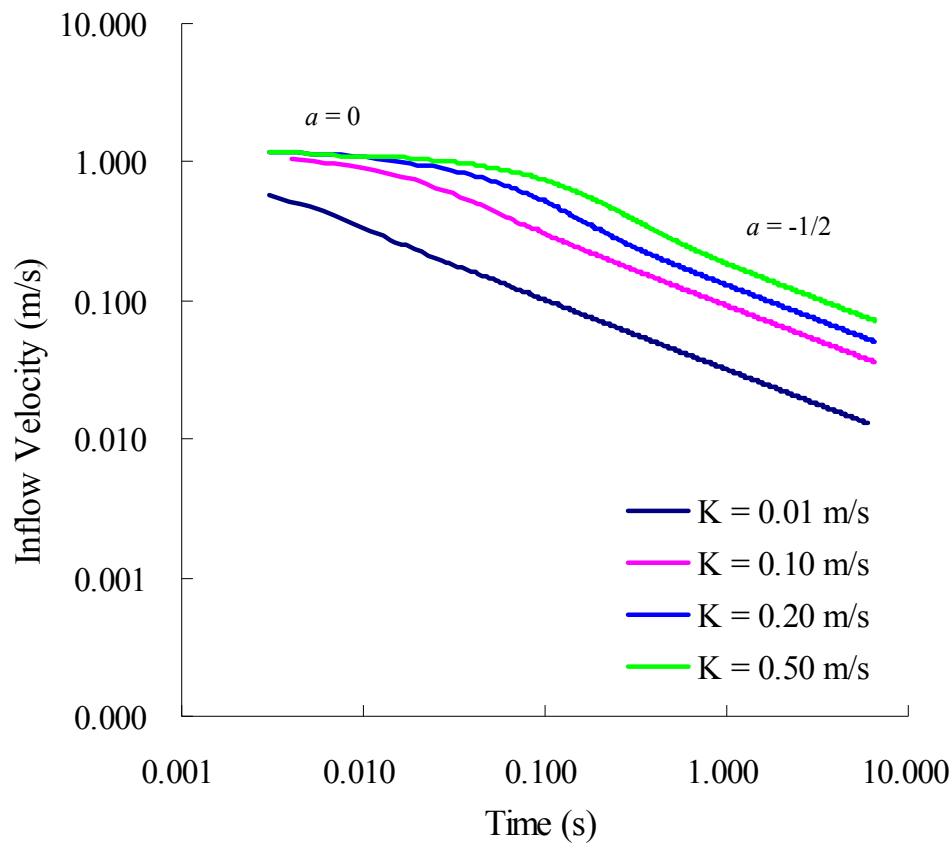
4.8(b)

Figure 4.8 Temporal values of (a) front position (b) entry velocity [case A: h_0 =0.085m]

Following figures are the results of the solution for integral formulation derived for case B. Figs. 4.9(a)-(c) show the plots of front position, depth at the origin and entry velocity with respect to time respectively. These plots clearly show the two flow regimes in the intrusion process. The early impulsive IP regime is followed by relatively milder PD regime. The transition from IP to PD regime is smooth and its occurrence time is highly dependent on the porous media characteristics. We can observe the longer dominance of IP regime in the case of highly permeable porous media. Also there is a clear shift of the transition time as the permeability increases. The values of temporal powers derived from similarity analysis are also shown in figures for comparison. They are in good agreement with the results of integral formulation.
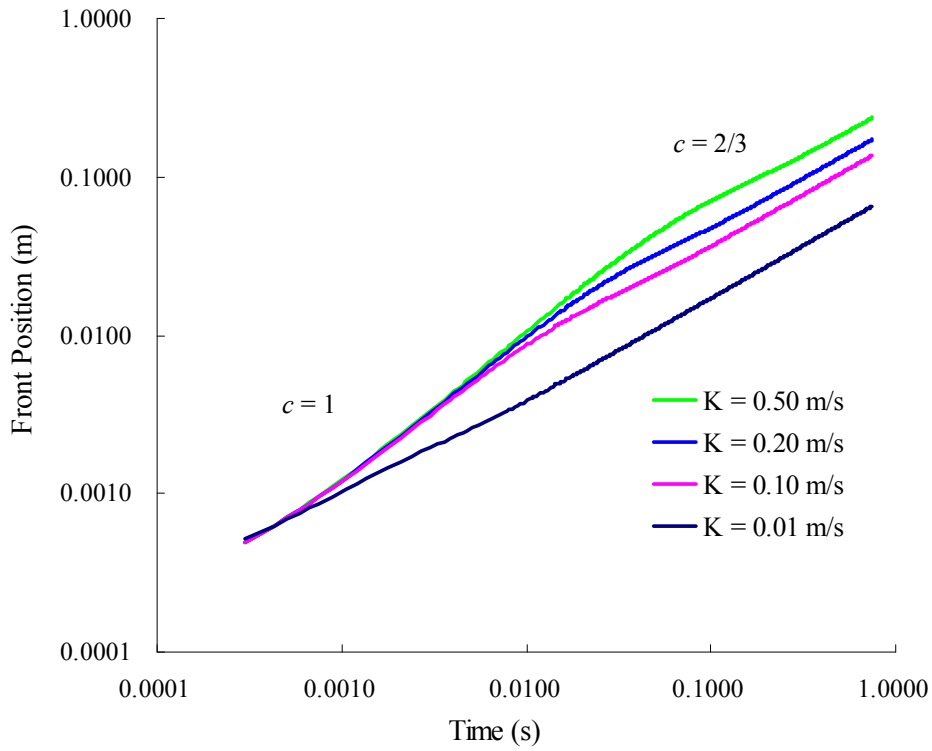
4.9(a)
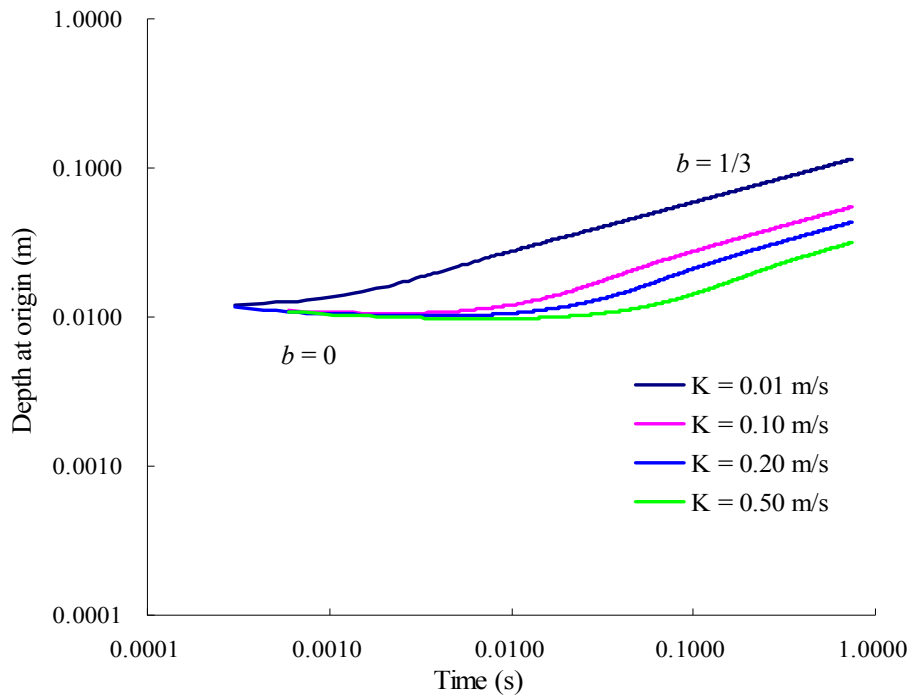
4.9(b)
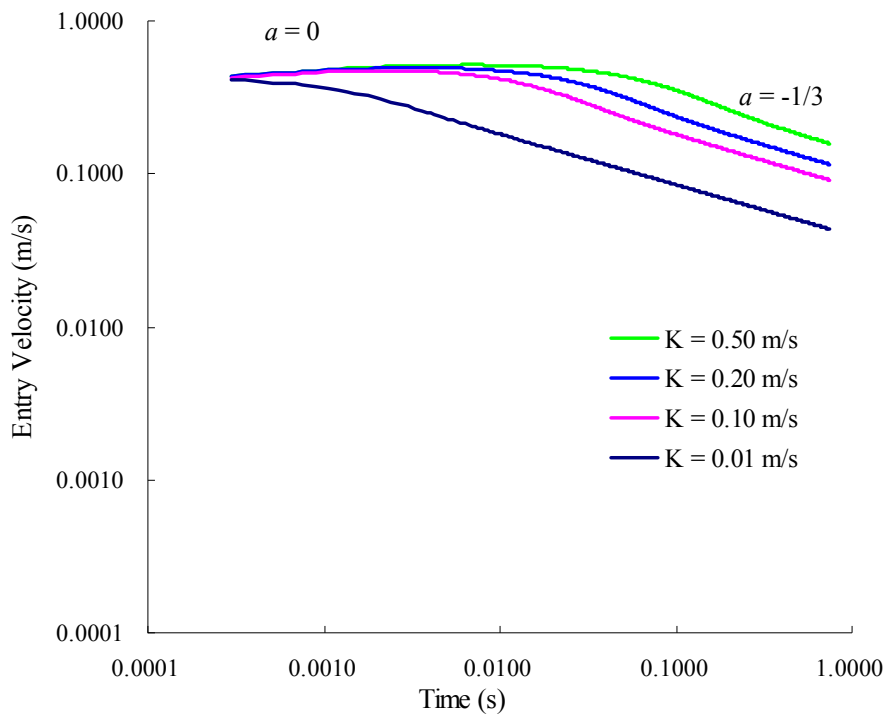
4.9(c)

Figure 4.9 Temporal values of (a) front position (b) depth at origin (c) entry velocity. [case B: q_0 = 5×10^{-03} m^3/s per m]

Integral model results of quadratic resistance law

Following plots are the results of integral model for the turbulent flows where quadratic resistance law is considered. Figs. 4.10(a) and 4.10(b) show the plots for front position and entry velocity with respect to time for pressure inlet condition. The CT value shown on the plots are the inertial coefficients [see Eq.(4.3)] for the square law consideration. The higher CT values means the low permeable porous media. The temporal powers derived are in good agreement with the results of integral models.

Figs. 4.11(a)-(c) show the plots for the turbulent flow with inflow flux boundary condition. In this case also the integral model shows both the flow regimes. The value of temporal powers a, b and c are also shown on the figures. They are in good agreement with the theoretical derivations.
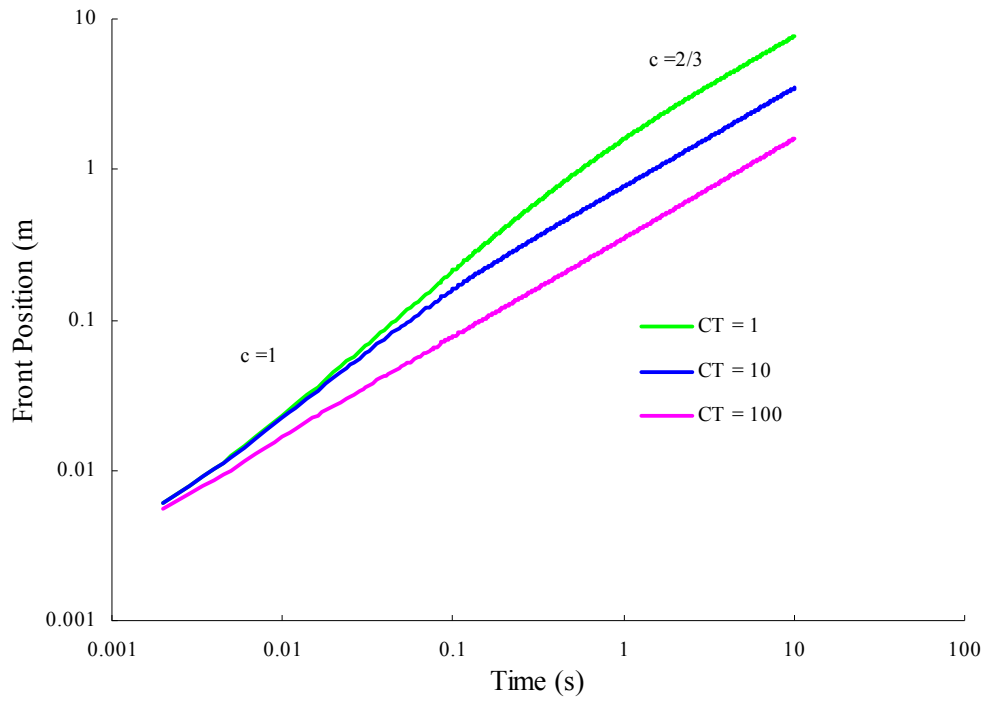
4.10(a)

4.10(b)

Figure 4.10 Temporal values of (a) front position (b) entry velocity. (case A quadratic law : h_0 =0.085m)
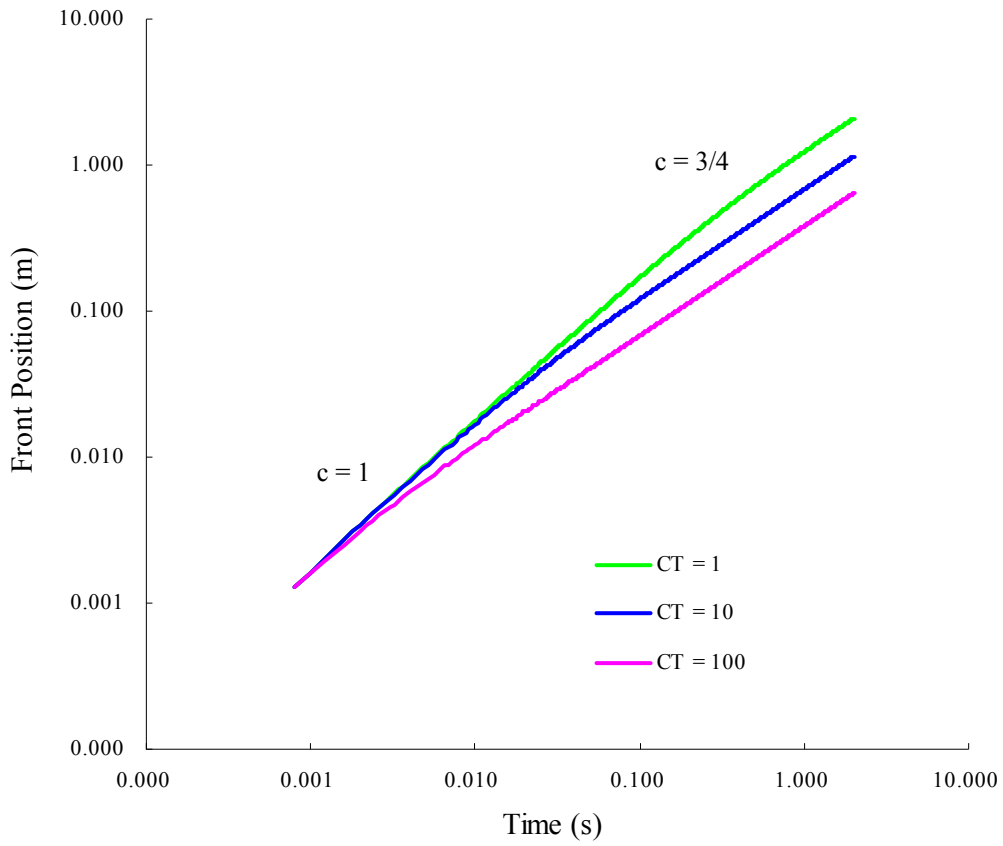
4.11(a)
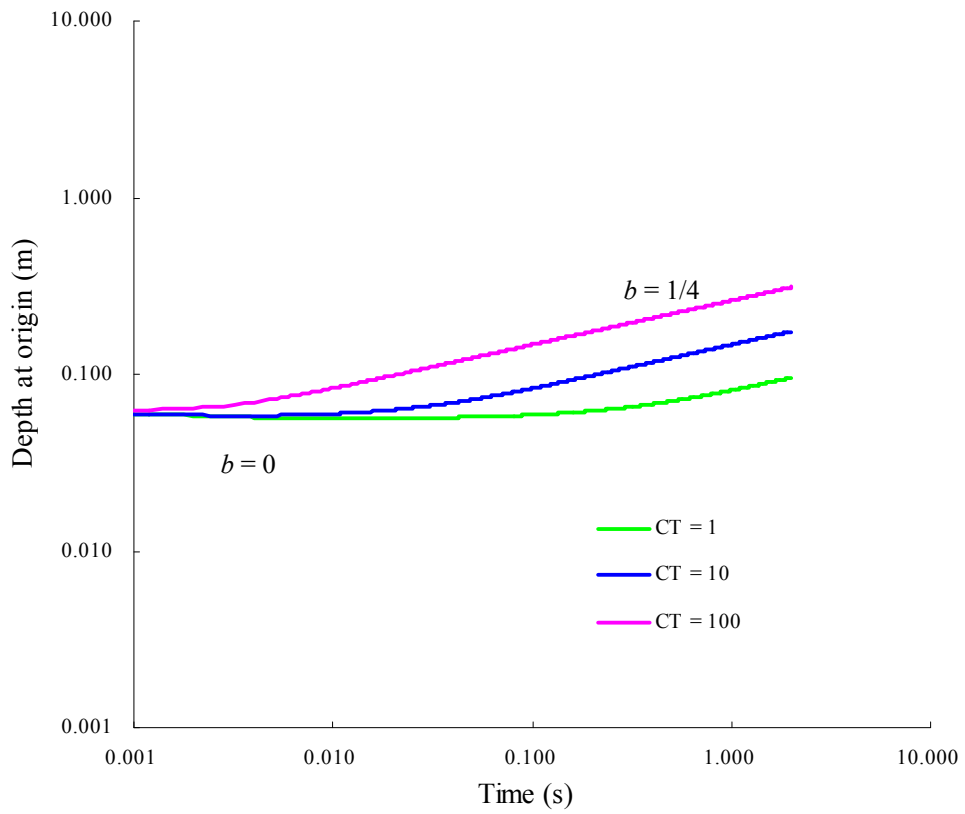
4.11(b)
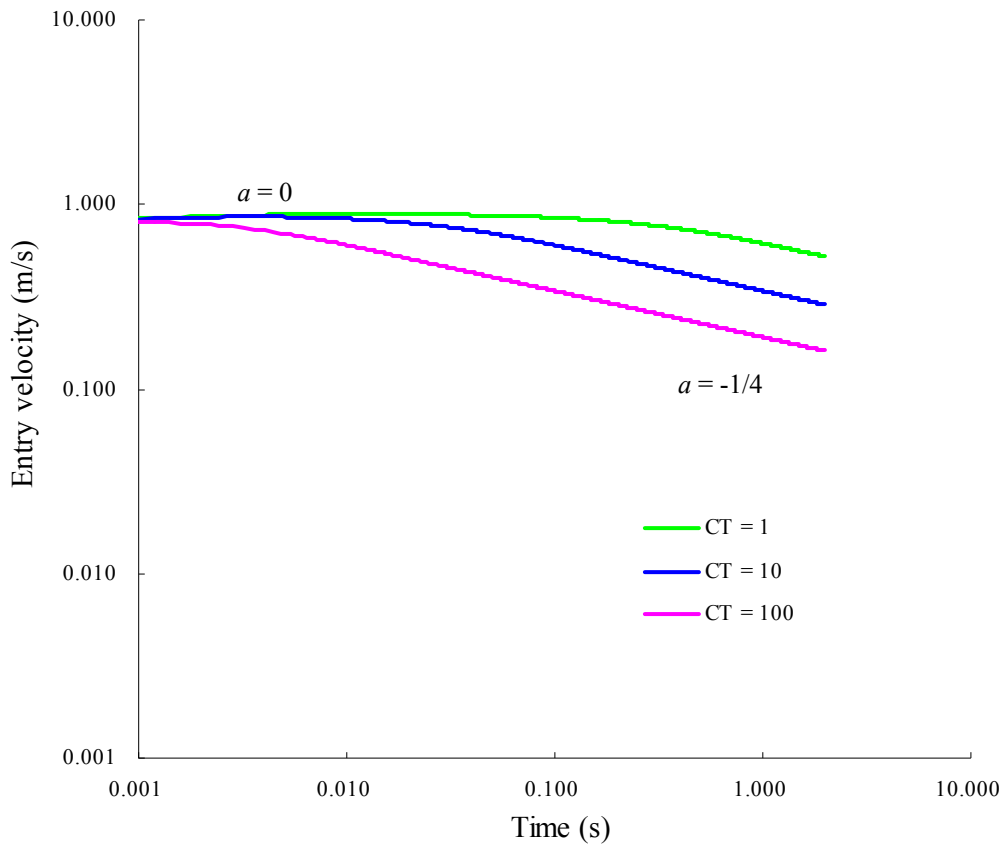
4.11(c)

Fig. 4.11 Temporal values of (a) front position (b) depth at origin (c) entry velocity. [case B quadratic law : $q_0 = 5 \times 10^{-03}$ m^3/s per m]
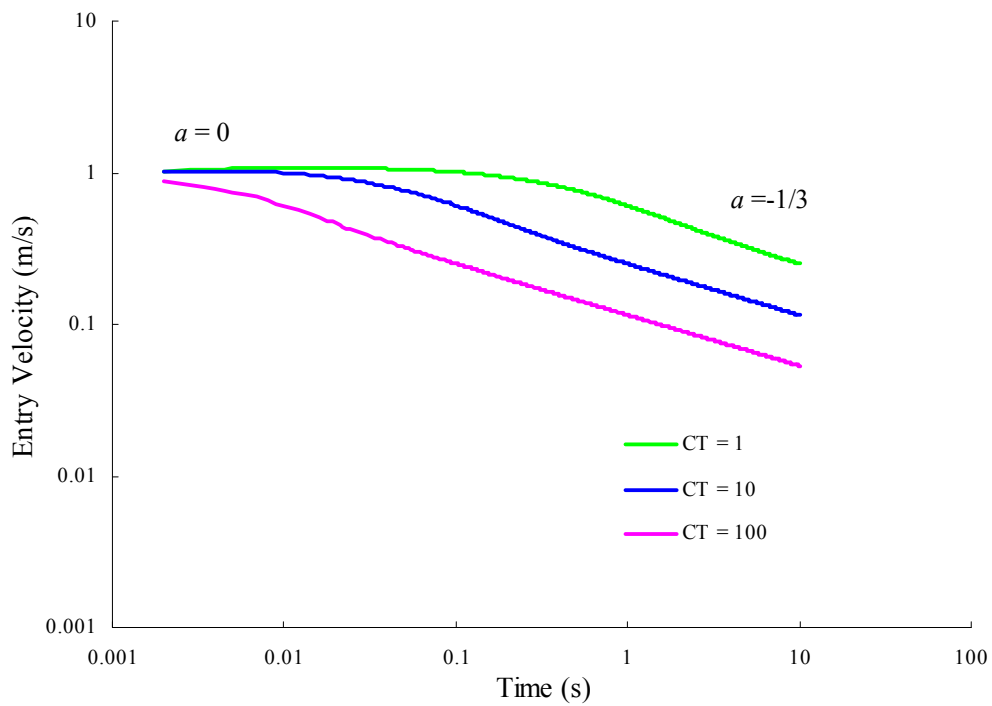
Results from numerical simulation and experiments

In Figs. 4.12 and 4.13, simulated flow profile showing velocity vectors and corresponding flow profile observed during the experiment are shown. The result shows a close agreement between the experiment and numerical simulation.
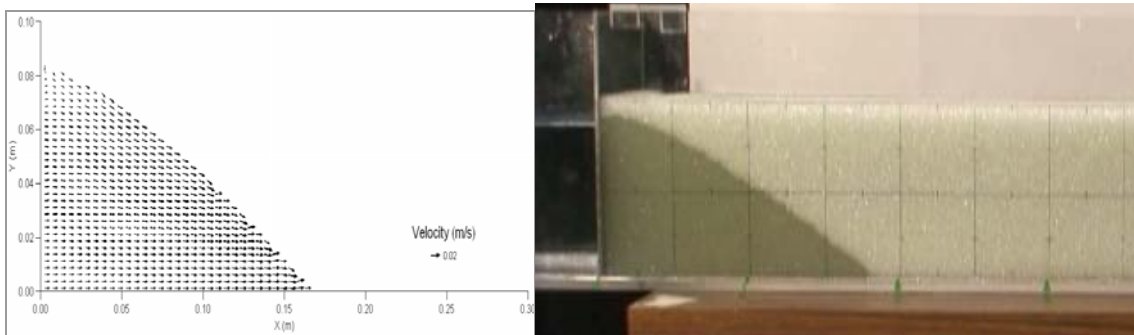
| 4.12 (a) | 4.12 (b) |

Figure 4.12 Flow profile at t = 5s (a) simulation [RUN1] (b) experiment [Expt I.]
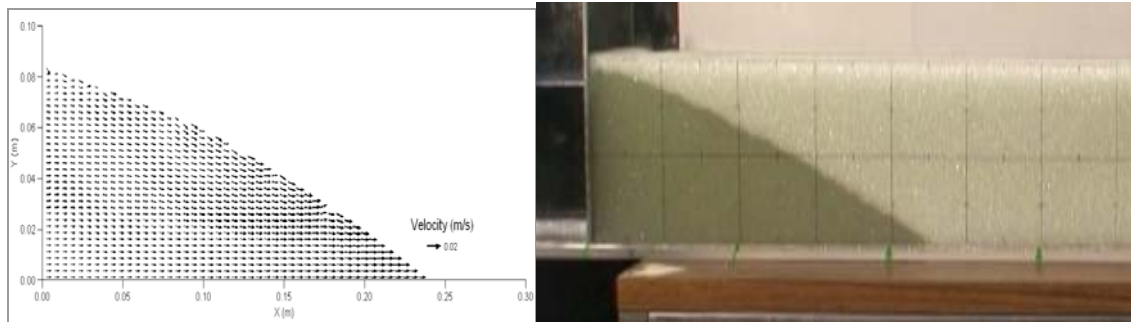
4.13 (a)   4.13 (b)
Figure 4.13 Flow profile at t = 10s (a) simulation [RUN1] (b) experiment [Expt I.]

Comparative results from numerical simulation, integral models and experiment

In the figures below the plots for the flows in porous media having different size and hydraulic conductivity are shown. The position of front in the unsteady free-surface flow inside porous media obtained from integral formulation, numerical simulation and experiment are shown. Figs. 4.14 - 4.16 show a comparison plot of temporal front position as obtained from the numerical run, integral model and the experiment in normal and log-log graphs for porous media of diameters 1mm, 5mm and 12mm respectively. It is also noticed here the PD regime is distinctly dominant for the flow in 1mm glass beads owing to its low permeability value. The discrepancy is very small in the case of 5mm diameter porous media. For the case of 12 mm diameter glass bead (Fig.4.16), the integral model results are confirmative to the square law. Square law for the intrusion through porous media holds good for the porous media of large permeability. The discrepancy in the case of 5mm bead (Fig.4.15) in the early periods might be due to the non confirming distribution of depth in the very early stage, error in the experimental timing etc. However the nonlinear natures of the phenomena are clearly depicted by these integral models.
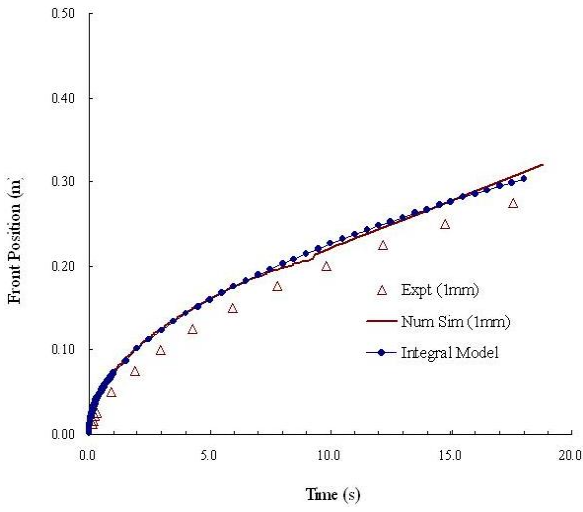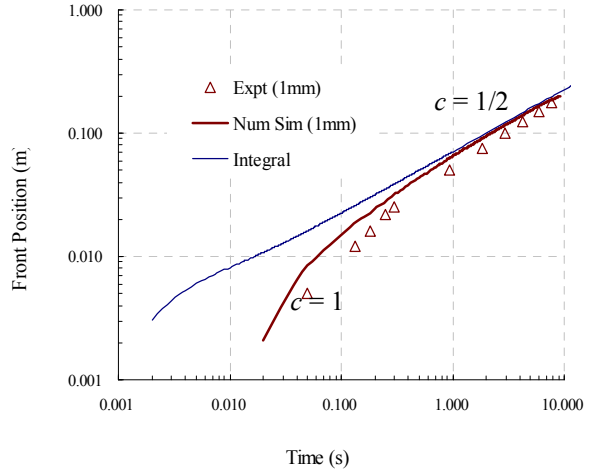
4.14(a)   4.14(b)

Figure 4.14 Temporal front position (a) normal plot (b) log-log plot (1mm glass bead)
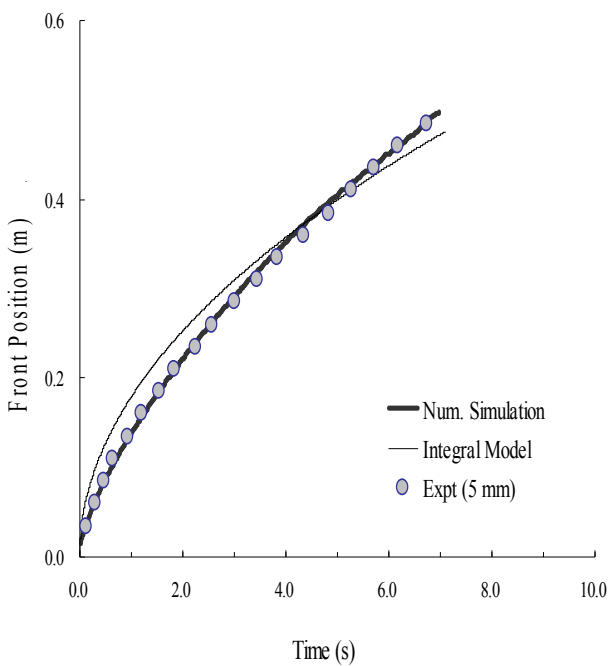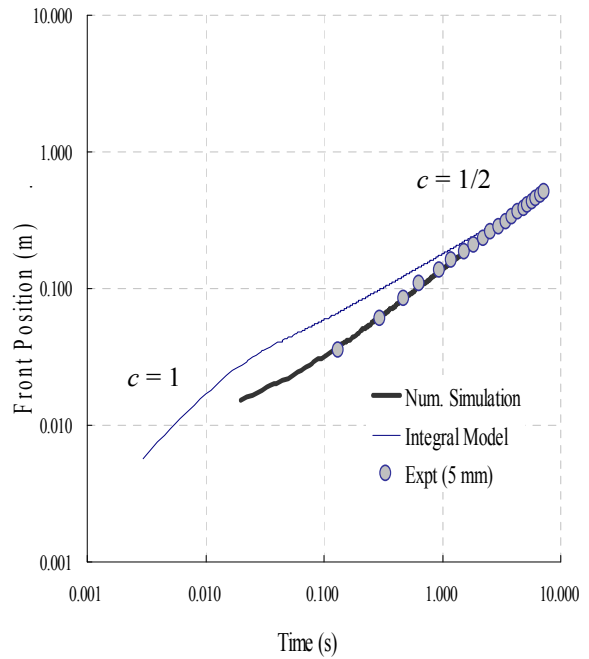
4.15(a)   4.15(b)

Figure 4.15 Temporal front position (a) normal plot (b) log-log plot (5mm glass bead)
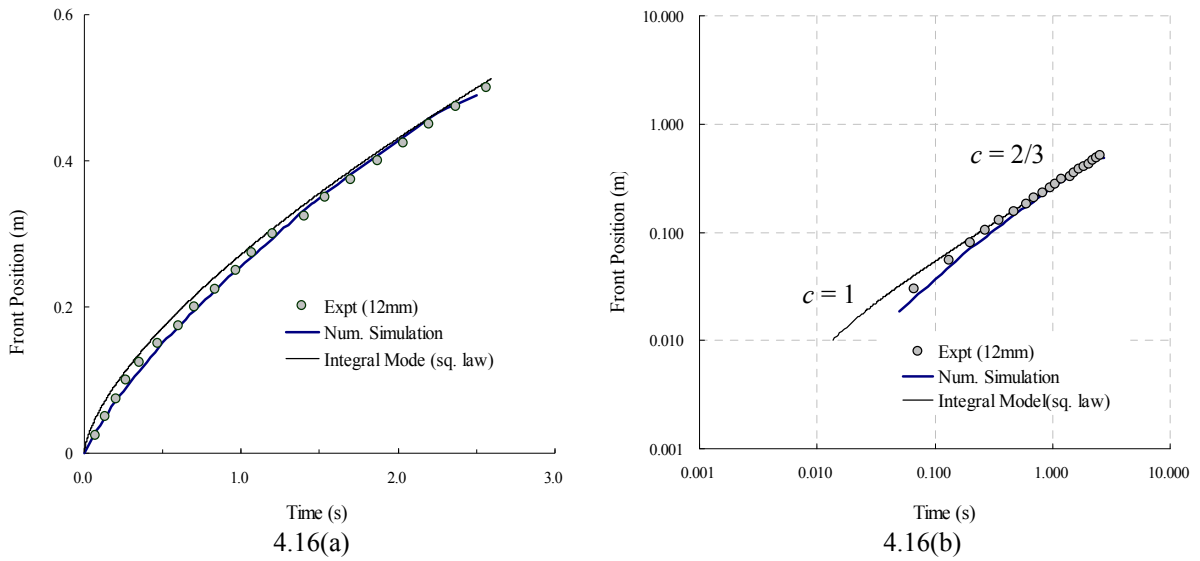
Figure 4.16 Temporal front position (a) normal plot (b) log-log plot (12mm glass bead)

Fig. 4.17 shows a plot for the front position for case B i.e. for flux inlet condition. The results from the integral model and numerical simulation are in good agreement. Integral model results presented here uses linear resistance law. Thus in the case of flux inlet boundary also the spatial integral models work well.
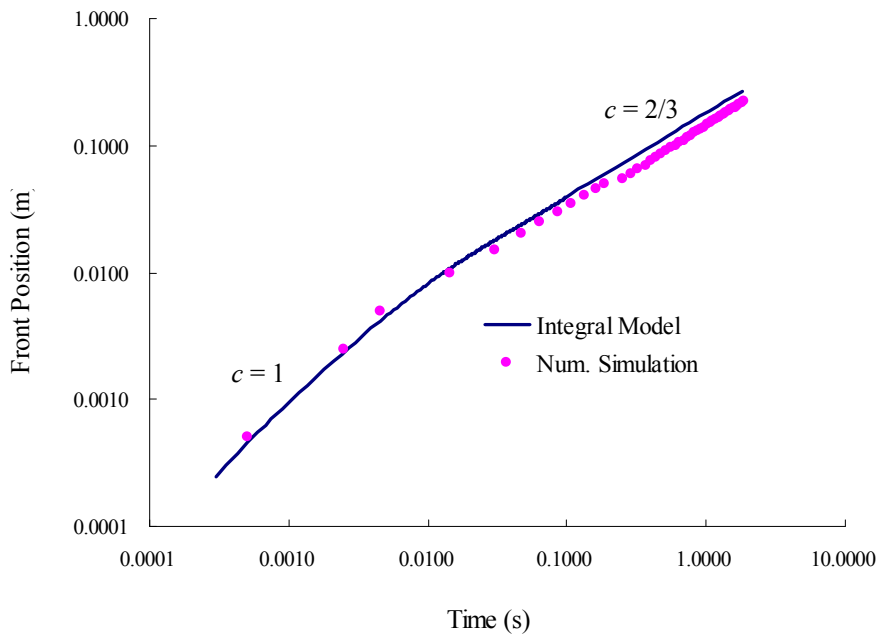
Figure 4.17 Position of front versus time (case B: [RUN 4])

4.10 Summary

Free surface transient flow through porous media has been analyzed for two different inlet conditions. It is pointed out that there are two flow regimes in the intrusion process of fluid into the porous media. An integral formulation for unsteady depth distribution, velocity and front speed under constant water level and constant flux discharge inlet conditions have been developed from similarity law. The two flow regimes are named as Inertia-Pressure (IP) and Pressure-Drag (PD) regimes. The integral models derived represent both IP and PD regimes effectively; where early IP regime is followed by PD regime. The analysis indicates that the integral model clearly represents this nonlinear flow behavior in the porous media. The formulation presented provides additional analytical insight about the intrusion dynamics. In addition, the method proposed can be successfully used for the solution of a host of other nonlinear flow problems that admit self-similarity. The developed solutions for constant inlet water level condition have been verified with the experimental observation. The unsteady distributions of drainage depth, inflow velocity and front speed have been compared for various porous media characterized by its corresponding permeability and porosity. The integral model results are in agreement with those obtained by similarity solution for the temporal change of velocity, depth at the origin and front positions.

We also carried out vertical 2D numerical simulations for the free-surface flow inside the porous media governed by Navier-Stokes type equations extended for porous media flow. The finite volume method is applied along with CIP method and highly simplified marker and cell (HSMAC) type pressure solver for the numerical solution. The evolution of moving free surface is governed by volume of fluid (VOF) method inside porous media. To prevent the spurious oscillation and generate diffusion-free sharp interface, a third order MUSCL-type total variation diminishing (TVD) schemes is used to discretize the convective terms in VOF convection equation. The results of analytical integral models were compared with the results of numerical simulation and hydraulic experiments. The close agreement in the results proves the applicability of the formulation. And also the algorithm used for the numerical solution proves to be a promising tool for the simulation of unsteady free-surface flow through porous media.

Chapter 5

FLOW ANALYSIS FOR A BACKSTEP CHANNEL FILLED WITH POROUS MEDIA

5.1 Introduction

5.1.1 Background

The free-surface flow of an incompressible fluid through a porous medium in a geometrically complicated domain is analyzed in this chapter. Lateral intrusion of water is a physical phenomenon of great importance in a wide range of engineering applications, varying from environmental applications to many industrial filtration processes. Application of such flow includes aquifer studies, contaminant transport studies, filter design, gas coolant system design, geologic flow simulations, groundwater remediation studies, oil exploration studies etc. An important application of porous media flow involves the modeling of unsteady inflow into the porous stratum. The newer technique for the urban flood management is emerging where storm water is allowed to intrude into a road sub-base porous formation. The viscous, laminar incompressible flow with small porosity is represented by Darcy equation (Beavers.and Joseph, 1967; Hanspal et al., 2006). The Darcy law assumes that the inertial force terms in the momentum equation is negligible compared with the other drag force and pressure terms. The law is inadequate in explaining the phenomena occurring near the boundary of the porous

medium bounded by a surface in the case of highly porous medium (K. Yamamoto and N. Iwamura, 1976). For this reason several works have been published by using the generalized Darcy's law where the convective acceleration and viscous-stress are taken into account.

The problem of unsteady gravity flow of liquids through porous media has not been solved by exact potential theory, even for special cases of simple boundary geometry. From Darcy's law and the equation of continuity, it is known that there must exist a velocity potential function that satisfies the Laplace equation. Although the existence of a velocity potential implies irrotational flow, one must remember that since Darcy's law deals only with velocities in a macroscopic and not microscopic way, the flow through a porous medium is not irrotational. Because of the existence of a velocity potential function, one may at first glance think that the problem reduces to one of finding a velocity potential function which satisfies both Laplace equation and the boundary conditions. If, however, one recalls that one of these boundaries, namely the free-surface, is the solution to the problem and hence is unknown a priori, the difficulty inherent in the nature of the problem becomes evident.

Assuming the power law in the front propagation, flow depth at origin and velocity at origin considering similarity transformation, the temporal powers for front propagation, velocity and depth at origin has been already derived for two types of upstream conditions in chapter 4. A simple rectangular channel filled with glass beads as porous media was used to verify the derived powers. Two types of upstream boundary conditions as constant water level and constant discharge at upstream boundary were assumed for the study of the intrusion behavior of the fluid into the porous media. The similarity solutions were also obtained for the assumed distribution of flow depth and velocity.

In this chapter, an attempt is made to derive the temporal power law solutions for a general inflow condition where the inflow discharge varies temporally as t^σ, thus making the solution applicable to account the unsteadiness in the inflow discharge. This power law solution is then applied to the flow in a channel with a backward facing step filled with porous media. The results of the analytical solutions will be compared with the outcomes of 2D-vertical numerical simulation using continuity and momentum equations.

5.1.2 Need of the study

Flood management is a broad spectrum of water resources activities aimed at reducing potential

harmful impacts of floods on people, environment and economy of the region. The main limitation of the current flood management methodologies comes from favoring mostly economic impacts and paying minor attention to the environmental and social impacts of floods. The conventional approach to flood management was based on river-basin oriented programs and plans that were needed during floods to minimize their impact on the individuals and the community. In this context the flow of water inside porous formation could be the interest to many researchers for in-site management of storm water. Also the initiation of the debris flow is another challenging field where the detailed insight of the unsteadiness in the inflow into porous hill slope can be utilized to save life and property.

5.1.3 Motivation for the study

In this study, we deal with the unsteady free-surface lateral intrusion of water into porous media consisting of large grain size, which can be applied to simulate the storm water storage into granular road sub-base from a side ditch, under prescribed boundary conditions. The newer practice for the management of urban flood has developed a concept of managing the flood in its source. On this backdrop the urban flood management using porous sub-base has become the attention of many researchers. The porous stratum acts as a retention basin helping reduce the peak flood flows and hence the damaging effect. In Fig. 5.1, storm water is allowed to intrude the porous formation from the side ditch so that the problem of clogging on the pavement surface can be avoided completely making the facility available for long period. An application of such flow is explained in chapter 8 of this thesis. In this section we check the validity of numerical model and make some analytical derivations for unsteady moving free surface boundary problem.

The fundamental characteristics of lateral intrusion process are firstly investigated theoretically using the depth averaged equations with the inertia term and porous drag force terms in the momentum equation. Assuming the self-similarity distributions of depth and velocity, we derive the power law solutions of intrusion process with the propagation of front position and the depth distribution under general inflow flux as an upstream boundary condition.
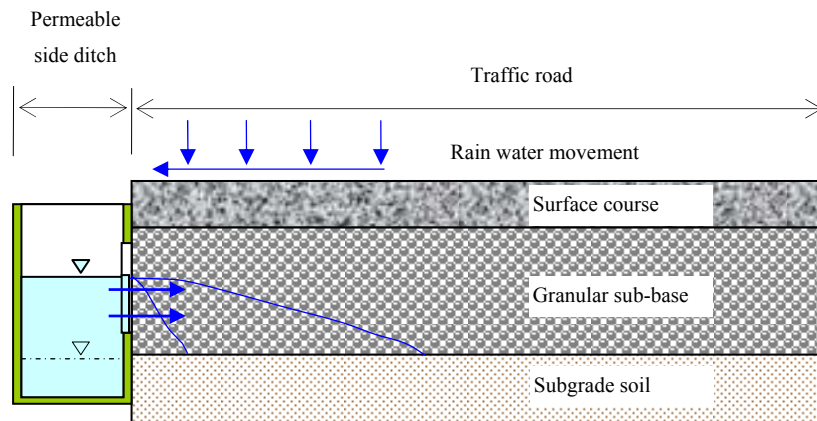
Figure 5.1 Schematic diagram showing lateral intrusion of storm water into porous sub-base from the permeable side drain in a typical road section

The common fundamental equations for solid-liquid multiphase flows with the inertia force term are used as the basic model of this study because the pervious road sub-base material consists of large grain size material and we expect nonlinear inertial effect in the flow. The theoretical results derived in this study are verified by carrying out the numerical simulations and hydraulic experiments.

5.2 Flow domain and boundary conditions

The flow domain and boundaries are shown in Fig. 5.2, in which 1-1 is a pressure boundary and 2-2 a time dependent flux boundary. At the pressure boundary 1-1, the depth of pool is kept at constant level. Due to the decaying nature of the inflow discharge at pressure boundary, the discharge received by the boundary 2-2 can be considered as a time dependent inflow i.e. $q(t) \propto t^{\sigma}$.
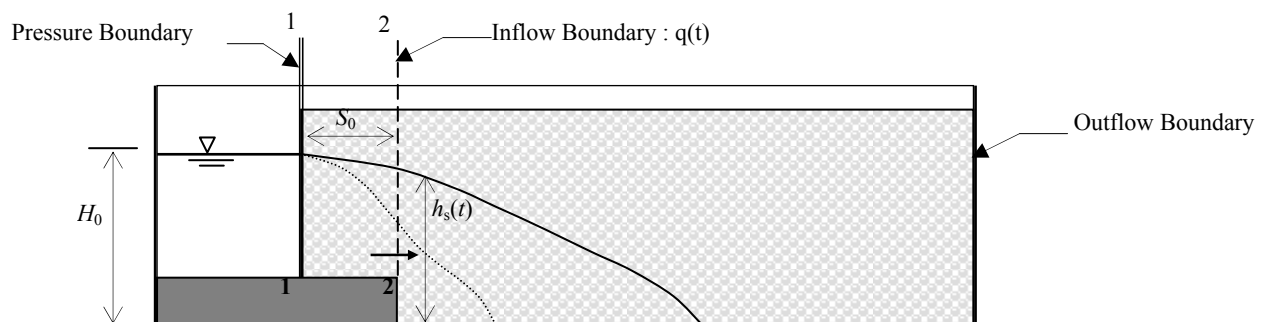
Figure 5.2 A backward-facing step channel filled with glass beads as porous

5.3 Theoretical considerations

5.3.1 Previous works on simple channels

In chapter 4, we derived the power laws for two cases: one with constant water level and other with constant inflow flux at the upstream end in simple rectangular channels filled with glass beads as porous media using similarity principle. Two power law regimes in the unsteady intrusion with free surface were observed namely inertia-pressure (IP) and pressure-drag (PD) regimes. In both the cases, the authors observed the early inertia-pressure regime lasts only for short period followed by the slower pressure-drag regime. The summary of results for different upstream boundary conditions can be seen in the Table 4.1 in the previous chapter. When the upstream boundary was set to a pressure boundary by creating a pool of water at a constant level, the front spreads as $t^{1/2}$. In such case, flow regime was already gone to pressure-drag regime because of the dominance of the pressure and drag forces on the flow. Similar results were also reported in Huppert and Woods [1995]. The decay of inflow discharge in the intrusion process was observed as $t^{-1/2}$. On the other hand in the case when the upstream boundary of the domain is subjected to a constant inflow flux, the spreading of the front in the dominance of the PD regime was observed as $t^{2/3}$. The depth at the origin varied as $t^{1/3}$ at the same time. These results are utilized to investigate a complex flow phenomena in a channel, having backward facing step, filled with porous media.

5.3.2 Power law analysis for time dependent flux inflow

Following set of continuity and momentum equations are taken for the intrusion analysis subjected to the boundary conditions as explained.

$$\frac{\partial h}{\partial t} + \frac{\partial hU}{\partial x} = 0 \tag{5.1}$$

$$\frac{\partial U}{\partial t} + U\frac{\partial U}{\partial x} + g\frac{\partial h}{\partial x} = -C_L U \tag{5.2}$$

with the parameters having their usual notation.

The same method as applied for constant discharge inflow is applied here based on the similarity law. The similarity transformation reduces the number of independent variables in the problem. The governing partial differential equations are reduced to ordinary differential

equations in the transformed co-ordinates. A time dependent phenomenon is said to be self-similar if the spatial distribution of its properties at different times can be obtained from one another by a similarity transformation. Consider the solution, $U(x, t)$, of a partial differential equation. We introduce a coordinate transformation,

$$\xi = \frac{x}{l(t)} \tag{5.3}$$

where $l(t)$ is a time dependent scale function for x. If $U(x, t)$ is self-similar, there will be two scale functions $l(t)$ and $U_0(t)$, so that the solution $U(x, t)$ can be represented by,

$$U(x,t) = U_0(t)G(\xi) \tag{5.4}$$

The coordinate transformation by Eq. (5.3) is called a similarity transformation. Choosing $U_0(t)$ as a scale for the solution $U(x, t)$, we can represent this scaled solution by $G(\xi)$. Thus, we have transformed the time-dependent problem into a steady-state problem, for new (self-similar) coordinates $\frac{U(x,t)}{U_0(t)}$ and ξ. The partial differential equation is then reduced to an ordinary differential equation. In this section, we derive the power law solutions considering the possible flow regimes under the prescribed inflow boundary conditions. The distribution of velocity at the origin U_0, depth at origin h_0, and the front position l are expressed by the temporal power a, b and c as,

$$U_0 = \alpha V_0 \left(t'\right)^{a}; \quad h_0 = \beta L_0 \left(t'\right)^{b}; \quad l = \gamma L_0 \left(t'\right)^{c} \tag{5.5}$$

In above expressions non-dimensional time $t' = t/T_0$ is used. where α, β and γ are the constant coefficients; V_0, L_0 and T_0 are the characteristic velocity , length and time respectively. It will be shown that the power laws with respect to time given by equation (5.5) are valid for the dominance of the combination of two terms of inertia-pressure and pressure-drag regimes. The similarity distributions of the depth $h(x,t)$ and velocity $U(x,t)$ are defined as,

$$h = h_0 F\left(\xi\right); \quad U = U_0 G\left(\xi\right) \tag{5.6}$$

where the functions F and G are the similarity distribution functions for depth and velocity. Now, we derive the temporal powers a, b and c for the condition where upstream boundary is set as a flux boundary i.e. there is inflow discharge q which is proportional to t^{σ} (see Fig. 5.3), where σ is any constant index.
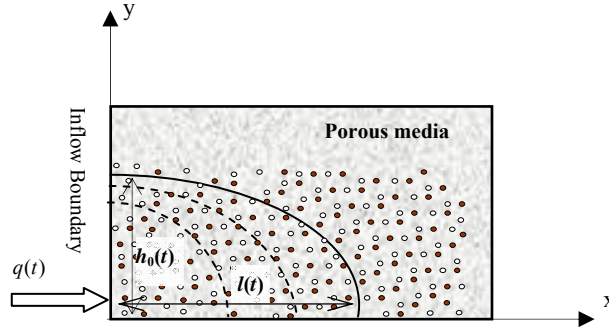
Figure 5.3 Definition sketch of the domain subjected to inflow boundary

The characteristic time, length and velocity are defined as,

$$T_0 = \left(\frac{Q_0}{g^2}\right)^{\frac{1}{3}}, \quad L_0 = \left(\frac{Q_0^2}{g}\right)^{\frac{1}{3}} \quad \text{and} \quad V_0 = (gQ_0)^{\frac{1}{3}} \tag{5.7}$$

where Q_0 is any reference inflow discharge. Using Eqs. (5.5) through (5.7), the equations for continuity and momentum as expressed by Eqs. (5.1) and (5.2) are reduced to Eqs. (5.8) and (5.9) as below,

$$F\frac{dh_0}{dt} - \frac{h_0}{l}\xi\frac{dl}{dt}\frac{dF}{d\xi} + q_0\frac{1}{l}G\frac{dF}{d\xi} + q_0\frac{1}{l}F\frac{dG}{d\xi} = 0 \tag{5.8}$$

$$G\frac{dU_0}{dt} - \frac{U_0}{l}\xi\frac{dl}{dt}\frac{dG}{d\xi} + \frac{U_0^2G}{l}\frac{dG}{d\xi} + g\frac{h_0}{l}\frac{dF}{d\xi} = -C_LU_0G \tag{5.9}$$

On simplification of above transformed equations for continuity and momentum using Eq. (5.5), we get following equations

$$\frac{BL_0}{T_0}bt'^{b-1}F - \frac{BL_0}{T_0}c(t')^{b-1}\xi\frac{dF}{d\xi} + \frac{E(t')^{\sigma-c}}{\gamma L_0}\frac{d(GF)}{d\xi} = 0 \tag{5.10}$$

$$\underbrace{\frac{AV_0}{T_0}at'^{a-1}G - \frac{AV_0}{T_0}ct'^{a-1}\xi\frac{dG}{d\xi}}_{\text{inertia (unsteady)}} + \underbrace{\frac{A^2V_0^2}{\gamma L_0}t'^{2a-c}G\frac{dG}{d\xi}}_{\text{inertia (convection)}} + \underbrace{\frac{B}{\gamma}gt'^{b-c}\frac{dF}{d\xi}}_{\text{pressure}} = \underbrace{-C_LAV_0t'^aG}_{\text{drag}} \tag{5.11}$$

The general inflow condition is given by $q = Dt^\sigma = DT_0^\sigma(t')^\sigma = Et'^\sigma$, where D and E are simply proportionality constants.

For the inflow boundary, we have

$$U_0h_0 = q \quad \text{or} \quad \alpha\beta V_0L_0t'^{a+b} = Et'^\sigma$$

i.e. $\qquad a + b = \sigma$ (5.12)

From transformed continuity Eq. (5.10), we have

$$b + c = \sigma + 1$$ (5.13)

For the determination of the values of power coefficients *a*, *b* and *c* each combination of Eq. (5.11) such as inertia-pressure and pressure-drag terms are taken and solved for. The results are shown below and Table 5.1 as well.

(a) Inertia-Pressure Regime

$$a = \frac{\sigma}{3}, \quad b = \frac{2\sigma}{3} \quad and \quad c = \frac{\sigma + 3}{3}$$ (5.14)

(b) Pressure-Drag Regime

$$a = \frac{\sigma - 1}{3}, \quad b = \frac{2\sigma + 1}{3} \quad and \quad c = \frac{\sigma + 2}{3}$$ (5.15)

(c) Inertia-Drag Regime

No solution obtained in this regime

Table 5.1 Summary of power law derivation for general inflow discharge

Assumed power law	Constant Water Level* [h_0 = const.]		Constant Discharge* [σ =0]		Time Dependent Discharge [q=Dt^σ]	
	IP	PD	IP	PD	IP	PD
$U_0 = \alpha V_0 t'^a$, $h_0 = \beta L_0 t'^b$, $l = \gamma L_0{}^c$; where α, β and γ are constant coefficients.	$a = 0$ $b = 0$ $c = 1$	$a = -1/2$ $b = 0$ $c = 1/2$	$a = 0$ $b = 0$ $c = 1$	$a = -1/3$ $b = 1/3$ $c = 2/3$	$a = \sigma/3$ $b = 2\sigma/3$ $c = (\sigma + 3)/3$	$a = (\sigma - 1)/3$ $b = (2\sigma + 1)/3$ $c = (\sigma + 2)/3$

* : These values are rewritten here for comparison

The theoretical results derived in this study are verified by carrying out the numerical simulations and hydraulic experiments. The vertical 2-D numerical simulation is done applying the finite volume method coupled with VOF method.

5.3.3 Application to back-step channel

The results obtained for the temporal powers so far are applied to an unsteady free-surface flow in a backward facing step channel. Due to very short negligible IP regime time we consider only the dominating PD regime. At the flux boundary 2-2, the depth $h_s(t)$ also varies as $(2\sigma+1)/3$ power of time t. The front position, after it crosses the brink of the step, varies as $(\sigma+2)/3$ power of time t.

To determine the values of *a b* and *c* for this typical flow problem, we first find the relationship of σ with any one of *a b* and *c* then numerical value of *a b* and *c* is possible for flow regime after it crosses the brink of the step.

After flow regime enters pressure-drag regime the front propagates as $t^{1/2}$ i. e. *c* = 1/2 which we have already proved for the constant water level at the upstream boundary. It can also be shown that the conventional Darcy law corresponds to this pressure-drag regime. Referring to Fig. 5.4, in which a simple porous stratum is subjected to constant water depth at its left boundary. Under the assumption of classical Darcy law and considering
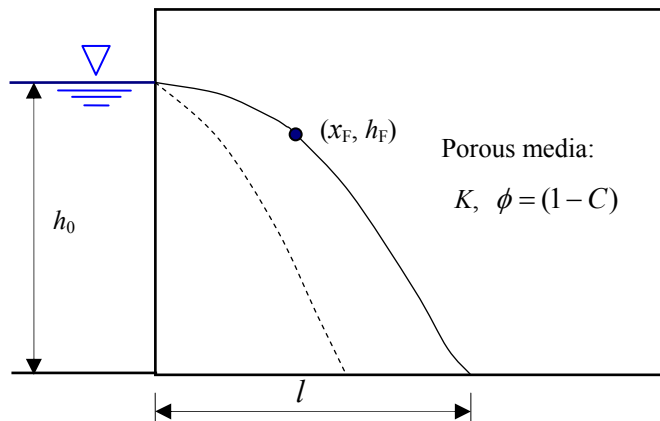
Figure 5.4 Intrusion under constant water depth

horizontal direction, for a point on the phreatic surface, we can write

$$u_D = K\,\frac{h_0 - h_F}{x_F}$$

$$\text{or,} \quad \phi u = K\,\frac{h_0 - h_F}{x_F} \tag{5.16}$$

where u_D is the Darcy's superficial velocity, ϕ is porosity and u is pore scale horizontal velocity. Using $\partial x_F/\partial t$ for u and on integration Eq. (5.16) after variable separation technique, we get,

$$l = \left(\sqrt{\frac{2Kh_0}{\phi}} \right) t^{\frac{1}{2}} \tag{5.17}$$

Eq. (5.17) shows that in Darcy flow, the front length is proportional to $t^{\frac{1}{2}}$. Hence we can write

$$c = 1/2$$

$$\therefore \quad \frac{\sigma+2}{3} = 1/2$$

hence, $\qquad \sigma = -1/2$ $\hspace{4cm}$ (5.18)

which is also true for the decaying of velocity proportional to $t^{-1/2}$ because as h_0 is constant we can deduce $q_0 \propto t^{-1/2}$. This can also be obtained if one considers the flux inflow, the powers for the front position and considering inflow volume.

Now using equation (5.18) in equation (5.15), we get

$$\sigma = -\frac{1}{2}, \quad a = -\frac{1}{2}, \quad b = 0 \quad \text{and} \quad c = \frac{1}{2} \tag{5.19}$$

These powers are verified using Numerical run using extended Navier-Stokes equation for porous medium by CIP method.

5.4 Experimental set up

Experiments were carried out in a rectangular channel having an impervious backward facing step filled with homogeneous (5mm, 12mm) porous media. The unsteady flow under constant water level at left boundary was made in the perspex channel as shown in Fig. 5.5.

The tank was filled with water to a depth H_0 above the bed level. The experiment starts when the gate is removed instantaneously at $t = 0$, leaving the water to flow out along the porous stratum. The released water also flows downwards through the bed to the lower part of the channel. A grid drawn equidistant at 50 mm on the sidewall of the tank facing the video camera enabled the determination of the position of front and flow profile as a function of time. The experiment was carried out separately for 5.0mm and 12mm diameter spherical glass beads as porous media in which water intrudes and runs on a solid impervious bottom. By analyzing the
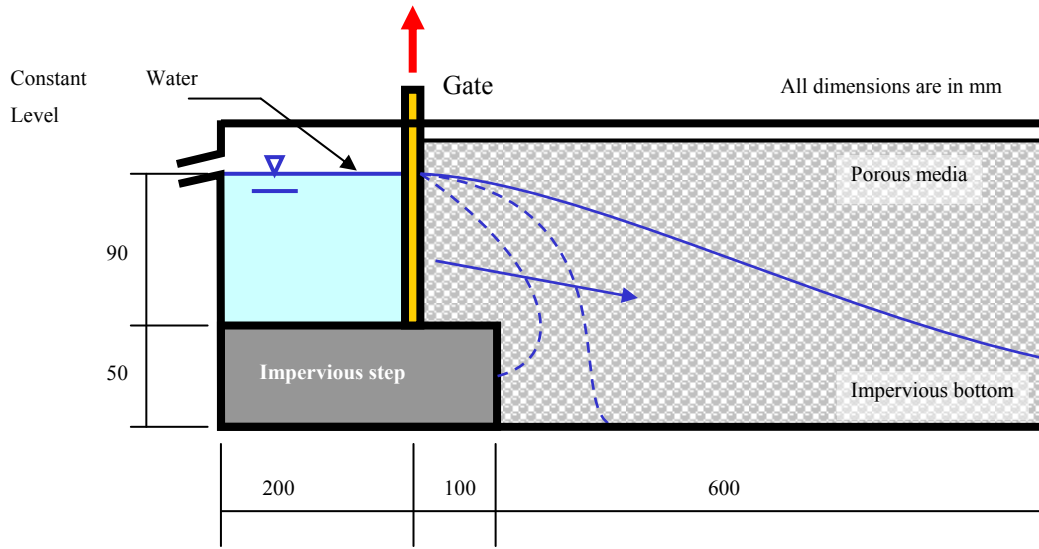
Figure 5.5 Experimental setup for back step full porous channel flow

digitized images taken from the video camera, the flow profile within the porous substrate, comparisons were made with that of the result from simulation and analysis. The bottom of the porous substrate is impermeable as shown.

5.5 Numerical Simulation

5.5.1 Governing Equation

The free-surface flow of viscous and incompressible fluid in porous media is governed by a set of continuity and extended Navier-Stokes equations with porous drag resistance terms as given below

$$\frac{\partial (1-C)u_i}{\partial x_i} = 0 \tag{5.18}$$

$$\rho \left[\frac{\partial (1-C)u_i}{\partial t} + \frac{\partial (1-C)u_i u_j}{\partial x_j} \right] = (1-C)\rho g_i - \frac{\partial (1-C)p}{\partial x_i} + \frac{\partial}{\partial x_j}\left((1-C)\mu \frac{\partial u_i}{\partial x_j} \right) + R_i \tag{5.19}$$

where u_i is the velocity vector, also called the pore water velocity in the porous medium, C is the volumetric concentration of the solids in the porous medium, R_i the flow resistance term due to porous medium and p the pressure. and μ dynamic viscosity of the fluid.

The total drag resistance force per unit volume of the fluid for a wide range of flow is

expressed by Ergun equation

$$R_i = -\left[\frac{\mu(1-C)^2 u_i}{k} + \rho \frac{F_{ch}(1-C)^3 u_i |u_i|}{\sqrt{k}} \right] \tag{5.20}$$

where k and F_{ch} are the permeability(m^2) and Forcheimer's inertia factor. For a randomly packed bed of spheres such coefficients can be expressed in terms of the solid concentration C and the mean diameter of the particles d_p in the porous medium as

$$k = \frac{(1-C)^2 d_p^{\;2}}{150 C^2}; \quad F_{ch} = \frac{1.75}{\sqrt{150}\sqrt{(1-C)^3}} \tag{5.21}$$

In the present study the second term known as Forchheimer' term in the Eq. (5.21) is assumed to be negligible for the assumption of linear resistance rule.

Boundary condition and free surface evolution

The model had been already tested by the authors for two types of upstream boundary conditions: constant discharge boundary and constant water level boundary in chapter 4. Here in the case of back-step channel, left boundary is treated as Dirichlet boundary condition where hydrostatic pressure due to water pool is supplied. At the bottom and impervious surfaces of the channel slip condition is applied to simulate the smooth perspex surface. The downstream boundary is treated as a Neumann type where zero gradient condition for velocity and pressure is applied to ensure the outflow boundary. At the free surface of the flow, the atmospheric pressure condition is applied. The free surface evolution inside the porous media is an important feature of this study. The evolution of the free surface is traced using VOF method [Hirt and Nichols, 1981]. The time evolution of the free-surface flow inside the porous domain is governed by the following equation, for incompressible fluids,

$$\frac{\partial (1-C)f}{\partial t} + \frac{\partial u_i (1-C)f}{\partial x_i} = 0 \tag{5.22}$$

where $(1-C)$ represents the fractional saturation of fluid in a cell. Equation (5.22) is the material derivative of the saturation volume of fluid within a cell [Jacimovic et al., 2005]. This equation is solved after the velocity field is calculated because the position of fluid surface cannot be known a priori.

5.5.2 Solution algorithm

The governing equations (5.18) and (5.19) are solved numerically on a uniform staggered Cartesian grid by finite volume method. The constrained interpolated propagation (CIP) method [Yabe and Aoki, 1991a, 1991b] is adopted as the base scheme for the solution.The numerical solution of the governing equations are carried out using *non-advection* and *advection phase* as explained in chapter 3.

5.6 Results and discussion

The experimental setup shown in Fig. 5.5 corresponds to the application of the model in full porous back-step channel flow. The lock release gate is provided at the left boundary of the channel along with the arrangement for maintaining water level constant. Both the speed of the front and the time evolution of the free surface during the experiment were recorded by a high speed video camera. The time recorded for the front to reach the right boundary during the experiment and the steady-state discharges measured and simulated are given in Table 5.2 which shows a close agreement in the numerical result and the experiment.

Table 5.2: Comparison between numerical simulation and experiment

S.N.	Bead Size (mm)	Steady state discharge (m^3/s per m)			Time to reach d/s end (s)		
		Expt.	Sim.	Error %	Expt.	Sim.	Error %
1	5.0	0.00101	0.00115	13.8	12.733	12.0	-5.76
2	12.0	0.00173	0.00181	4.6	4.967	4.50	-4.37

Figs. 5.6 and 5.7 below show the flow profile inside the porous media with free surface at different times of the simulation and corresponding photograph of the experiment side by side. The last figure with its corresponding photograph refers to the steady state profile. The left figures are the results of the numerical run and the figures at right are taken during experiment. For the numerical results vector plot profile is drawn for the fluid region so the free surface is easily understood. There is close agreement between the experiment and numerical results.

Following figures show the free surface evolution and velocity profiles inside the porous media (5mm) during numerical and experimental run.

5.5(a)

5.5(b)

5.5(c)

5.5(d)

Figure 5.6   Free surface and velocity profiles in a back step channel filled with 5.00 mm bead as porous media at time **(a)** 1.00s **(b)**3.75s **(c)** 13.00s and **(d)** 20.00s

Following figures show the free surface evolution and velocity profiles inside the porous media (12mm) during numerical and experimental run.

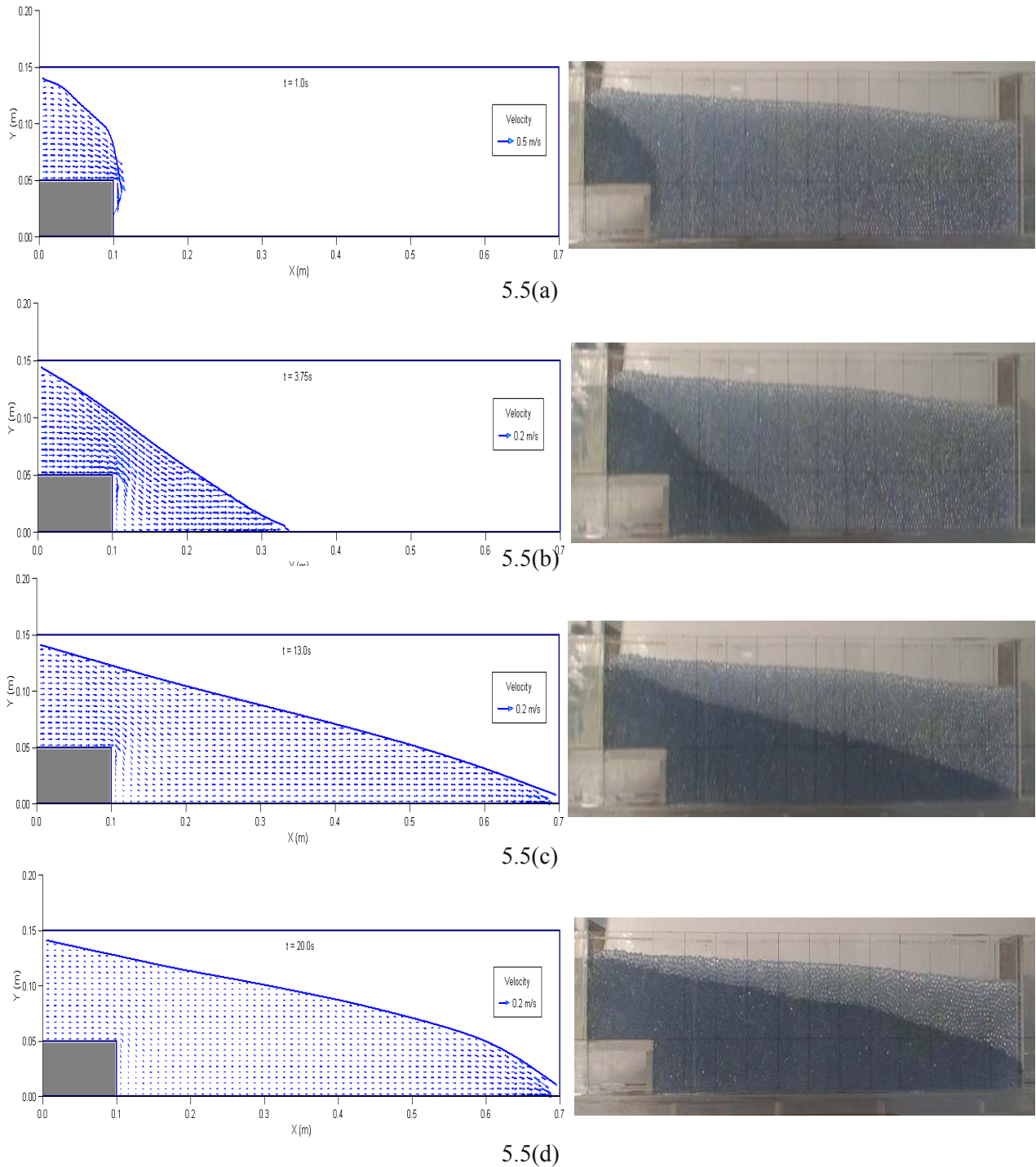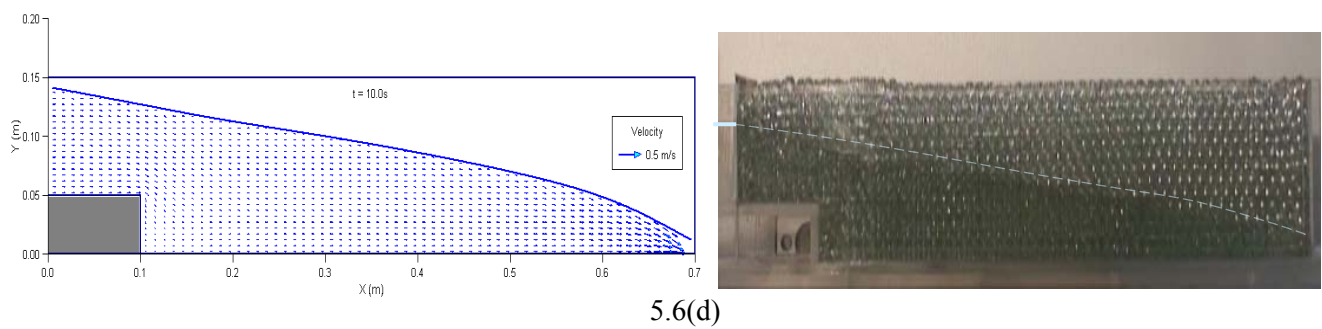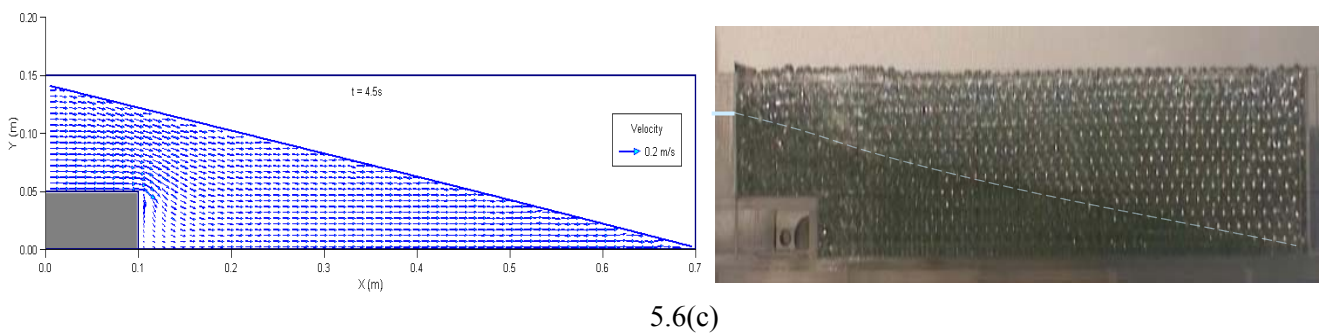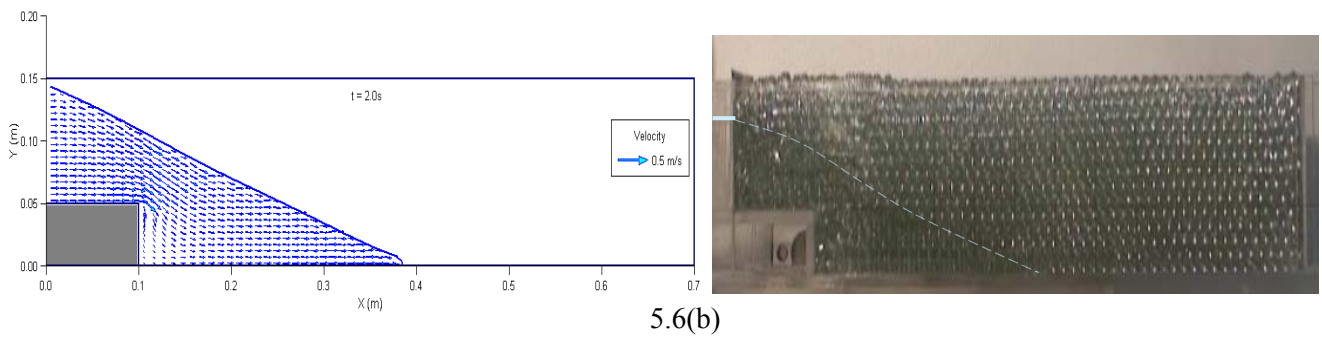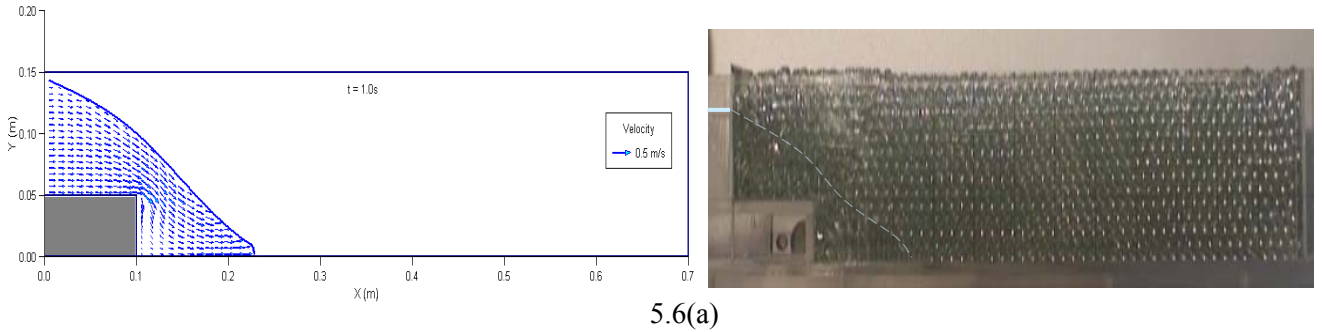5.6(a)

5.6(b)

5.6(c)

5.6(d)

Figure 5.7 Free surface and velocity profiles in a back-step channel filled with 12 mm bead as porous media at time **(a)** 1.0s **(b)** 2.0s **(c)** 4.50s and **(d)** 10.0s

Figure 5.8 below shows the inflow discharge at the leftmost boundary as a function of time. The plot shows that there is a clear decay of the inflow discharge and hence the inflow velocity owing to the fact that pressure gradient goes on decreasing as the flow forwards in later stages. The inflow discharge rapidly decays for very short time period and then becomes gradual approaching to a steady value. The two flow regimes: IP regime and PD regimes can be easily observed in the figure. During very early period the difference for two types of porous media is not so prominent but at later stage the difference becomes larger.
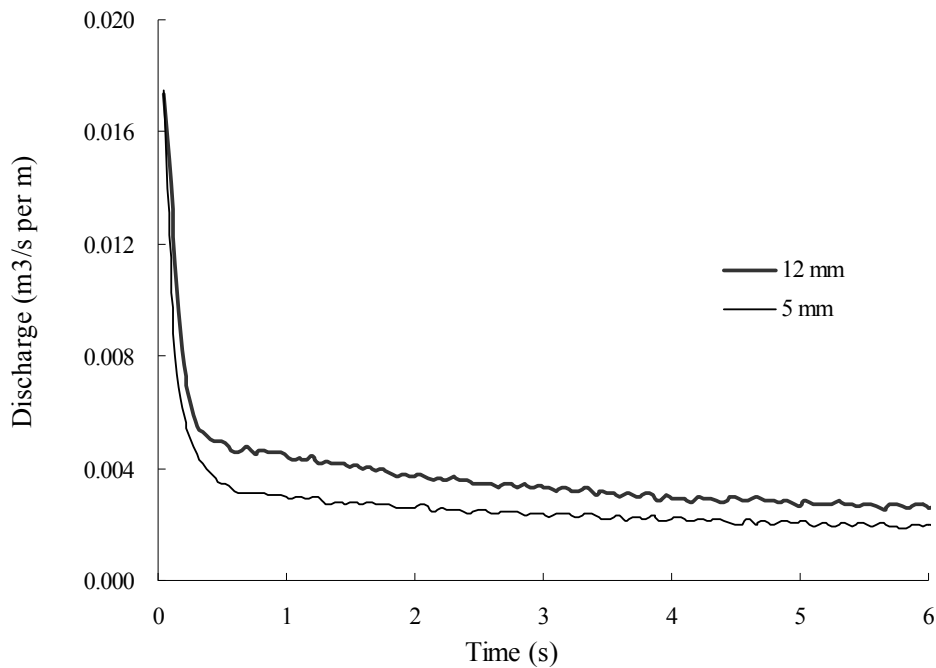
Figure 5.8 Inflow discharge for different sized beads ($H_0 = 0.90$m)

Figure 5.9 shows the log-log plot of the position of front versus time. The plot shows some discrepancies in the early inertial period but the result becomes closer in later phases after the flow regime enters into Pressure-Drag regime. The saddle in the curve represents the filling of the corner just after the brink of the step. Thus unsteady nature of the flow is clearly accounted by the model. The steep initial inertial-pressure regime lasts for very short period followed by a mild and steady pressure-drag regime. The temporal powers for corresponding variables are also shown on the plots for comparison.
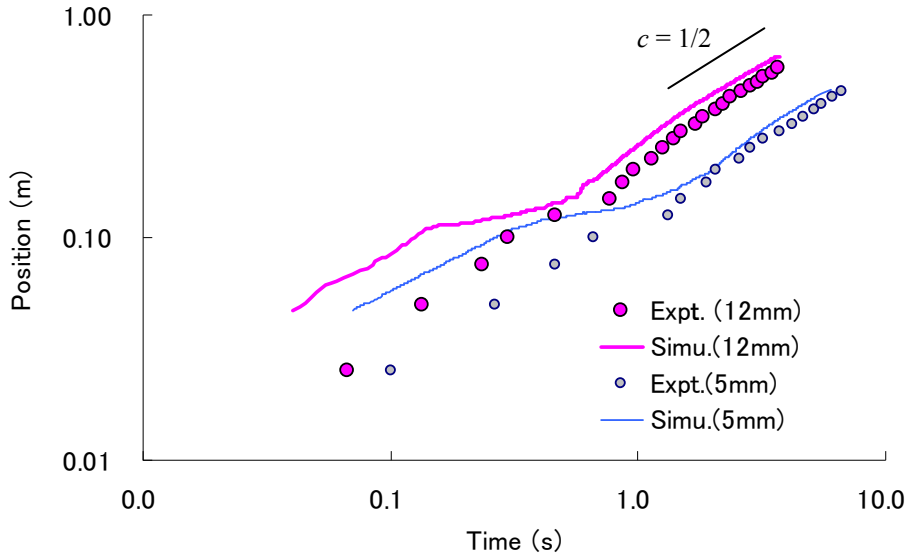
Figure 5.9 Position of front versus time for porous media of 12mm and 5mm in diameter
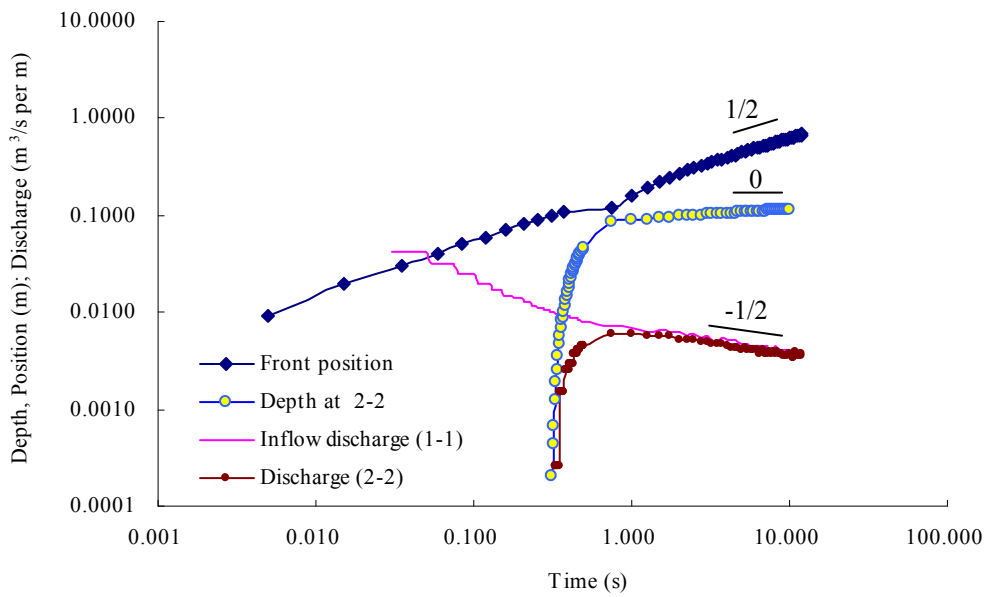
Figure 5.10 Front position, depth and discharges versus time showing their temporal power on them for 5.0 mm glass bead as porous media.
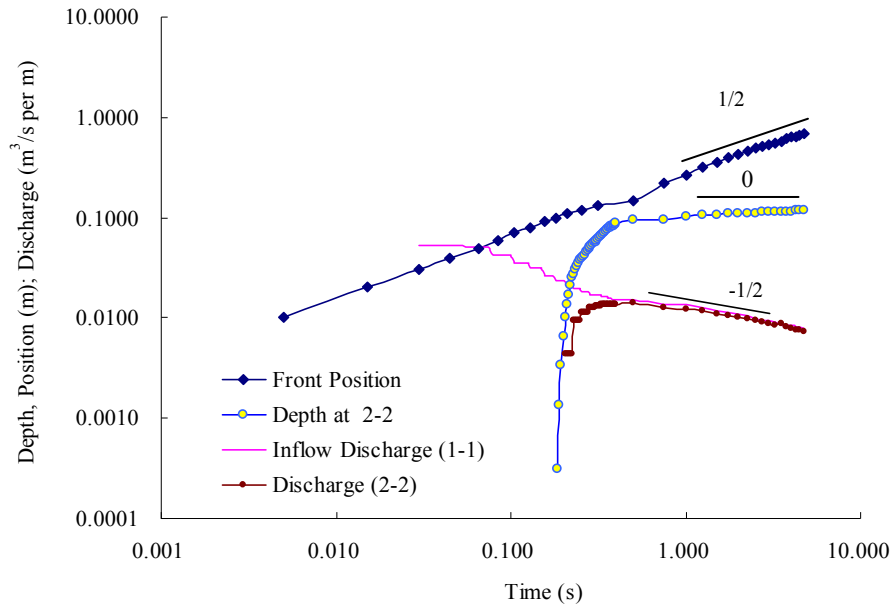
Figure 5.11 Front position, depth and discharges versus time showing their temporal power on them for 12 mm glass bead as porous media

Figs. 5.10 and 5.11 above shows a log-log plot of the front position, depth just after the brink of the step, inflow discharge from pressure boundary 1-1 and discharge at the flux boundary 2-2 for the channel considered filled with porous media consisting of 5.0mm and 12mm diameter, respectively. It is seen that the flow after it attains the PD regime in the case of flux boundary at 2-2 obeys the power law which is as it should be according to our assumption in the analytical derivation. The results are in close agreement with the analytical outcomes. There is a saddle in the plot showing the filling up of water into the immediate downstream corner of the step After this point we can observe that the power law for PD-Regime is valid for the inflow discharge condition at 2-2. The theoretical powers derived for each of the components is shown along with its corresponding value on the plot. We can observe that there is a close agreement between the derivation and numerical outcome.

5.7 Summary

The power laws for the unsteady intrusion process into a channel having impervious backward facing step, filled with porous media consisting of large grain size, is derived using the concept

of the similarity obedience in simple channel flows. We derived the power law solution for the channel having a backward facing step utilizing the concepts of previous power law for simple channels under two types of boundary conditions. The investigation on the front propagation speed, velocity and flow depth at the origin in relation to the temporal powers are done for the general inflow condition where the discharge varies as t^σ, where t is the time elapsed and σ a constant index. The analytical power derived by considering similarity transformation of variables is then compared with the result of numerical simulation. The applicability of the model is tested by applying it to a channel having backward facing step filled with glass beads as porous media. Numerical simulations showed the close agreement with what was derived analytically. The model can reproduce the depth of flow, velocity profile with negligible errors. Also the observed discharge and the numerically obtained results are matching. The analytically derived powers are verified using numerical simulations. The decay in the value of inflow discharge is observed and also produced in the numerical simulation owing to the fact that the pressure gradient which is responsible to drive the flow goes on decreasing during the later phase. It is pointed out that the flow profile and the rate of intrusion observed in the experiment are reproduced well by the numerical simulations.

Chapter 6

ACCELERATION IN RAPID FLOW THROUGH VERTICAL POROUS COLUMN

6.1 Introduction

Non-Darcy effects on natural convection in porous media have received a great deal of attention in recent years because of the experiments conducted with several combinations of solids and fluids covering wide ranges of governing parameters which indicate that the experimental data do not agree with the theoretical predictions based on the Darcy flow model. Due to this divergence in the rapid infiltration calculation, the efforts are thus being made to include the inertia terms in the flow equations and to examine their effects in order to develop a reasonable accurate mathematical model for accelerated or decelerated infiltration into porous media. Detailed accounts of the recent efforts on non-Darcy convection have been recently reported in Tien and Hong [1985], Cheng [1987], Prasad et al. [1988], and Kladias and Prasad [1989]. Poulikakos and Bejan [1985a, 1985b] investigated the inertia effects through the inclusion of Forchheimers's velocity-squared term.

Literatures show that several investigators have studied the steady-state characteristics of the hydrodynamics as well as the heat transfer behavior of flows through closed conduits partly filled with porous material. The steady hydrodynamics behavior of the fluid flow in channels

partly filled with porous material is first investigated by Beavers and Joseph [1967] who presented an empirically based correlation for the velocity gradient at the clear fluid/porous interface in terms of the velocities in the fluid layer and the porous region. The same problem was solved analytically using the matched asymptotic expansion technique by Vafai and Thiyagaraja [1987] and solved exactly by Vafai and Kim [1990]. The transient hydrodynamic behavior of the fluid flow in channels partly filled with porous material has been investigated by Al-Nimr and Alkam [1998], where the unsteadiness in the hydrodynamic behavior is due to a step change in the imposed pressure gradient. Keeping in view the practical applications of water release from the top of column filled with porous material, the goal of this study is to investigate the free convection of water movement from the top of a vertical porous formation. The significance of acceleration is investigated in the rapid downward intrusion of water into a porous column under gravity.

Various concise equations have been proposed, and used, to describe the dynamics of one-dimensional, vertical rapid infiltration into uniform porous media. The relative importance of inertia on natural convection in porous media is examined using vertical one-dimensional flow equation. The hydrodynamics of a system where there is a coupled flow above and below a free-porous interface are not completely understood. We analyze the flow as vertical unidirectional, unsteady/steady intrusion in the system of a vertical porous column using a coupled formulation between top and bottom flow layers. Experiments are conducted to determine the flow behavior. The vertical one dimensional flow equations are integrated to determine the pressure gradient exerted on the interface for coupling the free media flow at the top and porous media flow below the interface.

6.2 Theoretical consideration

6.2.1 Infiltration theories

Infiltration estimation methods are an integral part of the simulation of water movement and contaminant transport and fate in porous media. Numerous models are available for performing simulations related to the movement of water. There exists extensive documentation of these models. However, the practical application of these infiltration models has not been adequately addressed in the literature. In recent years, the use of vadose zone models has increased for the purpose of estimating contaminant levels in soils related to different types of remedial

decision-making. The rate of infiltration of water is generally the most important parameter required in such models. Often these models use an over-simplified estimate of the infiltration rate, which has little basis in reality and actual field conditions. A great majority of the models use either empirical or Green-Ampt type or Richards type of infiltration models. Most of the reported literatures deal with quasi-steady type of infiltration if not steady, in the very low permeable media. There is lacking of such infiltration models dealing with the acceleration in the unsteady intrusion that can be a significant phenomenon in the porous media having high value of perneability.

An investigation of rapid infiltration in a vertical channel filled with a porous medium including the effect of inertial forces is done by taking into account the effect of porous dissipations. The flow is modeled using the unidirectional flow equation extended with porous media resistance terms. The coupling of the free and porous domain is achieved from the continuity condition.

6.2.2 Formulations for rapid infiltration

The general problem of fluid draining vertically into a porous medium is formulated here and is analyzed in detail for the case of fixed-volume release and release under constant head.

Constant water depth at the top(Fixed head):

In this case, the depth of ponding above the top of the porous media is kept constant. Consider a layer of fluid with initial height H_0 above a deep and dry porous column. The governing equation for the assumed coordinate system as shown in Fig. 6.1, for the bulk fluid layer above the solid-liquid interface, is given by

$$\frac{\partial V}{\partial t} + V\frac{\partial V}{\partial y} = g - \frac{1}{\rho}\frac{\partial p}{\partial y} \tag{6.1}$$

where V is the bulk fluid velocity , g the acceleration due to gravity, p the pressure and ρ the fluid density. For uniform cross-section of the column and incompressible fluid, we can write equation (6.1) as

$$\text{i.e.} \qquad \frac{\partial V}{\partial t} = g - \frac{1}{\rho}\frac{\partial p}{\partial y} \tag{6.2}$$

Now integrating Eq.(6.2) from $y = 0$ to $y = H_0$, we get

$$\int_0^{H_0} \frac{\partial V}{\partial t} dy = \int_0^{H_0} \left[g - \frac{1}{\rho} \frac{\partial p}{\partial y} \right] dy \tag{6.3}$$

On simplification, we get:

$$\frac{p_0}{\rho} = gH_0 - H_0 \frac{\partial V}{\partial t} \tag{6.4}$$

where p_0 is the pressure at the interface H_0 is the constant depth above the top of porous medium. The second term on the right hand side of Eq. (6.4) is the contribution of vertical acceleration in the downward intrusion process. This term has a significant effect in the initial stage. In the long run the pressure at the interface becomes hydrostatic because the second term on the right side of Eq. (6.4) tends to zero.

While considering the flow through porous layer below the interface the governing equation can be written as:

$$\frac{\partial V_b}{\partial t} + V_b \frac{\partial V_b}{\partial y} = g - \frac{1}{\rho} \frac{\partial p}{\partial y} - \frac{g(1-C)}{K} V_b$$

Or,
$$\frac{\partial V}{\partial t} = g - \frac{1}{\rho} \frac{\partial p}{\partial y} - \frac{g(1-C)}{K} V_b \tag{6.5}$$

On integration Eq. (6.5) from $-h_b$ to 0, one can write,

$$\int_{-h_b}^{0} \frac{\partial V_b}{\partial t} dy = \int_{-h_b}^{0} \left[g - \frac{1}{\rho} \frac{\partial p}{\partial y} - \frac{g(1-C)}{K} V_b \right] dy \tag{6.6}$$

Or,
$$\frac{\partial V_b}{\partial t} h_b = \frac{p_0}{\rho} + gh_b - \frac{g(1-C)}{K} V_b h_b \tag{6.7}$$

Substituting the value of p_0/ρ in equation (6.7) from (6.4), we get

$$\frac{\partial V_b}{\partial t} h_b = gH_0 - (1-C)H_0 \frac{\partial V_b}{\partial t} + gh_b - \frac{g(1-C)}{K} V_b h_b \tag{6.8}$$

Or,
$$\frac{dV_b}{dt} = \frac{1}{\{h_b + (1-C)H_0\}} \left\{ gH_0 + gh_b - \frac{g(1-C)}{K} V_b h_b \right\} \tag{6.9}$$

in which the relations $V = (1 - C)V_b$, from mass conservation, has been used .Eq. (6.9) is solved in this study to describe the phenomenon of rapid infiltration through vertical porous media.

Variable head: a case of fixed volume release

In this case a fixed volume of water of depth L_0 is released from the top of vertical porous column instantaneously. Let $h(t)$ be the depth available at the top of porous media at any instant of time t. For the condition when $h(t) \geq 0$, we can write,

$$L_0 = (1 - C)h_b(t) + h(t) \tag{6.10}$$

Eq. (6.10) is an expression for mass conservation which can be utilized to find the ponding depth $h(t)$ above the interface in terms of the depth permeated $h_b(t)$ below the top of porous media or vice versa at any instant. Referring to Eq. (6.4) the expression for pressure at the interface can be written as

$$\frac{p_0}{\rho} = gh(t) - h(t)\frac{\partial V}{dt}$$

$$(6.11)$$

where $h(t)$ is the depth of ponding above the interface at any instant. Using Eqs. (6.7) & (6.11), we can write

$$\{h_b + (1 - C)h\}\frac{\partial V_b}{\partial t} = gh_b + gh - \frac{g(1 - C)}{K}V_b h_b$$

$$(6.12)$$

Eq. (6.12) can handle variable head if it is coupled with the mass conservation Eq. (6.10). In Eqs. (6.9) and (6.12), if we neglect the acceleration terms, we get,

$$\frac{(1 - C)}{K}\frac{dh_b}{dt} = 1 + \frac{h}{h_b} \tag{6.13}$$
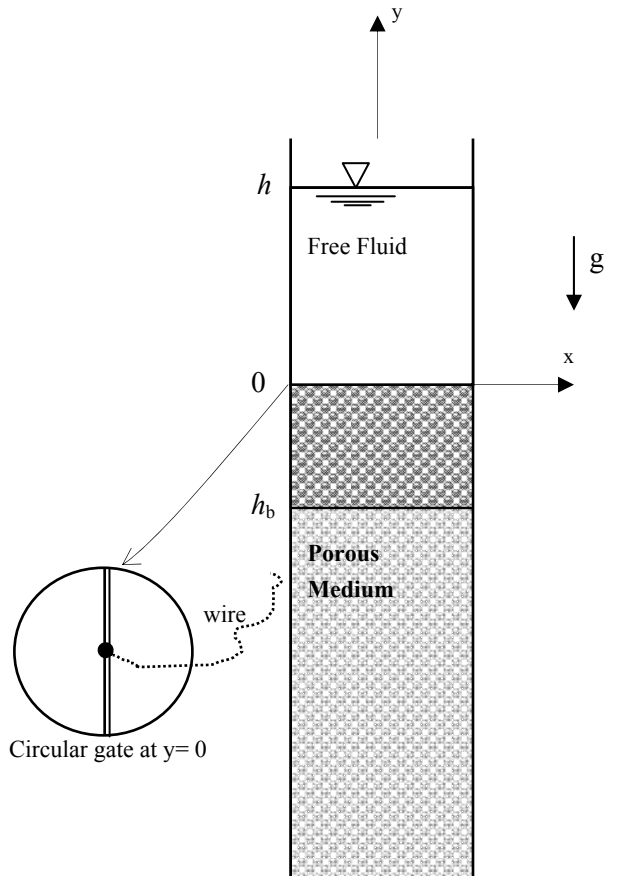

Circular gate at y= 0

Figure 6.1 Vertical infiltration through column of porous media and circular gate

which, on integration from $t = 0$ to t and assuming constant water depth h at the top, yields

$$\frac{K}{(1-C)}t = h_b + h\ln\left(1 + \frac{h_b}{h}\right)$$

(6.14)

which is the well known Green and Ampt infiltration expression. The expression is used in this chapter to compare with the effect of acceleration in the case of rapid infiltration. For the variable head case the instantaneous value of $h(t)$ can be found using the mass conservation Eq. (6.10) to implement it in solution considering small time increments.

6.3 Solution of governing equations

Eqs. (6.9) and (6.12) are solved using fourth order Runge-Kutta method and the results are shown in section 6.5. The equations are solved for corresponding initial and boundary conditions.

6.4 Laboratory Experiments

The experiments were carried out for different interface conditions regarding the top free water level and also for different sized porous media. The details of the experimental conditions are given in Table 6.1. To begin the experiment, water from the top of the porous media was released instantaneously and allowed to permeate down the vertical porous column. For the constant water level condition a continuous supply of water is ensured from the top reservoir. For the fixed volume release, a water column of depth L_0 is released instantaneously without further addition of the water volume. The arrangement is shown in Fig. 6.1 where a circular horizontal plate gate is positioned at the interface level from inside. The circular gate was formed by joining two thin semicircular flats. The flats were tied with a thin wire making water tight at the same time. During the experiment the wire was pulled instantaneously from the top open mouth so that the two flats would align together and impart negligible disturbance (see Fig. 6.1).

Table 6.1 Detail of vertical infiltration experiments

Name of the experiment	Glass bead size	Initial conditions	Remarks
TST1	1 mm	$h_0 = 0.5$m	Constant
TST 2	5 mm	$h_0 = 0.5$m	water level
TST 3	1 mm	$L_0 = 0.20$m	
TST 4	1 mm	$L_0 = 0.40$m	Variable
TST5	5 mm	$L_0 = 0.20$m	water level
TST6	5 mm	$L_0 = 0.40$m	

6.5 Results and discussion

Results for constant head at the interface:

Following figures show the plots for constant water depth condition above the interface. The results are shown for 1mm and 5mm diameter beads taken separately. Figs. 6.2 and 6.3 show the depth and velocity of front with time for the porous media having permeability 0.01 m/s, respectively.

Figure 6.2 Depth of penetration versus time [K=0.01m/s, H_0 = 0.50m]

Figure 6.3 Velocity at the front versus time [K=0.01m/s, H_0 = 0.50m]

Following figures show the similar results as above for the porous media having permeability 0.1 m/s. Figs. (6.4) and (6.5) show the plots of front depth and velocity, respectively. The results are also compared with the estimates from Green-Ampt formula.
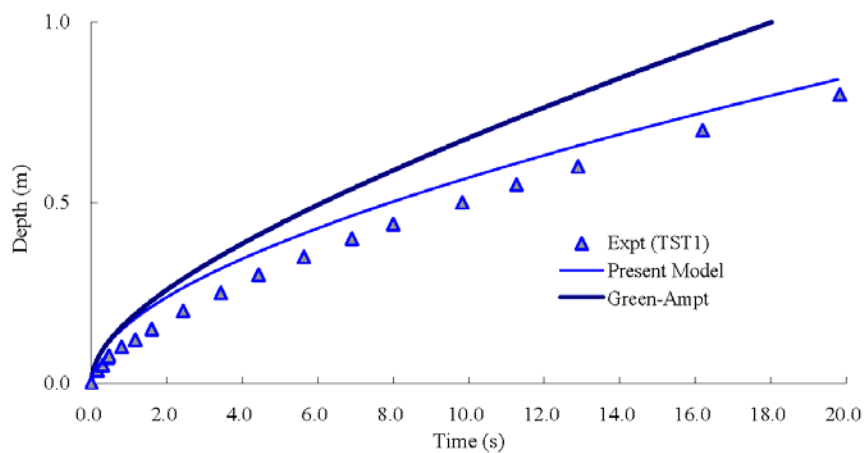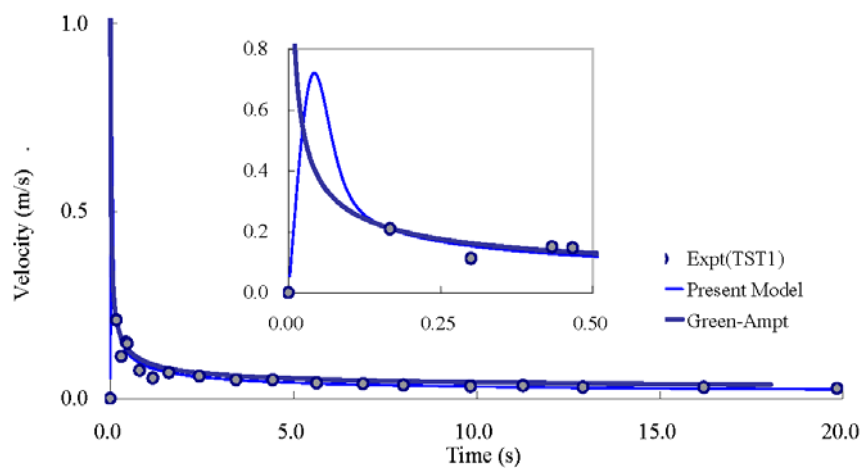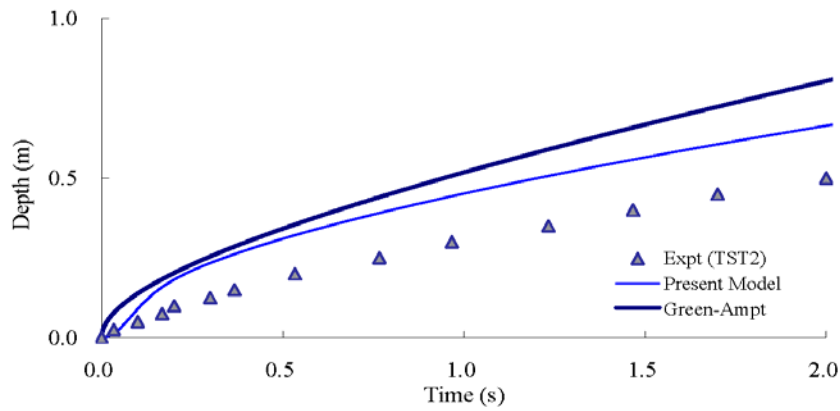
Figure 6.4 Depth of penetration versus time [K=0.1m/s, H_0 = 0.50m]
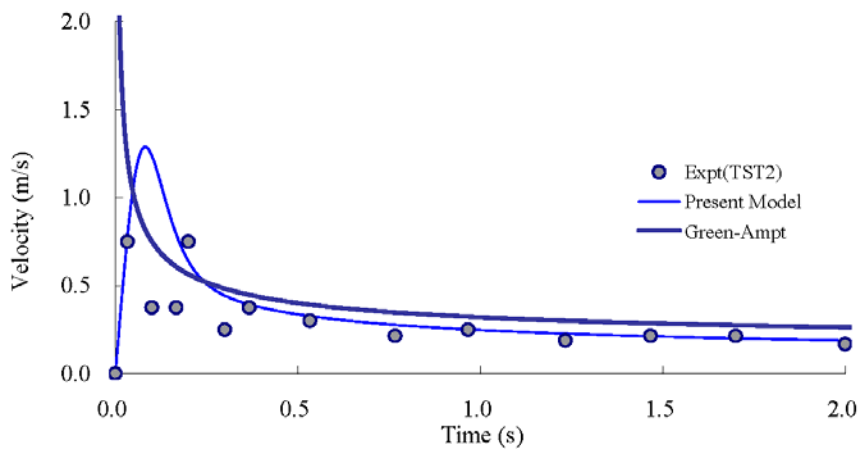
Figure 6.5 Velocity at front versus time [K=0.1m/s, H_0 = 0.50m]

The Green-Ampt formula overpredicts the infiltration volume and the velocity predicted is also unreasonably high at initial time stage. The results from the present model are reasonably satisfactory both for the infiltration volume and front velocity. Our formulation shows a gradual increase of acceleration at the initial time region and then decelerated before the front velocity becomes almost constant. Also the estimate of infiltrated volume is improved.

Results for variable head at the interface:

Following figures show the estimates of infiltration volume and velocity at the front with respect to time for constant volume (L_0) release i. e. decreasing depth with time at the interface. Figs 6.6 to 6.9 show the results for the case of 1mm [Figs. 6.6 and 6.7] and 5mm [Figs. 6.8 and

6.9] glass bead. The left figures show the front position and right figures shows the velocities of penetration. For each glass bead size the initial volume (L_0) taken is 0.20 and 0.40m as mentioned.

Figure 6.6 Results for 1mm glass bead (a) Front depth (b) velocity [L_0 = 0.20m, K =0.01m/s]

Figure 6.7 Results for 1mm glass bead (a) Front depth (b) velocity [L_0 = 0.40m, K =0.01m/s]

Figure 6.8 Results for 5mm glass bead (a) Front depth (b) velocity [L_0 = 0.20m, K =0.1m/s]

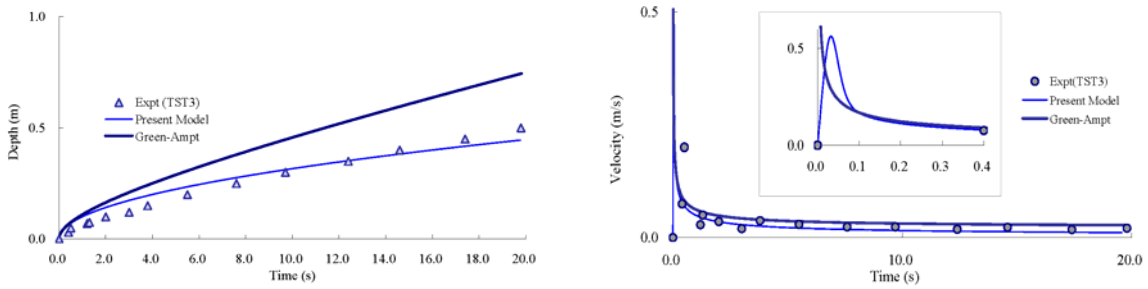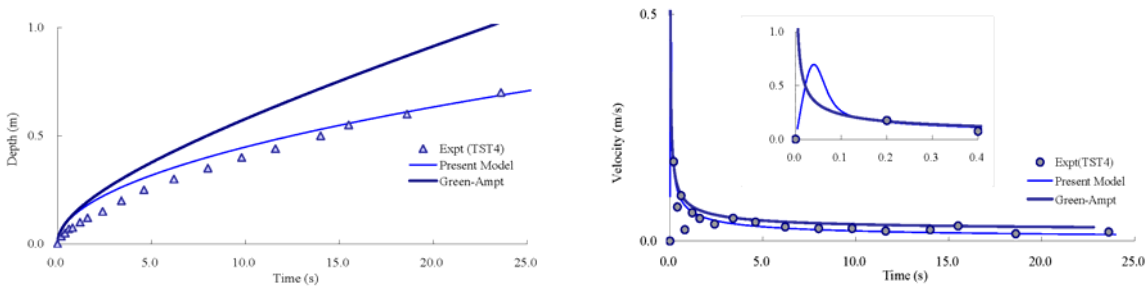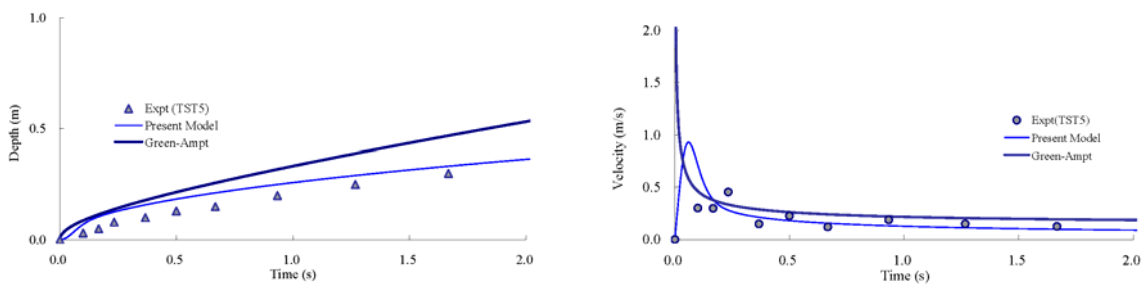
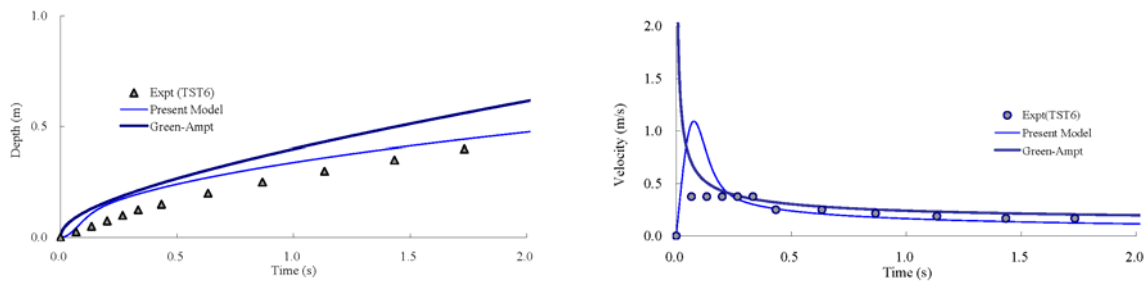**Figure 6.9** Results for 5mm glass bead (a) Front depth (b) velocity [L_0 = 0.40m, K =0.1m/s]

It is clearly observed that Green-Ampt formula overestimates the infiltration volume and also the velocity predicted is very high in the initial stage. In contrast, present model which takes into account the acceleration effects gives the satisfactory results. Velocity plots show that it takes certain time for the intruding water to get accelerated to its peak value. Then velocity gradually decreases to almost constant value in the later time stage. The rectangular inset is shown to see the results
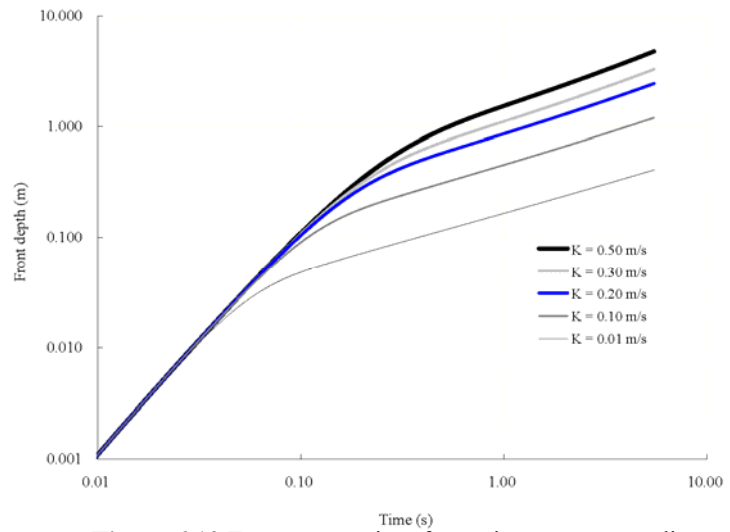
Figure 6.10 Front versus time for various porous media

closely in the initial time region. Fig. 6.10 shows a dependency of the time for peak velocity and subsequent retardation on the hydraulic conductivity. In almost all the cases the prediction by present model on infiltration volume is slightly higher than the experimental observations.

6.6 Summary

We first determined analytically the rate of drainage of a one-dimensional layer of fluid into a porous bed and found that the theoretical predictions for the downward rate of migration of the fluid front are in agreement with our laboratory experiments. The experiments also suggest a rapid and simple technique for the determination of the permeability of a porous medium. The values of permeability obtained from the experiments were used in the analytical calculation.

The effect of acceleration in the infiltration process can be observed at initial stage and it has a significant effect in the case of porous media with high permeability. It is revealed that it takes certain time for intruding water to be accelerated to its peak velocity and then it gradually decreases before attaining almost a constant value. For variable head case the difference between calculated results and experimental results is smaller than it is for constant head case.

It is pointed out that the conventional infiltration models like Green-Ampts infiltration model cannot account for the acceleration effect in the case of high velocity flow. It overestimates the infiltrated volume. The acceleration effect is not so significant for low permeable media. In almost all the case the experimental permeated depths are less than the calculated one. This may be due to the effect of compressed air in the front region during unsteady penetration process.

Chapter 7

DAM BREAK FLOW OVER POROUS BED: A CASE OF COMPOSITE FLOW DOMAIN

7.1 Introduction

The study of flow systems composed of a porous medium and a homogenous fluid has attracted much attention since they occur in a wide range of the civil and environmental applications. Examples of practical applications are: flow through porous walls, drying process, various filtration processes, overland flow during rainfall, and surface-subsurface flows etc. Two different approaches; the single domain approach [Mercier et al., 2002; Jue, 2004] and the two-domain approach [Silva and Lemos, 2003; Costa and Oliviera, 2004], are usually used to solve this type of problems. One of the several early studies on the interface boundary conditions is that by Beavers and Joseph [1967]. In their approach, the fluids in a homogenous fluid and a porous medium are governed by the Navier-Stokes and Darcy equations, respectively. In the single-domain approach, the composite region is considered as a continuum and a single set of general governing equations is applied for the whole domain. The explicit formulation of boundary conditions is avoided at the interface and the transitions of the properties between the fluid and porous medium are achieved by certain artifacts [Goyeau,2003]. In the present study, the single-domain approach is considered.

The combination of free flow and flow through porous media occurs in a wide range of fluid processes. When the layer along which the fluid spreads is not quite impermeable, the current loses mass by drainage through this layer, and in this situation the usual self-similar solutions are no longer valid. Indeed, the current may exhibit behavior such as spatially limited spreading which cannot be described by similarity solutions. The first study of how this drainage might affect the spreading of a gravity current in a porous medium was carried out by Pritchard, Woods & Hogg [2001] who investigated drainage, driven by hydrostatic pressure, through a thin, spatially uniform underlying layer releasing of a constant volume of fluid.

The diversity of underlying phenomena and the complexity of interactions between free and porous flow systems have prevented development of a general theoretical analysis of coupled flow systems. The objective of the present study is to apply a developed numerical model based on finite volume method to treat the composite system having both porous and free flow domain. The stresses at the interface are assumed to be continuous and there is no any special boundary condition applied at the interface because the single set of governing equations are used to simulate the complex flow behavior.

7.2 Flow domain and its relevance

There are many geological situations in which fluid spreads through a layered porous medium. Important examples of such systems include aquifers and oil or geothermal reservoirs [Bear, 1972], and the flows may be natural or artificial. In many instances, the fluid spreads laterally along a permeable layer in the medium, driven by the buoyancy contrast between it and the ambient fluid: the resulting overland flows are generally known as gravity currents.

During the last four decades, several numerical formulations and specialized software have been developed in response to studies about dam break wave propagation and its hydraulic and environmental impacts on downstream hydraulic structures and valleys. These methods cannot, however, be used to predict the flow when there is a sudden release of water over a porous substrate as it is a very practical case of dam break over the permeable bed. In fact, such problems require the modeling of the complex transition from a free-surface flow into a pressurized one. Hosoda et al. [1993] studied the flow comprising of the propagation of an interface between the open channel free-surface flow and pressurized pipe flow in hydraulic transients that occur in underground floodways constructed for urban flood mitigation.

The main objective of the present work lies in the application of the model in various flow domains. The composite domain we mean the computational domain where different types of flow domains are in coexistence as shown in Fig. 7.1. Furthermore, in our study, the flow comprises of pressurized as well as open channel flow. In zone A, there is pressurized flow and in B it is open channel flow. The interface between pressure flow and open channel flow moves forward as the front propagates.
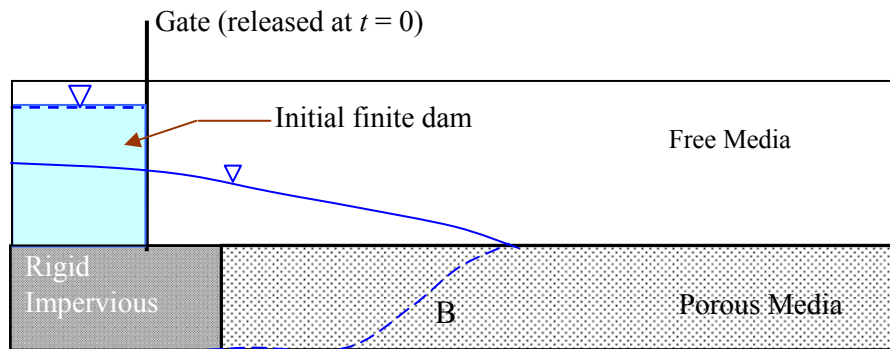
Figure7.1 Definition sketch for the dam break flow over porous bed

The flow domain chosen here consists of a short impervious bed in the immediate downstream of the gate. Then this impervious bed is followed by a porous substrate with an open outlet at the right end. The area above the porous bed is free whereas the bottom of the porous substrate is an impervious boundary.

7.3 Experimental setup

Overland shallow flow gravity currents are generated in a channel (900 mm long, 100 mm wide and 150 mm deep) with transparent Perspex sidewalls and bottom by means of the lock-release system as depicted in Fig 7.2. The porous substrate was formed by packing glass beads of 12 mm placed up to 50mm above the impermeable bottom, thus separating the tank into two parts. A video camera was placed at a fixed position far away (about 1.8m) from the side of the channel to record the whole experiment on a digital memory card.

The tank was filled with water to a depth H_0 above the bed level. The experiment starts when the gate is removed instantaneously, leaving the water to flow out along the porous bed. The released water also flows downwards through the bed to the lower part of the channel. In order to provide the impervious bed portion in the dam break flow, a short impervious stretch is left between the porous bed and the release gate. Thus water rushes through this passage before it

meets the porous infiltrating substrate. There is significant infiltration of water into the porous bed which gets arrested due to shallow depth of bottom and again moves forward after the build up of the pressure gradient there within the porous media.
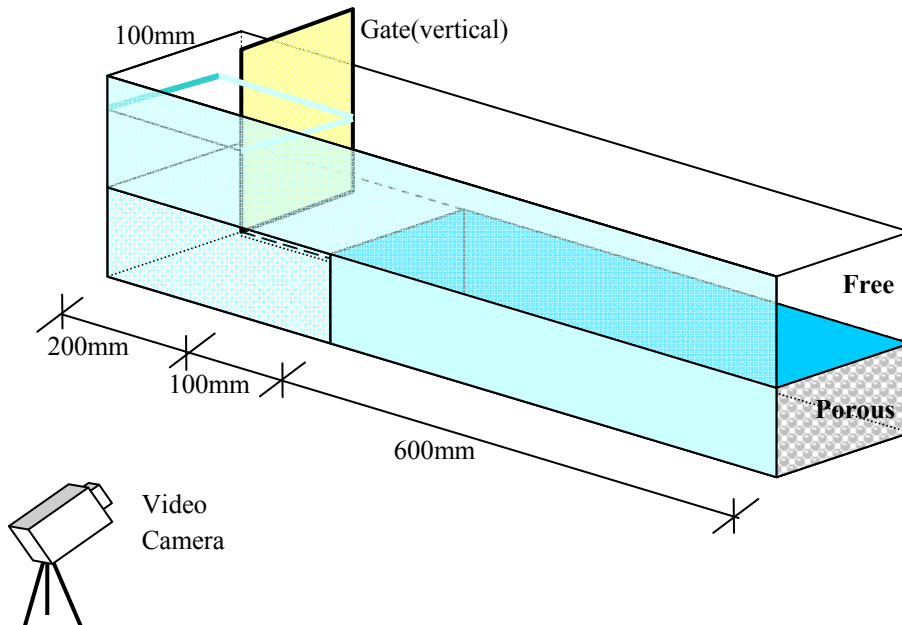
Figure 7.2 Schematic diagram of the experimental setup

A series of equidistant lines at 50 mm on the sidewall of the tank facing the video camera enabled the determination of the position of front measured from the gate as function of time. A video of the experiment was taken by a digital movie camera placed near the side of the flume. The video was converted into a series of still images at an equal time interval of 1/30 (frame rate of video camera) seconds. Then the position of front and depth distribution for different time is traced by the image interpretation manually with the help of grids drawn at 50mm interval on the perspex plate of the flume facing the camera. In this study, the thickness of the horizontal porous bed is of finite depth with impermeable bottom. The arrangement allows us to determine how, where and when water penetrates the porous surface. A video camera is used for obtaining the depth distribution of the current inside and outside of the porous substrate. This enabled the detailed internal profile of the current to be measured, and provided physical insight into the interaction of the gravity current with the porous substrate.

7.4 Numerical Simulation

The governing equations for the dam break flow are solved in vertical 2D in the composite domain, but its extension to 3D is straightforward. The flow is represented by a single set of governing equations as presented in section 3.1, which are solved numerically on a uniform

staggered Cartesian grid by finite volume method. The constrained interpolation propagation (CIP) method is adopted as the base scheme for the solution.

The governing equations are split into two steps: advection and non-advection phase. The advection phase is solved by the CIP method whereas the non-advection phase is solved by usual finite difference schemes. A HSMAC type iteration algorithm is implemented to update the velocity vector and the pressure. The evolution of free surface above and in the porous media is governed by the advection of the VOF function.
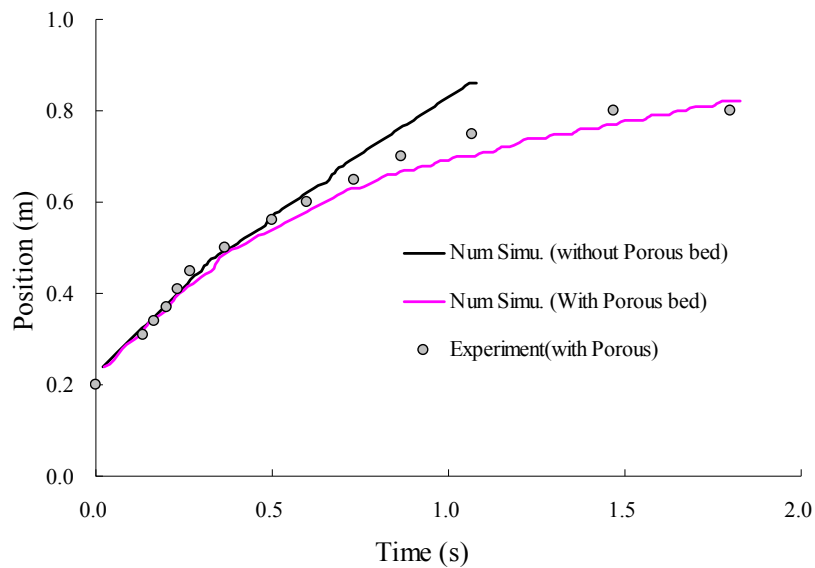
7.5 Result and discussion

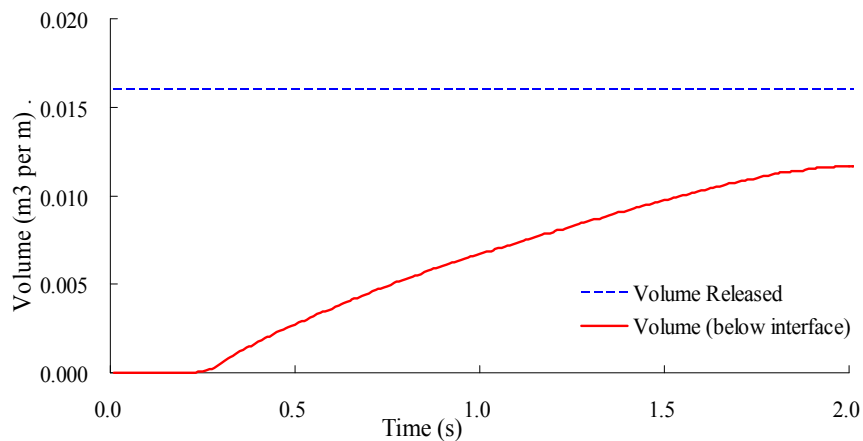**Figure 7.3** Comparison of Front position versus time

**Figure 7.4** Temporal change of volume of water in the porous stratum

Fig. 7.3 shows a comparison between the numerical and experimental values of front position. The initial portion of the plot has a steep slope before the front reaches porous bed. Then the flow speed gets retarded showing the slower speed due to the loss of the mass into porous bed and further resistance to the flow front. The plot also shows the curve for the case when there is no porous bed i. e. representing the conventional dam break over impervious bed. The effect of porous bed can be seen easily from this comparison.

A plot of temporal change of the volumes above and below the interface of free and porous media is shown in Fig. 7.4. At the starting the infiltrated volume is very small due to small horizontal propagation along the interface. After the significant flow occurs along the interface, the rate of volume accumulation in the porous layer is also increasing rapidly before it again becomes slower due to the significant mass loss by the flowing current.

Figures below show some of the snapshots during the experiment and simulation as well for the dam break over the porous substrate. As already stated, the nature of flow in this case is a composite one. Both the flow occurs above and inside of the porous medium, this is clearly observed in these figures. In Fig. 7.5(a) significant part of the water is above the bed and little inside the porous media, while the front is going further making the overland flow. The front current goes on ahead while losing more mass as it traverses the velocity is gradually becoming smaller and smaller. In Fig. 7.5(b), the current acquires its foremost position above the porous bed and simultaneously the front head starts vanishing and in Fig. 7.5(d) almost all the water is inside the porous layer.

Figs. 7.6(a)-(d) show the results of numerical simulations at different time steps. The evolution of free surface and velocity plots are shown in the increasing time steps corresponding to the experimental figures shown above [Fig. 7.5(a)-(d)]. The results are in good agreement with the experimental observation.

Figure 7.7 shows the evolution of pressures in the simulation. Initially the pressure profile changes nonlinearly and it becomes linear in later times. The figures also show the pressurized and open channel zones during the early stages of the propagation. The initial nonlinear pressure profile suggests the inertial dominance in the flow whereas as the time elapses the pressure contours are seem to be linear.
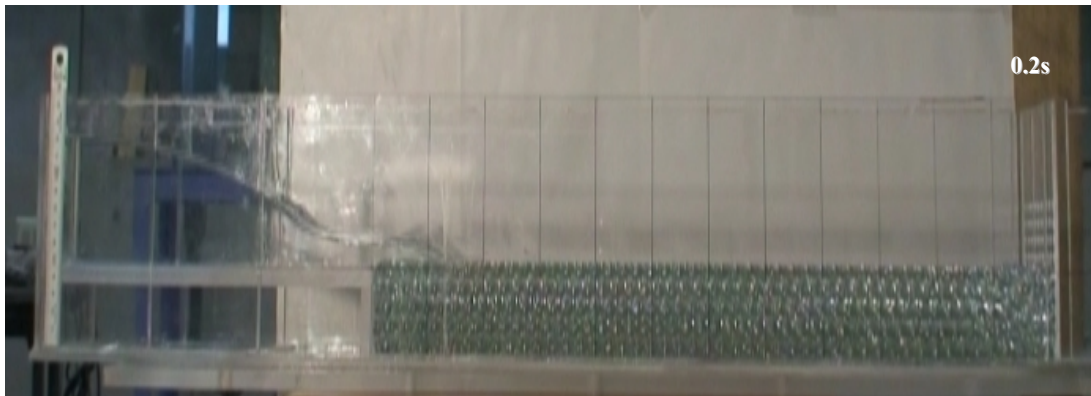
7.5(a)
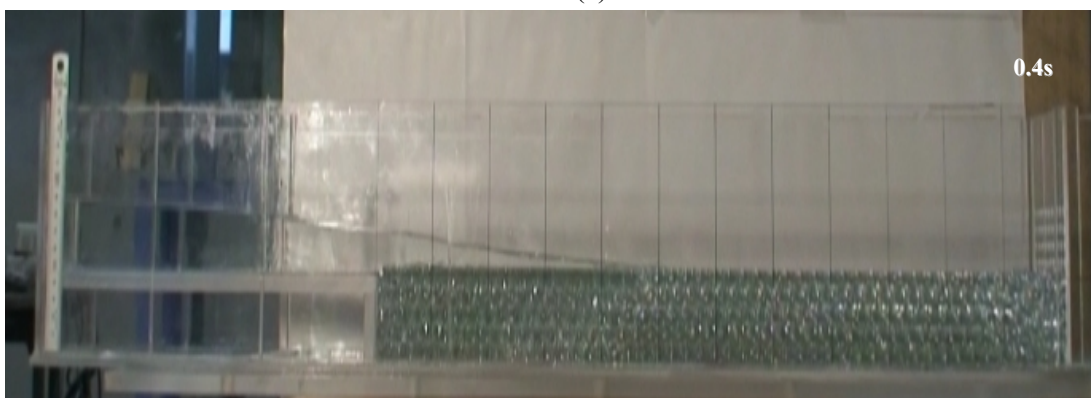
7.5(b)

7.5(c)

7.5(d)

Figure 7.5 Flow profiles during experiment at (a) t = 0.2s (b) t = 4.0s (c) t = 1.0s and (d) 2.0s

7.6(a)

7.6(b)

7.6(c)

7.6(d)

Figure 7.6 Flow profiles during simulation at (a) *t* = 0.2s (b) *t* = 4.0s (c) *t* = 1.0s and (d) 2.0s

Figure 7.7 Evolution of pressure profiles during simulation at (a) $t = 0.1$s (b) $t = 0.2$s (c) $t = 0.4$s (d) 1.0s and (e) 2.0s

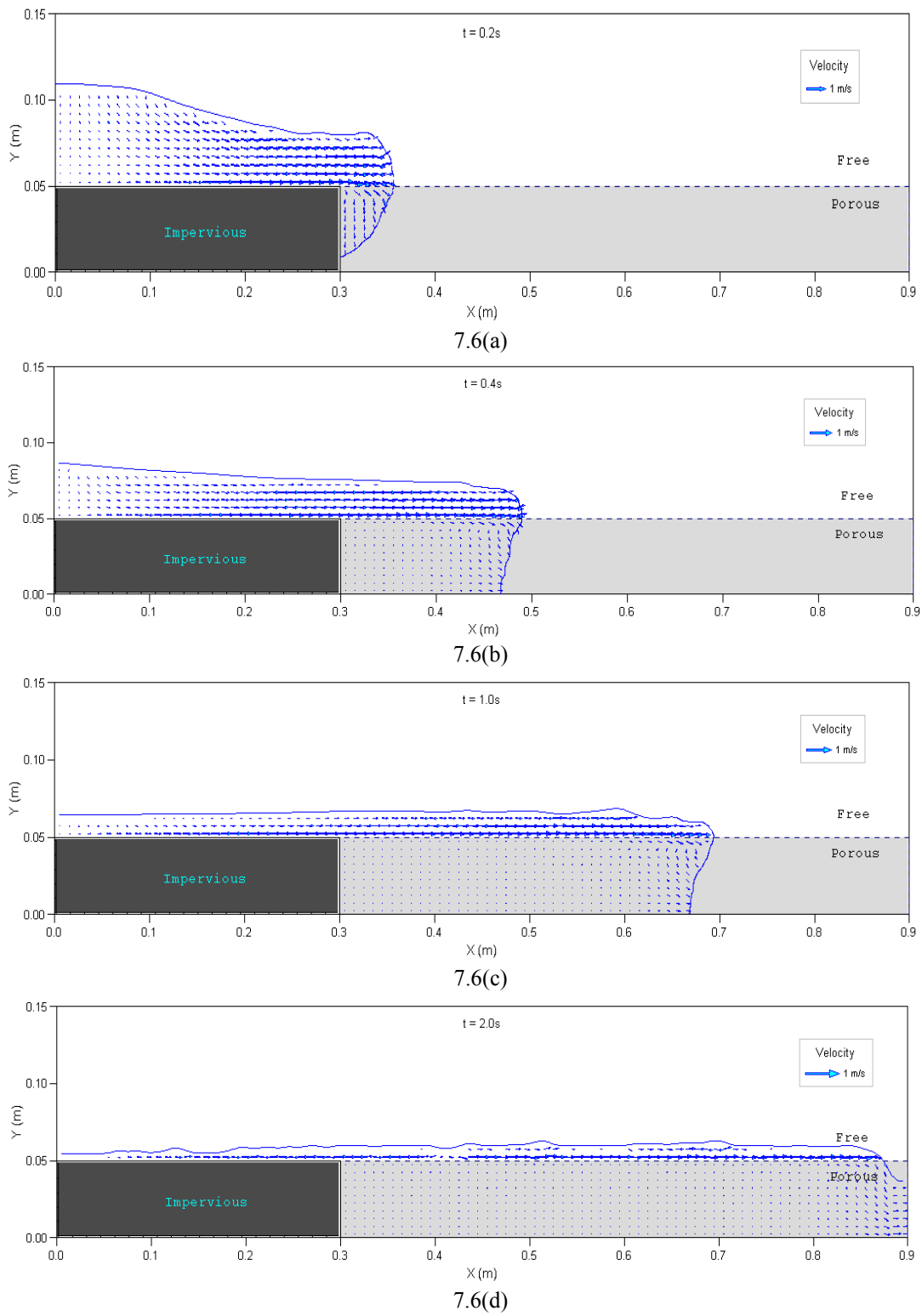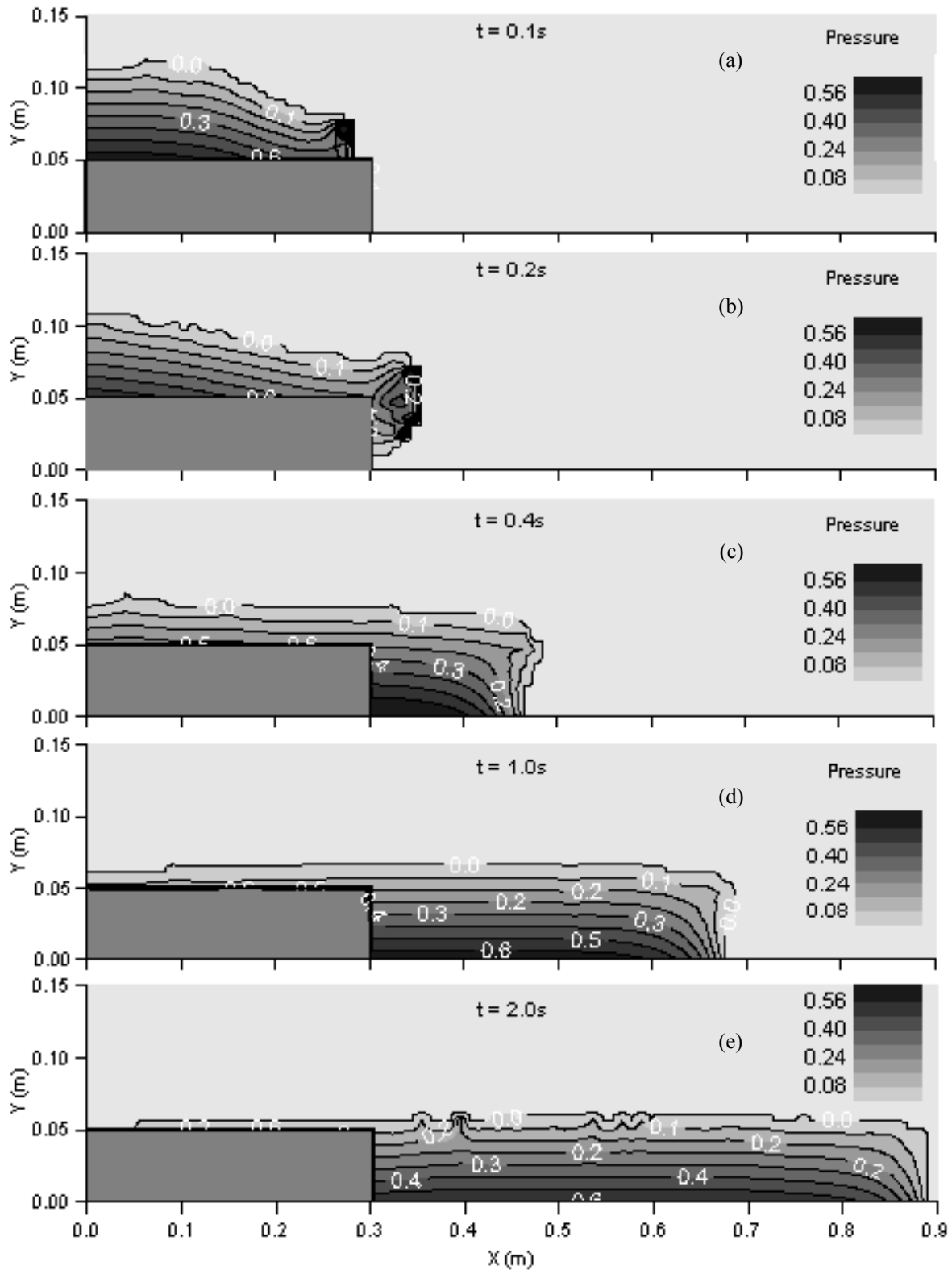From these experiments it is well-known that the gravity current so produced passes through two distinct phases. In the first stage, or slumping phase, the head of the current maintains nearly constant depth and travels at constant velocity. As the current goes ahead the Reynolds number of the gravity current drops sufficiently, another phase occurs in which viscous forces are important. However, as the drainage becomes established, the spreading slows, and in fact the fluid only spreads a finite distance before it has fully drained into the underlying layer which has been reproduced well in the simulation.

7.6 Summary

The proposed model is applied for problems with interface between a homogenous fluid and a porous medium. The numerical model is based on finite volume method with VOF method for the free-surface evolution, which is effective for dealing with complex boundary conditions at the interface between different domains.

The dynamics of unsteady flow with free interface, induced by sudden release of water in and over the porous media is investigated taking into account the influence of the inertia. The complex flow phenomenon, in which interface between pressurized flow and open channel flow moves forward within the porous media, has been successively captured. It is almost very difficult, if not impossible, to predict the flow using classical shallow water flow models coupled with infiltration models. The downstream boundary is taken as an outflow boundary. We observed that for some early time the flow near front region is open channel flow but shortly after the whole porous substrate gets saturated there is pressurized flow and the region moves forward near the bottom of the bed.

For solving the flow equations time splitting CIP method has been used with HSMAC type pressure solver. A finite dam with finite extent is instantaneously released over the porous bed. There are many effects to discuss in this experiment, but for clarity we restrict ourselves to the global behavior of the propagation and free surface profile inside and outside of the porous media. We observed and showed that for early short times the inertial effects are dominant. A single set of equation is solved numerically and the results are compared with the experimental outcomes. The capacity of model can be extended with the consideration of water Table, saturation, rainfall etc to get the prediction of overland runoff and ground storage. The model can account the unsteady flow behavior both in the bulk fluid flow and flow inside porous media. The simulated results for the depth distribution and velocity profiles show satisfactory

results. The model can be applied for the design of flood water detention facilities using granular porous media in some urban flood mitigation measures.

The occurrence of infiltration excess (Hortonian) or saturation excess (dunnian) overland flow can be completely determined by rainfall and ground surface infiltration characteristics. The model can account for dynamic infiltration when computing lateral inflow/outflow rates such that the effects of the relationship between microtopography and infiltration characteristics on run-off could be explored. Therefore, there are no limitations to the surface and subsurface water components for the model described which would disallow future incorporation of saturation excess runoff generation. The developed method may also be useful for simulating irrigation, coastal dynamics and floods.

The influence of the drag term is clearly seen with the varying speed of propagation and intrusion into porous bed. The future works will be directed towards the refinement for drag resistance in early high velocity stage incorporating the turbulent models. But the model proves to be a robust of its kind to capture the transient flow behavior regarding the free-surface profile and velocity. The application of the model in various geometry, boundary conditions and domain itself proves robustness of its application.

.

Chapter 8

SIMULATION OF UNSTEADY STORM WATER STORAGE INTO GRANULAR ROAD SUB-BASE

8.1 Introduction

Urban drainage systems are vital infrastructure assets which protect our towns and cities from flooding and the transmission of waterborne diseases. They are usually constructed as a network of buried pipelines which are unseen at the ground surface and hence their importance is often taken for granted by the public. Systems for both foul wastewaters and surface water runoff have been developed since the middle of the last century. Initially single pipes, known as combined sewers, were used to convey both types of water to nearby watercourses. Since the last war most new developments have adopted separate systems of sewerage which transport foul sewage to a treatment works and storm water directly to the nearest river.

It is now realized that these schemes, whilst removing a potential threat from one area, often

simply pass large quantities of water forward in the catchment so that it becomes someone else's problem downstream. Uncontrolled, rapid urban runoff presents not only an increase in the risk of downstream flooding, but also has an adverse effect on river corridor habitat due to changes in channel morphology through natural processes, or man's actions in the name of flood defense. The modern drainage engineer is therefore faced with some interesting challenges in maintaining the levels of flood protection demanded by society, whilst not causing damage to the natural environment or rapidly transmitting his problems further down the catchment.

Emphasis on controlling the discharge of storm water runoff has therefore changed with a catchment wide approach now being recommended. This requires plenty of storage to be retained or created in the developments in the higher reaches of a catchment to attenuate peak flows. Furthermore, the use of source control to reduce the total quantity of runoff from increasingly urbanized catchments is being encouraged. As more development takes place and the amount of impermeable surfaces increase, the use of soakways, swales, infiltration galleries and porous pavements have an important role to play in allowing storm water to enter the ground directly and not to place unrealistic loads on the downstream water network. These solutions are a vital part of catchment management.

Urban runoff does not only pose a flood risk but can also have serious polluting effects and can cause damage to urban watercourses from the frequent operation of storm sewer overflows. As the natural river catchment is ultimately the sink for urban runoff it is vital that storm water discharges are managed effectively both in terms of quantity and quality. New approaches in developing sustainable urban drainage systems using alternatives to conventional piped drainage systems are getting attentions recently.

Flow through porous media has great importance in many facets of engineering practice. In particular such flows with free or moving boundaries make up a significant part of the seepage

phenomena that occur in nature. Some examples of these are seepage through earth dams; seepage from open channels such as rivers, ponds, irrigation systems, and recharge basins; unconfined aquifer flow; and flow to wells. In the analysis of seepage through porous media in the presence of a free or moving boundary, numerous solution approaches have been used [Bear, 1972]. In addition, numerical schemes using the finite element or finite difference techniques have extended the solvable types of problems to a wider range of applications [Cryer, 1977].

During the storm, the runoff goes on increasing up to a peak value and again recesses. Our main concern is to trap some of the storm water in some kind of granular storage like pervious road sub-base, during peak hours, so that the in-site management of storm is achieved. The same mathematical model as applied in chapter 7 is used here with little modification for the composite flow domain where both bulk fluid and porous substrate coexist.

8.2   Motivation for the study

Over recent decades, many megacities around the world have been through chaotic urbanization, producing changes on hydrological processes. Economic instruments for inducing the reduction of such impacts have been studied and employed, especially on urban drainage services. The most obvious effect of urban development on the hydrological behavior of a catchment is the increase in impervious area producing larger quantities of runoff, which occur within shorter times leading to higher peak flow rates. Flow velocities will be increased in surface water sewerage and culverted channels. Other effects include the lowering of the local ground water table as a result of reduced pervious area which limits soil moisture recharge. This can affect stream base-flows and water resources.
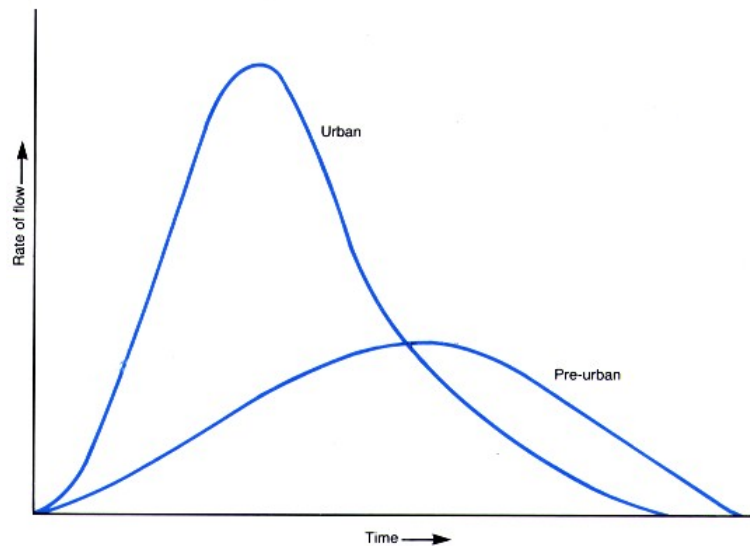
Figure 8.1 Effect of urbanization on volume and rates of surface runoff

Figure 8.1 displays hydrographs before and after such development. The hydrograph after urbanization peaks sooner and recedes much faster than the natural conditions hydrograph. The water after urbanization travels at a much faster rate because of the increase in impervious and smooth surfaces. Water will travel down the impervious formations much faster than it will through the adjacent lawn. Flashiness tends to damage streams by causing increased erosion with moderately large storm events. Storm water management is partly meant to control this increased flashiness and keep it from damaging property and the natural environment. The usual means of doing so is to provide detention storage, releasing water more slowly than it would be otherwise.

Storm water runoff will carry a significant pollution load including road grit, soil from construction work, hydrocarbons and occasional spillages from vehicles. These effects can lead to an increase in flood levels which are unacceptable. The objectives of urban runoff control are therefore to limit the quantity, location and frequency of flooding to acceptable levels and to maintain natural watercourses fit for their other functions such as conservation, water supply,

amenity and navigation.

Existing techniques towards sustainability

Techniques have been developed to reduce the impact of urban runoff on the receiving watercourse and downstream catchment. These often require changes to the traditional approach of upgrading or rehabilitating urban drainage by simply increasing the capacity of the system, and are collectively known as Best Management Practice techniques. In the context of urban drainage the term "best management practice" can be defined as that which is used for a given set of conditions, such as: land use, groundwater/soils, topography and local cost, in order to achieve satisfactory water quantity and quality enhancement at a minimum cost [Wanielista and Yousef, 1993].

These techniques can be categorized into three broad groups :

- Reduction of flows entering the drainage system (source control techniques)

- Attenuation of flows within the drainage system (using storage tanks, ponds and permeable conveyance systems)

- Passive treatment to collected surface water before discharge to a watercourse (end of pipe systems).

Source control techniques are located upstream in a catchment near the source of run-off. They divert runoff into the ground, minimizing the quantities of water collected, thus allowing more efficient utilization of the downstream conveyance system. Benefits of upstream control include greater flexibility in choosing sites for control facilities, standardization of storage unit design, and increases in system capacity through the use of real time flow control. Their use may avoid the need for laying expensive surface water sewers.

Among various source control measures for effective infiltration, porous pavements are very

common which use porous macadam, permeable concrete surface, grass concrete surface, porous concrete block surfaces etc. Infiltration basins, swales, soakways and infiltration trenches are also in use for the storage of a portion of the storm water. Our effort is to assist by modeling in the design guidelines for such source control systems described above. One such new typical drainage facility is proposed [see Fig. 8.2 (rewritten for clarity from chapter 5)] to overcome the shortcomings of the above mentioned methods and to enhance the effectiveness in the existing practices.
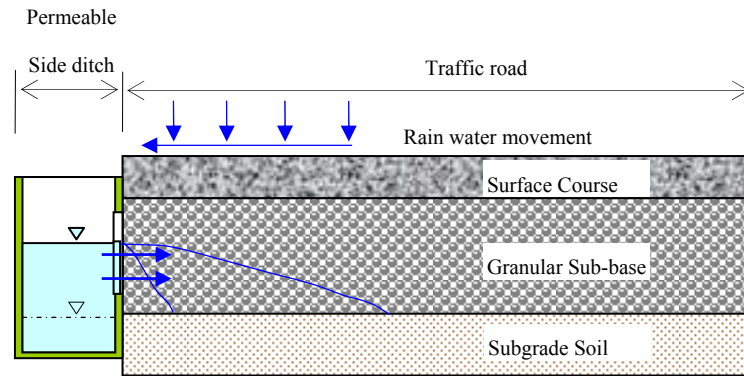
Figure 8.2 Schematic diagram showing the intrusion of storm water into porous sub-base from the permeable side drain in a typical road section.

8.3   Governing Equations

The free-surface flow of viscous and incompressible fluid through both the porous and bulk fluid region are described by a set of continuity and Navier-Stokes type equations extended with porous drag resistance terms. The equations are rewritten as:

$$\frac{\partial(1-C)u_i}{\partial x_i} = 0 \tag{8.1}$$

$$\rho\left[\frac{\partial(1-C)u_i}{\partial t} + \frac{\partial(1-C)u_iu_j}{\partial x_j}\right] = \rho(1-C)g_i - (1-C)\frac{\partial p}{\partial x_i} + \mu\frac{\partial}{\partial x_j}\left(\frac{\partial(1-C)u_i}{\partial x_j}\right) + R_i \tag{8.2}$$

where u_i is the velocity vector, also called the volume averaged intrinsic velocity in the porous

medium, C is the volumetric concentration of the solids in the porous medium, R_i the flow resistance term due to porous medium, p the pressure and the μ dynamic viscosity of the fluid. The above equations for conservation of mass and momentum can be used for anisotropic porous media and variable porosity.

The total drag resistance due to the presence of the solid particles per unit volume R_i in Eq. (8.2) represents the sum of the pressure drag and viscous friction. The total drag resistance force per unit volume of the fluid for a wide range of flow is expressed by Ergun's correlation Eq. (8.3) which can be written as

$$R_i = -\left[\frac{\mu(1-C)^2 u_i}{k} + \rho \frac{F_{ch}(1-C)^3 u_i |u_i|}{\sqrt{k}} \right] \tag{8.3}$$

where k and F_{ch} are the permeability(m^2) and Forchheimer's inertia factor. For a randomly packed bed of spheres such coefficients can be expressed in terms of the solid concentration C and the mean diameter of the particles d_p in the porous medium as

$$k = \frac{(1-C)^2 d_p^{\,2}}{150 C^2} \; ; \;\; F_{ch} = \frac{1.75}{\sqrt{150}\sqrt{(1-C)^3}} \tag{8.4}$$

It should be noted that the Eqs. (8.1) and (8.2) governing the flow in porous media is very much similar to the classical continuity and Navier-Stokes equation for the open channel flow. The equations are made applicable for both free and porous domain by switching the values of C and K. In doing so, the term dealing with the drag of the solid matrix will be vanished outside the porous media resulting the usual open channel flow in free domain.

Boundary condition and free surface evolution

The model has been already tested for two types of upstream boundary conditions: constant discharge boundary and constant water level boundary. Here, in this case the bottom of the left channel ($0 \leq x \leq 0.20$m) is treated as Dirichlet boundary condition where the vertical velocity is supplied as a function of time as given in the Table 8.1 to check the applicability of the model to simulate the unsteadiness in the water depth and velocity in the left channel. All other boundaries are treated as no flow boundary. At the free surface of the flow, the atmospheric pressure condition is applied. The method introduces a volume of fluid function to define the water region and its saturation within the cell.

Table 8.1 Time dependent vertical velocity

S.N.	Time (s)	Velocity (m/s) [+ for upward]	Remarks
1.	0.0 -2.0	+0.07	Applied at the bottom of left channel for its full width 0.20m.
2.	2.0 -5.0	+0.03	
3.	5.0 onward	-0.03	

8.4   Numerical approach

The governing Eqs. (8.1) and (8.2) are solved numerically on a uniform staggered Cartesian grid by finite volume method. The constrained interpolated propagation (CIP) method [Yabe and Aoki, 1991a and 1991b] is adopted as the base scheme for the solution. The basic idea of the CIP method is that for advection computation of any flow variable, not only the transportation equation but also the transportation equation of its spatial gradients are solved. Thus applying the fractional time step approach, the numerical solution of the governing equations can be divided into the following two steps: *non-advection* and *advection phase* as explained in chapter 3.

The evolution of the free surface is traced using VOF method [Hirt and Nichols, 1981]. The governing equation for such free-surface flow is already given in previous chapters [see Eq. (3.11)] Given the volumetric nature of function *f* and in order to maintain its sharpness at the interface, discretization of equation (3.11) requires special treatment. The donor-acceptor concept [Hirt and Nichols, 1981] along with MUSCL type TVD [Van Leer, 1979] scheme is used for the non-oscillatory convection of the VOF function.

8.5   Results and discussion

The results from the numerical simulation are presented in this section. Figures 8.3(a)-(c) show the velocity and flow profile evolution in the free-surface flow in the composite flow domain. The left channel is the free flow domain and the right shaded one is porous domain (K=0.10m/s). The flow dynamics for gradually increased water level in the channel has been shown in the figures for different time instants after the start of the simulation. During the recession the backflow to the channel occurs but some portion is still moving to the porous storage basin. The delayed response of porous media flow seems very useful characteristic in the effective management of storm severity.

We can observe that when intrusion starts the velocity are higher inside the porous media which is as it should be because these velocities are the volume averaged intrinsic velocities. The level reaches its peak at *t* = 5s. Then it gradually recesses showing some backflow into the side channel forming there a sort of water divide. During recession also some of the water is still flowing towards the porous storage. The delayed response phenomenon of the porous flow could be a very positive aspect in the peak reduction.
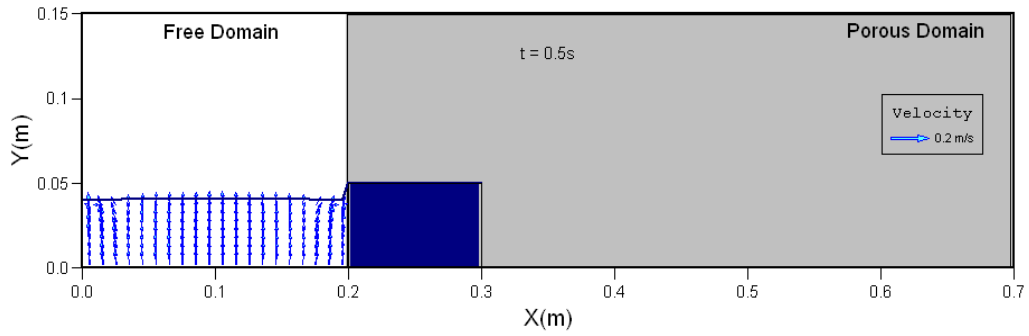
8.3(a)
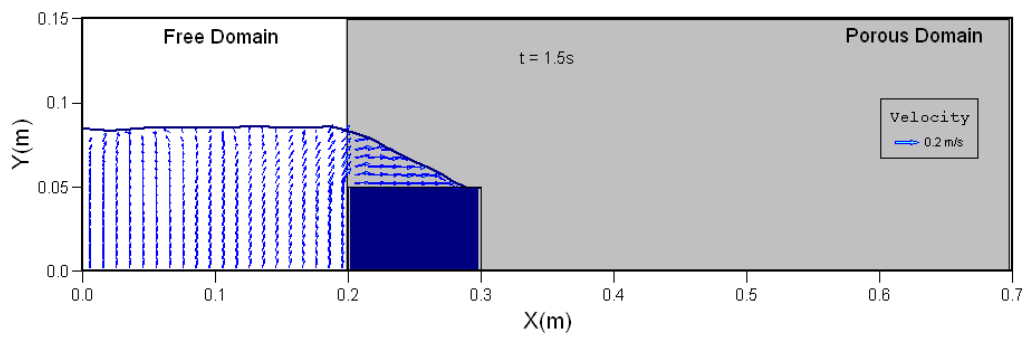
8.3(b)
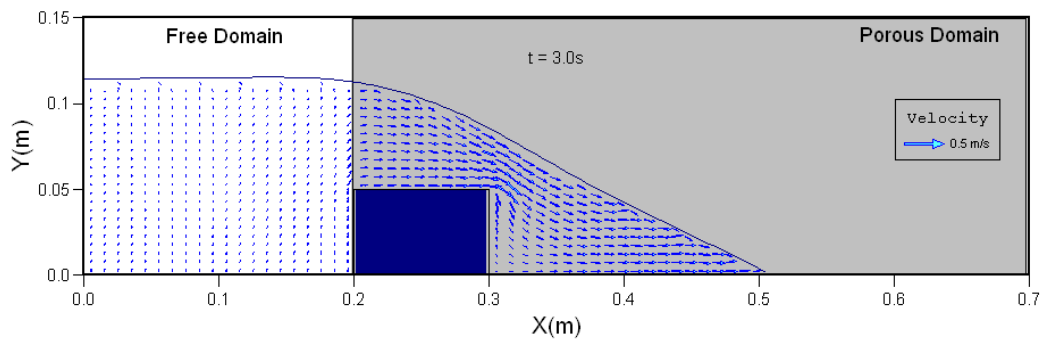
8.3(c)
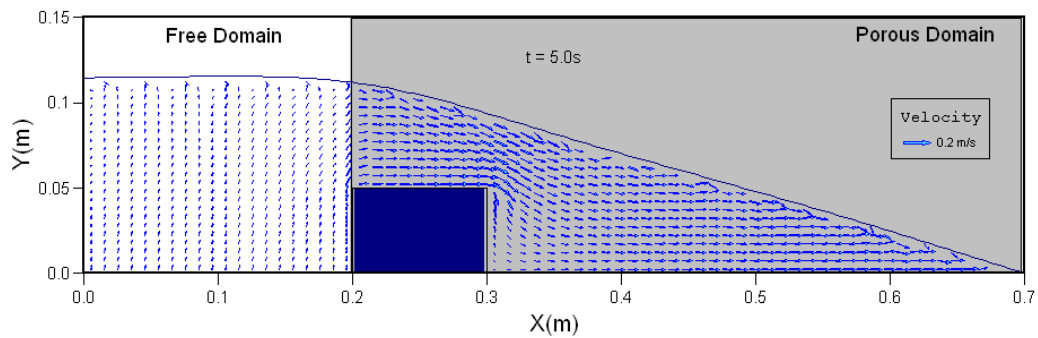
8.3(d)
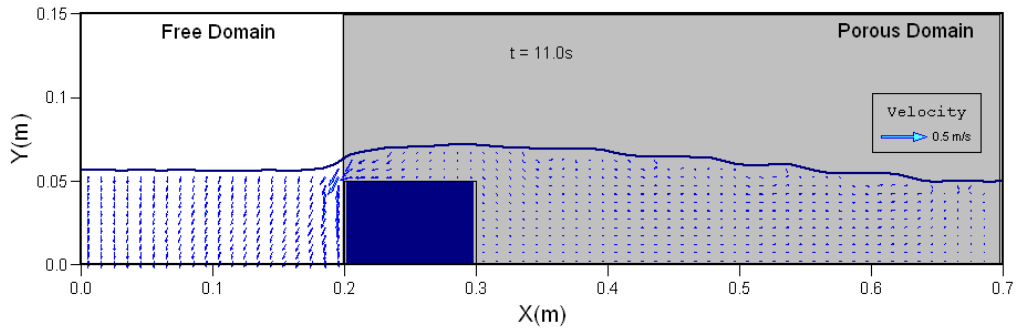
8.3(e)
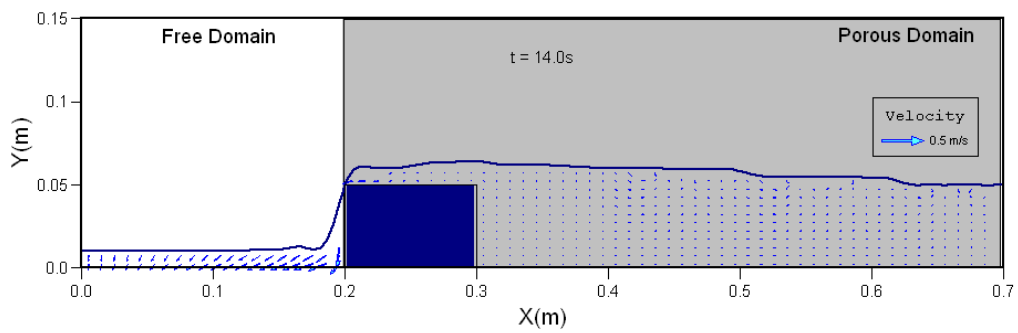
8.3(f)

Figure 8.3 Velocity and flow profiles by numerical simulation at different times as indicated [(a)-(f): 0.5s, 1.5s, 3.0s, 5.0s, 11.0s, 14.0s).]
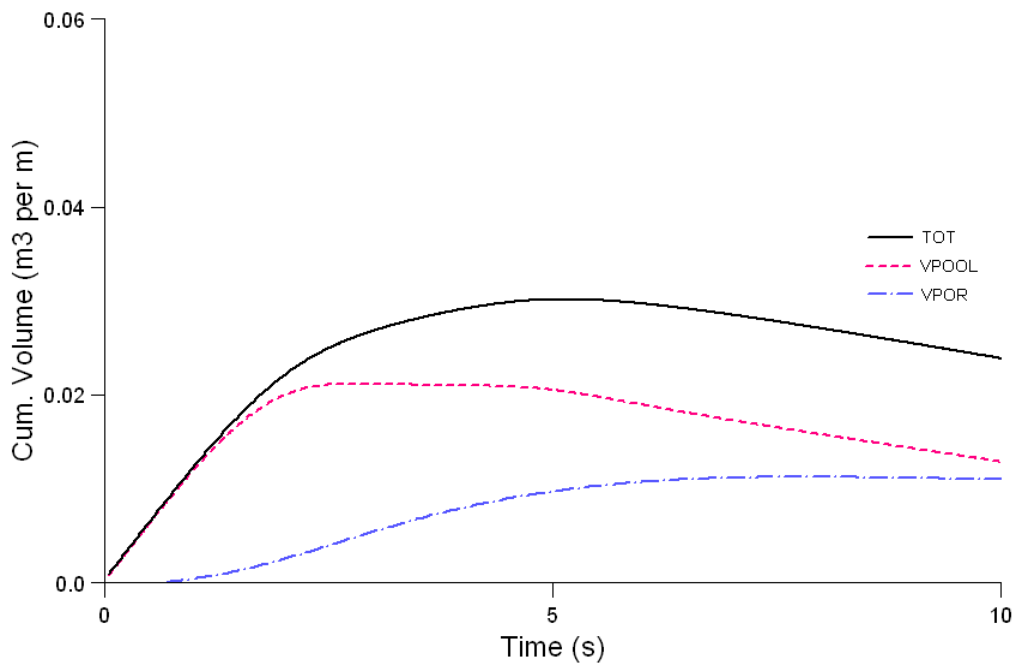
Figure 8.4 Temporal variation of storage in the side channel and porous basin.

Fig. 8.4 shows the temporal change of various hydrological parameters obtained in response to the assumed total inflow. The model seems very useful in predicting precisely the storage volume in a storm event. It could be used as a hydrological decision tool for event based calculation.

8.6 Summary

Limited land space and the need for more housing and infrastructure means greater emphasis is being given to how we handle flood management. This of course impacts on watercourses and drainage systems with increased risk of localized flooding and pollution. To make matters worse, handling this added pressure of volume and water quality is fast becoming a developer's responsibility rather than the local water authorities'. So what's the solution? Total flood protection is unrealistic and unwise. The ultimate goal of flood loss prevention is the improvement of the quality of life by reducing the impact of flooding. The answer lies underground, not with the current drainage system, but with a new Sustainable Drainage System.

Planning and design of storm water drainage systems, culverts, detention basins, and other storm water facilities require information on storm peak flows and runoff volumes. The model of this kind can be utilized to estimate the information about the temporal storage volumes, variability and complexity, functionality, and applicability to a given region or storm type, through a process of calibration and verification for reliable results.

Chapter 9
OVERALL CONCLUSION

9.1 Overall conclusion

In this study a physically based mathematical model is proposed and solved numerically. It is applied for different types of domains with various boundary conditions. The model results are verified with the results of analytical solution and experiments. Also an integral model is formulated using similarity distribution functions for depth and velocity. The partial differential equations are transformed into ordinary differential equation. The model can represent both inertia-pressure and pressure-drag flow regimes as obtained in the analytical derivations.

A comprehensive approach including mathematical, numerical and experimental programs has been taken in order to develop new models for describing free-surface flow behavior in porous media. The study suggested that modeling free-surface flow in porous media is possible using a single integral equation with proper transition between inertial and classical Darcian fow, based on the similarity distribution functions of depth and velocity. The developed integral model

inherits both the flow regimes as depicted in the analysis. Both for the laminar and turbulent flows through porous media, the integral models give satisfactory results. The proposed algorithm for numerical simulation is capable of solving various problems of free-surface flow through porous media.

This study adds a new dimension to fluid flow in porous media by replacing Darcy's equation with new models that are capable of representing both Darcy and non-Darcy flow behaviors. These are new nonlinear ordinary differential equations inherited all the flow regimes. The integral formulation for unsteady depth distribution, velocity and front speed under constant water level and constant flux discharge inlet conditions have been developed from similarity law. Analysis is done for both laminar and turbulent flows. The formulation presented provides additional analytical insight about the intrusion dynamics. In addition, the method proposed can be successfully used for the solution of a host of other nonlinear problems that admit self-similarity. The developed solutions for constant inlet water level condition have been verified with the experimental observation. The unsteady distributions of drainage depth, inflow velocity and front speeds have been compared for various porous media characterized by its corresponding permeability. The analysis indicates that the integral model clearly represents the nonlinear flow behavior in the porous media both in laminar and turbulent flow conditions. The integral model results are in agreement with those obtained by similarity solution for the temporal change of velocity, depth at the origin and front positions.

The thesis also presents a computational fluid dynamics (CFD) model developed for the analysis of transient free-surface flows in porous media, transient flow problems in porous strata. Vertical two-dimensional numerical simulations are carried out for the free-surface flow inside the porous media governed by a set of Navier-Stokes equations extended for porous media flow. This model includes the convective and local inertia terms along with viscous diffusion terms

and a resistance terms comprising Darcy's linear resistance and Forchheimer's inertial resistance terms. The Finite volume method is applied using constrained interpolated propagation (CIP) method and highly simplified marker and cell (HSMAC) type pressure solver for the numerical solution. The evolution of moving free surface is governed by volume of fluid (VOF) method employed for the flow through porous media. To prevent the spurious oscillation and generate diffusion-free sharp interface, a third order MUSCL type total variation diminishing (TVD) schemes is used to discretize the convective terms in VOF convection equation.

In the case of rapid vertical infiltration of water through a vertical column filled with porous media, a number of experiments and analytical investigations are carried out to see the effect of acceleration in the intrusion process. It is concluded that the conventional infiltration models like Green-Ampts infiltration equation cannot account for the acceleration effect in the case of high velocity flow. It is also revealed that it takes certain time for intruding water to be accelerated to its peak velocity and then its velocity gradually decreases as the gradient goes on decreasing.   The investigations are made for two different cases; constant and variable water level (fixed water volume release) at the top of the porous media. For the media having low permeability, the effect of acceleration is not so significant in the downward intrusion.

The power law derivation and validation for the general inflow condition has been made for a channel having a backward facing step. The result of theoretical analysis has been compared with that of the numerical simulation and it showed a good agreement. The effect of characteristics of porous media has been identified with respect to inflow discharge and front position. The model could be a tool for the proposition of some empirical relations using multivariate correlation.

In the case of dam break flow over horizontal porous strata, the model has been applied to a

very complicated domain regarding both geometry and boundary conditions. The single set of governing equation is capable of simulating a complex phenomenon. The model showed its robustness in simulating the flow where the interface between pressurized and open channel flow moves forward. The rapid vertical infiltration has significant effect due to the acceleration which the shallow water equations cannot account. In particular, it is shown that vertical two dimensional numerical solutions that couples the fluid and solid systems simultaneously at the macroscopic scale are feasible and are extremely beneficial, shedding a new light into phenomena unavailable otherwise.

It is also found that the proposed numerical model can be used for the determination of the storm storage in the porous sub-base in a typical road section. The capability of the model has been assessed by using the unsteady inflow condition so as to simulate the condition during high precipitation. The model could be a promising tool for the planners and decision makers for the effective drainage calculations to mitigate the urban flood. The model is successful in modeling the free-surface flow in the bulk fluid as well as in the porous region. In contrast to earlier proposed boundary conditions at the two domain interface, in this model a continuity of velocities and stresses is assumed; for both regions a single set of governing equations is solved. The robustness of the model can be demonstrated by the capability of the numerical approach proposed in this thesis. The proposed mathematical model for flow in porous media, which would be able to simulate the incompressible free-surface flow in the porous media having high permeability and assist in the design of various hydraulic facilities. An integral model formulation gives a reliable and quick method for the prediction of flow parameters in the case of simple flow geometry.

9.2 Recommendation for future research

The results from the proposed analytical integral as well as numerical models are expected to be useful for the real world application with unbounded possibilities of its expansion in the future. The results of the model could be used as reference states to assess the results of other model approaches. The incorporation of turbulent models in the proposed model could be made to increase its accuracy and robustness. The expansion and optimization can be performed as the needs may arise. Further research is required to incorporate capillarity, surface tension etc. Analysis is necessary for determining the limit of validity of different flow regimes so that a generalized resistance can be formulated to use in the momentum equation. The current formulation cannot account for the movement of porous media. The analysis in this direction may be useful in the studies of various natural processes like debris flow, landslides etc. The model maybe extended for the movement of pollutants in the groundwater studies.

Protecting the environment is essential for the quality of life of current and future generations as well as for economic growth. Given that the Earth's natural resources and the man-made environment are under pressure from growing population, urbanization, continuous expansion of the agriculture, transport and energy sectors, as well as climate variability and warming at local, regional and global scales, newly envisaged global objective of human security cannot be met as expected. The proposed models may contribute to achieving sustainable use of resources, to mitigating and adapting to climate change, and to protecting the ecosystems and the man-made environment. etc. The model could be a tool to study the consequences of construction of various hydraulic facilities where there is porous stratum as a whole or a part of the solution domain

REFERENCES

Ahmed, N. and Sunada, D. K., Nonlinear flow in porous media, *J. Hydr. Div.*, *ASCE*, 95:1847-1857, 1969.

Al-Nimr, M. A. and Alkam, M. K., Unsteady non-Darcian fluid flow in parallel-plates channels partially filled with porous materials, *Heat Mass Transfer*, 33:315-318, 1998.

Amsden, A. A. and Harlow, F. H., A Simplified MAC Technique for Incompressible Fluid Flow Calculations, *J. Comput. Phys.*, 6:322-325, 1970.

Anderson, T. B. and Jackson, R., A fluid mechanical description of fluidized beds, *Ind. & Eng. Chem. Fund.*, 6(4):527-539, 1967.

Bachmat, Y., Basic transport coefficients as aquifer characteristics, International Association of Scientific *Sympo. on Hydrology of Fractured Rocks*, Dubrovnik, 1:63-75, 1965.

Barenblatt, G. I. and Vazquez, J. L., A new free boundary problem for unsteady flows in porous media, *Euro. J. Applied Maths.*, 9:37-54, 1998.

Bauer, T. H., A General Analytical Approach toward the Thermal Conductivity of Porous Media, *J. Heat Mass Transfer*, 36:4181-4191, 1993.

Bear, J. and Bensabat, J., Advective fluxes in multiphase porous media under nonisothermal conditions, *Transport in Porous Media*, 4(5):423-448, 1989.

Bear, J., Dynamics of Fluids in Porous Media, *Elsevier*, NY, 1972.

Beavers, G. S. and Joseph, D. D., Boundary conditions at the natural permeable wall, *J. Fluid Mech.*, 30:197-207, 1967.

Beavers, G. S. and Sparrow, E. M., Non-Darcy Flow through Fibrous Porous Media, *J. Applied Mechanics*, ASME, 36(4):711-714, 1969.

Brinkman, H. C., A calculation of the viscous force extended by a flowing fluid on a dense swarm particles, *Appl. Science Res*. A1, 1947.

Buckingham, E., Studies on the movement of soil moisture, Bulletin 38, U. S. Department of Agriculture, Bureau of Soils, Washington, 1907.

Buckley, S. E. and Leverett, M. C., Mechanism of fluid displacement in sands, Trans. AIME, 146:107-116, 1942.

Chen, Z. X., Bodvarsson, G. S., Witherspoon E. A. and Yortsos, Y. C., An integral equation

formulation for the unconfined flow of groundwater with variable inlet conditions, *Transport in Porous Media*, 18:15-36, 1995.

Cheng, P., Wall effects on fluid flow and heat transfer in porous media. *Proc.* ASME/JSME Thermal Engng. Joint Conf., 2:297-303, 1987.

Chorin, A. J., Numerical solution of the Navier-Stokes Equations, *Mathematics of Computation*, 22(104):745-762, 1968.

Costa, V. A. F., Oliveira, L. A., Baliga, B. R. and Sousa, A. C. M., Simulation of coupled flows in adjacent porous and open domains using a control-volume finite-element method, *Numerical Heat Transfer A,* 45:675-697, 2004.

Cryer, C.W., A bibliography of free boundary problems, MRC Technical Summary Report, University of Wisconsin, Madison, 1793, 1977.

Darcy, H., Les Fontaines Publiques de la Ville de Dijon, Victor Dalmont, Paris, 1856.

Drew, D. and Prassman, S., Theory of multicomponent fluids, first ed., *Springer*, 1999.

Dracos, T., Multiphase flow in porous media, In: Bear, J. and Buchlin, J. M., Editors, *Modelling and applications of transport phenomena in porous media*, 203–217, 1991.

Ergun, S., Fluid flow through packed columns, *Chem Engng Prog.* 48:89-94, 1952.

Fand, R. M., Kim, B. Y. K., Lam, A. C. C., and Phan, R. T., Resistance to the flow of fluids through simple and complex porous media whose matrices are composed of randomly packed spheres, ASME, *J. Fluids Engng.*, 109:268-274, 1987.

Forchheimer, P.,Wasserbewegung durch Boden, *Zeitschrift Verein Deutscher Ingenieure*, 45:1782-1788, 1901.

Fuentes, C., Haverkamp, R. and Parlange, J. Y., Parameter constraints on closed-form soilwater relationships, *J. of Hydrology*, 134:117-142, 1992.

Ghimire, B., Hosoda, T. and Nakashima, S., An investigation on lateral intrusion process of water into porous media under different upstream boundary conditions, *J. Applied Mechanics*, JSCE, 10:839-846, 2007.

Goyeau, B., Lhuillier, D., Gobin, D. and Velarde, M. G., Momentum transport at a fluid-porous interface, *Int. J. Heat Mass Transfer*, 46:4071-4081, 2003.

Gray, W. G. and Lee, P. C. Y., On the theorems for local volume averaging of multiphase systems, *Int. J. Multiphase Flow*, 3:333-340, 1977.

Gray, W. G. and Hassanizadeh, S. M., Paradoxes and realities in unsaturated flow theory, *Water Resources Research*, 27(8):1847-1854, 1991.

Hall, W. A. , An analytical derivation of the Darcy equation, EOS Trans., AGU, 37:185-188, 1956.

Hanspal, N. S., Waghode, A. N, Nassehi, V., Wakeman, R., Numerical analysis of coupled Stokes/Darcy flows in industrial filtrations, *Transport in Porous Media*, 64:73-101, 2006.

Harlow, F. H., Shannon, J. P., Welch, J. E., A computing technique for solving viscous, incompressible transient fluid flow problems involving free surface, Los Alamos Scientific Laboratory Report LA-3425; 1965.

Harlow, F. H. and Welch, J. E., Numerical calculation of time-dependent viscous incompressible flow of fluids with free surface, *Phys. Fluids*, 8:2182, 1965.

Harry, R. C., Seepage drainage and flow nets, John Wiley & Sons, New York, 1989.

Harten, A., High resolution schemes for hyperbolic conservation laws, *J. Comput. Phys.*, 49:357-393, 1983.

Hassanizadeh, S. M. and Gray, W. G., General conservation equations for multi-phase systems: I. averaging procedure, *Advances in Water Resources*, 2(3):131, 1979a.

Hassanizadeh, S. M. and Gray, W. G., General conservation equations for multi-phase systems: 2. mass, momentum, energy, and entropy equations, *Advances in Water Resources*, 2(4):191-203, 1979b.

Hassanizadeh, S. M. and Gray, W. G., General conservation equations for multi-phase systems: 3. constitutive theory for porous media flow, *Advances in Water Resources*, 3(1):25-40, 1980.

Hassanizadeh, S. M. and Gray, W. G., Thermodynamic basis of capillary pressure in porous media, *Water Resources Research*, 29(10):3389-3405, 1993.

Hassanizadeh, S. M. and Gray, W. G., Recent advances in theories of two-phase flow in porous media, In: Plessis, P. du, editor, Fluid Transport in Porous Media, *Advances in Fluid Mechanics*, chapter 13(3):104-160, 1997.

Hlushkou, D. and Tallarek, U., Transition from creeping via viscous-inertial to turbulent flow in fixed beds, *J. Chromatography*, *Elsevier*, 1126:70-85, 2006.

Hirsch, C., Numerical computation of internal and external flows, vol. 2: Computational

methods for inviscid and viscous flows, John Willey & Sons, 1990.

Hirt, C. W. and Cook, J. L., Calculating three dimensional flows around structures and over rough terrain, *J. Comput. Phys.*, 10:324-340, 1972.

Hirt, C. W. and Nichols, B. D., Volume of fluid (VOF) method for the dynamics of free boundaries, *J. Comput. Phys.*, 39:201–225, 1981.

Hosoda, T., Inoue, K. and Tada, A., Hydraulic transient with propagation of interface between open-channel free surface flow and pressurized pipe flow, *Proc*. of the 5th *Int. Symp. on Computational Fluid Dynamics*, JSCFD, Japan, 1:291-296, 1993.

Hosoda, T., Kokado, T. and Miyagawa, T., Flow characteristics of viscous fluids on the basis of self-similarity law and its applications to high flow concrete, *J. Applied Mech.*, JSCE, 3:313-321, 2000.

Hsu, C. T. and Cheng, P., Thermal dispersion in a porous medium, *Int*. *J. Heat Mass Transfer*, 33:(8):1587-1597, 1990.

Hubbert, M. K., Darcy law and the field equations of the flow of underground fluids, *Trans. Amer. Inst. Min. Metal Engng.*, 207:222-239, 1956.

Huppert, H. E., The propagation of two-dimensional and axisymmetric viscous gravity currents over a rigid horizontal surface, *J. Fluid Mech.*, 121:43-58, 1982.

Huppert, H. E. and Woods, A. W., Gravity-driven flows in porous layers, *J. Fluid Mech.*, 292:55-69, 1995.

Ingham, D. B. and Pop, I., Transport Phenomena in porous media second ed., Pergamon, *Elsevier*, London, 2002.

Ishii, M., Thermo-Fluid Dynamic Theory of Two-Phase Flow, Eyrolles, Paris, 1975.

Jacimovic, N., Hosoda, T., Kishida, K. and Ivetic, M., Numerical Solution of the Navier-Stokes equations for incompressible flow in porous media with free surface boundary, *J. Applied Mech.*, JSCE, 8:225-231, 2005.

Jue, T. C., Numerical analysis of vortex shedding behind a porous square cylinder, *Int. J. Numer. Methods Heat Fluid Flow*, 14:649-663, 2004.

Kaviany, M., Principles of Heat Transfer in Porous Media, Springler-Verlag, New York, 1991.

Kladias, N. and Prasad, V., Natural convection in horizontal porous layers: effects of Darcy and Prandtl numbers. *J. Heat Transfer* **111**:926–935, 1989.

Kothe, D. B., Rider, W. J., Mosso, S. J., Brock, J. S. and Hochstein, J., Volume tracking of interfaces having surface tension in two and three dimensions, Los Alamos National Laboratory Report AIAA96-0859, 1996.

Leonard, B. P., A stable and accurate convective modeling procedure based on quadratic upstream interpolation, *Comp. Methods in Appl. Mech. Engng*, 19(1): 59-98, 1979.

Manz, B., Gladden, L. F., and Warren, P. B., Flow and dispersion in porous media: Lattice-Boltzmann and NMR studies, *AIChE Journal*, 45(9):1845-1853, 1999.

Martys, N. S. and Hagedorn, J. G., Multiscale Modeling of Fluid Transport in the Heterogeneous Materials Using Discrete Boltzmann methods, *Material and Structures*, 35:650-659, 2002.

Mercier, J., Weisman, C., Firdaouss, M. and Quéré P. L., Heat transfer associated to natural convection flow in a partly porous cavity, ASME, *J. Heat Transfer*, 124:130-143, 2002.

Muskat, M., The flow of homogeneous fluids through porous media, J. W. Edwards, Michigan, 1946.

Neuman, S. P., Theoretical derivation of Darcy's law, Acta Mechanica, 25:153-170, 1977.

Prasad, V., Lauriat, G. and Kladias, N., Reexamination of Darcy-Brinkman solutions for free convection in porous media, ASME, *Proceedings of the 1988 National Heat Transfer Conference,*1, ASME HTD 96:569-580, 1988.

Poulikakos, D. and Bejan, A., The departure from Darcy flow in natural convection in a vertical porous layer, *Phys. Fluids*, 28:3477-3484, 1985a.

Poulikakos, D., A departure from the Darcy model in boundary layer natural convection in a vertical porous layer with uniform heat flux, *J. Heat Transfer*, 107:716-720, 1985b.

Press, W. H., Teukolsky, S. A., Vetterling, W. T., Flannery, B. P., Numerical recipes, second ed., Cambridge University Press, 1996.

Pritchard, D., Woods, A. W. and Hogg, A. J., On the slow draining of a gravity current moving through a layered permeable medium, *J. Fluid Mech.*, 444:23-47, 2001.

Pullan, A. J., The quasilinear approximation for unsaturated porous media flow, *Water Resources Research*, 26(6):1219-1234, 1990.

Richards, L. A., Capillary conduction of liquids through porous medium, Physics, 1:318- 333, 1931.

Rider, W. J., and Kothe, D. B., Reconstructing volume tracking, *J. Comput. Phys.*, 141:112-152, 1998.

Raptis, A., Perdikis, C., Flow of a viscous fluid through a porous medium bounded by a vertical surface, *Int. J. Engng Sci.*, 21(11):1327-1330, 1983.

Reynolds, O., Papers on mechanical and physical subjects, Cambridge University Press, 1900.

Scheidegger, A. E., Statistical hydrodynamics in porous media, *Journal of Applied Physics*, 25(8):994-1001, 1954.

Silva, R. A. and de Lemos, M. J. S., Numerical analysis of the stress jump interface condition for laminar flow over a porous layer, *Numer. Heat Transfer* A 43:603-617, 2003.

Slattery, J. C., Single-phase flow through porous media, *AIChE Journal*, 15:866-872, 1969.

Slattery, J. C., Flow of viscoelastic fuids through porous media, *AIChE Journal*, 13:1066-1071, 1967.

Sweby, P. K. High resolution schemes using flux limiters for hyperbolic conservation laws, *SIAM Journal on Numerical Analysis*, 21(5): 995-1011, 1984.

Thompson, K. E. and Fogler, H. S., Modeling flow in disordered packed beds from pore-scale fluid mechanics, *AIChE Journal*, 43(6), 1377-1389, 1997.

Thompson, K. E., Pore-scale modeling of fluid transport in disordered fibrous materials, *AIChE Journal*, 48(7):1369-1389, 2002.

Tien, C. L. and Hong, J. T., Natural convection in porous media under non-Darcian and non-uniform permeability conditions, In: Kakas, S., Aung, W. and Viskanta, R., Editors, *Natural Convection*, Hemisphere Publishing, Washington, DC, 373-587, 1985.

Vafai, K. and Tien, C. L., Boundary and Inertia Effects on Flow and Heat Transfer in Porous Media, *Int. J. Heat Mass Transfer*, 24:195-203, 1981.

Vafai, K. and Thiyagaraja, R., Analysis of flow and heat transfer at the interface region of a porous medium, *Int. J. Heat Mass Transfer*, 30:1391-1405, 1987.

Vafai, K. and Kim, S. J., Fluid mechanics of the interface region between a porous medium and a Fluid layer an exact solution, *Int. J. Heat Fluid Flow*, 11:254-256, 1990.

Van Genuchten, M. T., A closed-form equation for predicting the hydraulic conductivity of unsaturated soils, *Soil Sci. Soc. Am. J.*, 44:892-898, 1980.

Van Leer, B., Towards the ultimate conservative difference scheme, *J. Comput. Phys.*, 32:101-136, 1979.

Viecelli, J. A., A Computing Method for Incompressible Flows Bounded by Moving Walls, *J. Comput. Phys.*, 8:119-143, 1971.

Wanielista M. P. and Yousef, Y. A., Storm water management, John Wiley and Sons, New York, 1993.

Washburn, E. W., The dynamics of capillary flow, Physical Review, Second Series, 17(3):273-283, 1921.

Welch. J. E., Harlow, F. H., Shannon, J. P. and Daly, B. J., A computing technique for solving viscous, incompressible, transient fluid-flow problems involving free surfaces, Los Alamos Scientific Laboratory Report, LA-3425, 1965.

Whitaker, S., The equations of motion in porous media, *Chem. Engng. Sci.*, 21:291-300, 1966.

Whitaker, S., Diffusion and dispersion in porous media, *AIChE Journal*, 13(3):420-427, 1967.

Whitaker, S., Advances in theory of fluid motion in porous media, *Ind. & Eng. Chem.*, 61(12):14-28, 1969.

Whitaker, S., Flow in porous media I: a theoretical derivation of Darcy's law, *Transport in Porous Media*, 1:3-25, 1986.

Wright, D. E., Non-linear flow through granular media. *J. Hydraulic Div.*, ASCE 94(H74):851–872, 1968.

Yabe, T. and Aoki, T., A universal solver for hyperbolic equations by cubic-polynomial interpolation I: One dimensional solver, *Comput. Phys. Communications*, 66:219-232, 1991a.

Yabe, T., and Aoki, T., A Universal solver for hyperbolic equations by cubic-polynomial interpolation II. Two- and three-dimensional solver, *Comput. Phys. Communications*, 66:233–242, 1991b.

Yamamoto, K. and Iwamura, N., Flow with convective acceleration through a porous medium, *J. Engng. Maths.*, 10:41-54, 1976.

Youngs, D., L., Time-dependent multi-material flow with large fluid distortion, In: Morton, K. W. and Baines, M. J., Editors, *Numerical methods for fluids dynamics*, Academic Press, New York, 273-285, 1982.

River System Engineering and Management Laboratory
Department of Urban Management
Graduate School of Engineering
Kyoto University